FINAL REPORT TO

NATIONAL AERONAUTICS AND SPACE ADMINISTRATION

GODDARD SPACE FLIGHT CENTER
LABORATORY FOR ATMOSPHERES

CONTRACT NAS5-30957

/N -4/
/4/3-/4/
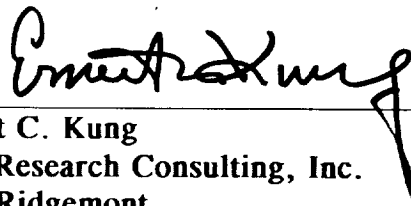*P- 104*

Title: Long Range Forecasts of the Northern Hemisphere Anomalies
with Antecedent Sea Surface Temperature Patterns

Period Covered: March 5, 1991 - June 4, 1994

June 4, 1994

Principal Investigator and Contractor:

Ernest C. Kung
ECK Research Consulting, Inc.
1719 Ridgemont
Columbia, Missouri 65203
(314) 446-3296

REPORT DOCUMENTA. AGE

Public reporting burden for this collection of information is estimated to average 1 hour per response, including the time for reviewing instructions, searching existing data sources, gathering and maintaining the data needed, and completing and reviewing the collection of information. Send comments regarding this burden estimate or any other aspect of this collection of information, including suggestions for reducing this burden, to Washington Headquarters Services, Directorate for Information Operations and Reports, 1215 Jefferson Davis Highway, Suite 1204, Arlington, VA 22202-4302, and to the Office of Management and Budget, Paperwork Reduction Project (0704-0188), Washington, DC 20503.

1. AGENCY USE ONLY *(Leave blank)*	2. REPORT DATE June 1994	3. REPORT TYPE AND DATES COVERED Contractor Report

4. TITLE AND SUBTITLE
Long Range Forecasts of the Northern Hemisphere Anomalies with
Antecedent Sea Surface Temperature Patterns

5. FUNDING NUMBERS

910.4

6. AUTHOR(S)
Ernest C. Kung

7. PERFORMING ORGANIZATION NAME(S) AND ADDRESS(ES)

ECK Research Consulting, Inc.
1719 Ridgemont
Columbia, Missouri 65203

8. PERFORMING ORGANIZATION REPORT NUMBER

9. SPONSORING/MONITORING AGENCY NAME(S) AND ADDRESS(ES)

National Aeronautics and Space Administration
Washington, D.C. 20546–0001

10. SPONSORING/MONITORING AGENCY REPORT NUMBER

CR-189358

11. SUPPLEMENTARY NOTES

Technical Monitor: J. Susskind/910.4

12a. DISTRIBUTION/AVAILABILITY STATEMENT
Unclassified–Unlimited
Subject Category 47
Report is available from the NASA Center for AeroSpace Information, 800 Elkridge
Landing Road, Linthicum Heights, MD 21090; (301) 621-0390.

12b. DISTRIBUTION CODE

13. ABSTRACT *(Maximum 200 words)*

The research has been conducted in the following three major areas:

1) Analysis of numerical simulations and parallel observations of atmospheric blocking;
2) Diagnosis of the lower boundary heating and the response of the atmospheric circulation;
3) Comprehensive assessment of long-range forecasting with numerical and regression methods;

the results of which are presented in this document.

14. SUBJECT TERMS
General Circulation Model (GCM), Sea Surface Temperture

15. NUMBER OF PAGES
102

16. PRICE CODE

17. SECURITY CLASSIFICATION OF REPORT Unclassified	18. SECURITY CLASSIFICATION OF THIS PAGE Unclassified	19. SECURITY CLASSIFICATION OF ABSTRACT Unclassified	20. LIMITATION OF ABSTRACT Unlimited

NSN 7540-01-280-5500

1. **SUMMARY STATEMENT OF CONTRACT RESEARCH, CONCLUSIONS, AND ACCOMPLISHMENTS**

The contract research has been conducted in the following three major areas:

1. Analysis of numerical simulations and parallel observations of atmospheric blocking.
2. Diagnosis of the lower boundary heating and the response of the atmospheric circulation.
3. Comprehensive assessment of long-range forecasting with numerical and regression methods.

The essential scientific and developmental purpose of this contract research is to extend our capability of numerical weather forecasting by the comprehensive general circulation model. The systematic work as listed above is thus geared to developing a technological basis for future NASA long-range forecasting.

Experiments have been conducted for a 46-day summer period from July 1 to August 15, 1979, using the high resolution 2 x 2.5 degree version of the Goddard Laboratory for Atmospheres (GLA) general circulation model (GCM), to simulate the summer blocking observed during the period in the Northern Hemisphere. During the simulation, sea surface temperature (SST) anomalies were updated daily with observations to provide a realistic surface heating field. A parallel control run used climatology SSTs, in lieu of observed SSTs. Both the SST updating experiment and the control run were able to simulate the persistent blocking patterns in Eurasia and the eastern Pacific during July. However, only the SST updating experiment was able to generate the realistic blocking episodes in the last 10-day period during the 46-day simulation. Forecast skill was examined in terms of 500 mb anomaly correlation and error kinetic energy. When the blocking patterns develop or become reinforced, a high forecast skill is apparent in nearly half of

1

the Northern Hemisphere, including the area of blocking and its downstream region. Unlike the major winter blockings, which may be treated as the manifestation of wave number one and two, the summer blockings are localized, and have a smaller scale than that of winter blockings. However, summer blockings treated in this study are persistent, and possess a considerable predictability. The effort in this simulation is detailed in Kung, Min, Susskind and Park (1992).

In an attempt to examine the association of SST anomalies with major winter blocking, twelve major blocking episodes in the Northern Hemisphere winter are selected for examination from a 34-year data period: four episodes for each category of Pacific, Atlantic and double blocking. It is shown in Kung, Susskind and DaCamara (1993) that the major single blocking in the Pacific or Atlantic is formed through constructive interference of the traveling zonal wave of $n=1$ and the stationary wave of $n=2$. The $n=1$ is supported by the energy input through the nonlinear wave-wave interaction, and the $n=2$ by *in situ* warming over the Pacific and Atlantic. The concurrent double blocking in the Pacific and Atlantic is formed by the stationary $n=2$ when the traveling $n=1$ is weak. The cooling of the Pacific and Atlantic is associated with the single blocking in the Pacific and Atlantic. On the contrary, the warming in both the Pacific and Atlantic is associated with concurrent Pacific and Atlantic blockings, indicating the baroclinic nature of the double blocking. The hemispherical and regional energetics of blocking areas are examined in terms of kinetic energy and nonlinear kinetic energy transfer in $n=1$, 2, and 3.

Large-scale modes of variations in SSTs and the tropospheric circulation are examined with major principal components utilizing monthly mean fields of the global SSTs and Northern Hemisphere geopotential height (Z) at 700, 500 and 300 mb levels in Kung, Chern and Susskind (1994). The data period covered is from 1955 to 1992. It is found that the

heterogeneity of SST data due to availability of satellite observations and difference of analysis schemes may result in a large systematic bias in the dataset. However, the bias may be effectively corrected through elimination of an appropriate principal component, n=1 in this case. The first three components of monthly SST and Z fields during the 38-year period are scrutinized. The El Niño-Southern Oscillation (ENSO) mode of variation is observed in both 1st and 2nd components of SSTs. The inter-annual variations of principal components of monthly SST and Z fields are utilized to probe the association of SST components and Z components. Further, cross-correlation patterns of principal components of SSTs in reference to the tropospheric circulation are studied with 500 and 300 mb fields. It is shown that the tropospheric response to SST anomalies are consistent at 500 and 300 mb levels, and the seasonal-range predictability of the tropospheric circulation is recognized with SST anomaly fields.

Long-range predictability of the Northern Hemisphere circulation with numerical-dynamical and empirical-regression methods has been critically evaluated in reference to prominent circulation phenomena, including blocking, monsoon, and others (Kung, Chern, Susskind and Lin 1992). Whereas the deterministic model forecasting can be accomplished to 1.5 months with the current GCM, it appears necessary and desirable to formulate the multiple regression forecast scheme at the range of 1 month to 1 year.

Accomplishments of this contract research are detailed in 4. Technical Details of Accomplished Results.

2.   RECOMMENDATIONS

It has long been stipulated that SSTs may affect the formation of blocking. It has been shown in this contract research that SSTs are an essential forcing function for blocking development. Blocking is the persistent feature in the global circulation which can be tagged as the basic

3

circulation pattern to be forecasted in the long-range. Other features of the general circulation may be considered in reference to the predicted blocking occurrence.

This contract research specifically revealed that there is a significant predictability of blocking if the SST component of the global circulation is properly prescribed. In the model forecast, it should mean the development of the joint ocean-atmosphere model. We have indicated that at least a 1.5 month, and possibly longer, forecast is feasible with GCMs. For the seasonal-range forecast up to 1 year, which is not in the immediate reach of the GCM forecast, a development of the empirical regression scheme should be considered. The results obtained in this study offer useful information for further diagnosis of the SST and circulation field, which will be vital in the joint development of ocean-atmosphere model forecasting and empirical-regression forecasting.

3. **PAPERS UNDER THE CONTRACT (Refereed Publications)**

Kung, E.C., W. Min, J. Susskind and C.-K. Park, 1992: An analysis of simulated summer blocking episodes. *Quart. Jour. Roy. Meteor. Soc.*, 118, 351-363.

Kung, E.C., J.-G. Chern, J. Susskind, and M.-S. Lin, 1992: Long-range forecasting of the Northern Hemisphere circulation with numerical-dynamical and empirical-regression models. *Trends in Atmos. Sci.*, 1, 189-216.

Kung, E.C., J. Susskind, and C.C. DaCamara, 1993: Prominent Northern Hemisphere winter blocking episodes and associated anomaly fields of sea surface temperatures. *Terr. Atmos. Ocea. Sci.*, 4, 273-291.

Kung, E.C., J.-G. Chern, and J. Susskind, 1994: Large-scale modes of variations in the global sea surface temperatures and Northern Hemisphere tropospheric circulation. *Atmosfera*, 7. (In Press)

4. <u>TECHNICAL DETAILS OF ACCOMPLISHED RESULTS</u>

Technical details of accomplished results are presented in the following form of publication reprints for 4.1, 4.2, and 4.3, and in prepublication form for 4.4.

4.1 An analysis of simulated summer blocking episodes

By ERNEST C. KUNG and WEI MIN

Department of Atmospheric Science, University of Missouri-Columbia, Columbia, Missouri 65211

and

JOEL SUSSKIND and CHUNG-KYU PARK*

Laboratory for Atmospheres, Goddard Space Flight Center/NASA, Greenbelt, Maryland 20771

SUMMARY

Using the high-resolution 2 × 2.5 degree version of the Goddard Laboratory for Atmospheres general circulation model, experiments were performed for a 46-day summer period from 1 July to 15 August 1979. During the simulation, sea-surface-temperature (s.s.t.) anomalies were updated daily with observed s.s.t.s to provide a realistic surface heating field. A parallel control run used climatology s.s.t.s. in lieu of observed s.s.t.s.

Both the s.s.t. updating experiment and control run were able to simulate the persistent blocking patterns in Eurasia and the eastern Pacific during July. However, only the s.s.t. updating experiment was able to generate the realistic blocking episodes in the last 10-day period during the 46-day simulation. Forecast skill was examined in terms of 500 mb anomaly correlation and error kinetic energy. When the blocking patterns develop or become reinforced, a high forecast skill is apparent in nearly half of the northern hemisphere including the area of blocking and its downstream region. Unlike the major winter blockings, which may be treated as the manifestation of wave number one and two, the summer blockings are localized, and have a smaller scale than that of winter blockings. However, summer blockings treated in this study are persistent, and possess a considerable predictability.

1. INTRODUCTION

In a preceding paper Kung *et al.* (1990) reported that simulation experiments, using the high-resolution Goddard Laboratory for Atmospheres (GLA) general circulation model (GCM) with a realistic sea-surface-temperature (s.s.t.) field, were able to generate two successive major blocking events over the northern hemisphere Pacific and Atlantic oceans during January 1979. It was suggested that the development of the second blocking episode over the Atlantic toward the end of the month was due to the realistic heating field that provided an adequate baroclinic energy source for wave–wave kinetic-energy transfer, whereas adequate baroclinic energy existed within the initial data for the development of the Pacific blocking immediately following the initialization of the GCM. The formation of realistic blocking during the month was associated with the improved forecast skill of the ultralong waves.

In the simulation experiments the ocean surface heating field was provided with daily updating of observed s.s.t.s (the procedure was developed by the third and fourth authors of this paper). One view on this series of experiments is that what was being tested is the upper limit of what would be possible with a coupled ocean–atmosphere model, since updating the observed s.s.t.s during the atmospheric-model integration may imply a correct ocean-model integration. Despite the encouraging results, however, a number of important questions were left unanswered in the preceding study. Only one initial state was involved in the experiments, and as such, the results cannot be generalized. The effects of uncertainties in initial conditions and the dependence of simulations on the initial regime of flow must be considered (see Palmer 1988; Tracton *et al.* 1989; Tribbia and Baumhefner 1988). Although the improved blocking simulation resulted from the use of a realistic s.s.t. field, it was not determined whether this was due to the

---

* Affiliated with General Sciences Corporation, Laurel, Maryland.

improved initial s.s.t. field or the realistic time variations of s.s.t.s during the simulation. The skill of blocking simulations in the northern hemisphere winter is often a major concern in medium-range forecasting, and it is of interest to investigate the simulation of summer blocking episodes in similar GCM integrations.

In the subsequent study two simulations during the summer of 1979 were performed. Using an identical high-resolution version of the GLA GCM with the GLA initial data set for 0000 GMT 1 July 1979, a model integration was carried out for the period 1 July–15 August 1979. The s.s.t. anomalies were updated daily with observations in the same manner as in the preceding winter simulations. A parallel control run was performed in the same way, except that the s.s.t. climatology for the simulation period was utilized in lieu of observed s.s.t.s. Both the simulation with updated s.s.t.s and the control run are compared with observations. Blocking episodes and their patterns in the northern hemisphere are identified. The forecast skill is examined in terms of anomaly correlation and error kinetic energy at the 500 mb level. Considerable forecast skill is achieved in the summer simulation in association with blocking development and maintenance. Effects of s.s.t. updating on the simulation are studied with the time variation of s.s.t. anomalies during the period.

2. SIMULATION EXPERIMENTS

Two 46-day simulations were performed using the 2 × 2.5 degree version of the GLA GCM for the period 1 July–15 August 1979. The GCM was the same high-resolution version as employed in Kung et al. (1990). The GLA fourth-order global atmospheric model is described in Kalnay-Rivas et al. (1977) and Kalnay et al. (1983). The high-resolution version is identical to the original coarse-resolution version with respect to physical parametrizations. The model was initialized with the GLA gridded analyses of the First GARP (Global Atmospheric Research Program) Global Experiment (FGGE) for 0000 GMT 1 July 1979.

A blended global monthly s.s.t. analysis at the GLA based on *in situ* (ship and buoy) and satellite-retrieved data by the third and fourth authors of this paper was described in Kung et al. (1990) and detailed in Susskind et al. (1984) and Susskind and Reuter (1985). For the GCM experiment, daily gridded s.s.t. fields were obtained by linear interpolation of the blended monthly fields, assuming that the observed monthly means are located in the middle of each month. The interpolation in this manner is valid because of the smallness and slowness of the time variation in s.s.t.s. The GCM simulation of the global atmosphere, with the s.s.t.s updated during the model integration using this set of daily fields, is referred to as the 'experiment' in this paper to contrast with the parallel control run and observed atmosphere. Daily s.s.t. fields obtained by the interpolation of monthly climatological s.s.t.s (Reynolds 1982) were utilized in the control run of the simulation. The Geophysical Fluid Dynamics Laboratory analyses of the FGGE observations during the simulation period were used to describe the observed circulation. The simulation and observation fields analysed in this study include twice-daily values of the circulation fields at 0000 and 1200 GMT.

3. OBSERVED SEA-SURFACE-TEMPERATURE ANOMALIES AND BLOCKING EPISODES

Observed anomaly patterns of blended s.s.t.s from 30°S to 60°N are illustrated in Fig. 1 with four selected 5-day period averages during the simulation. The National
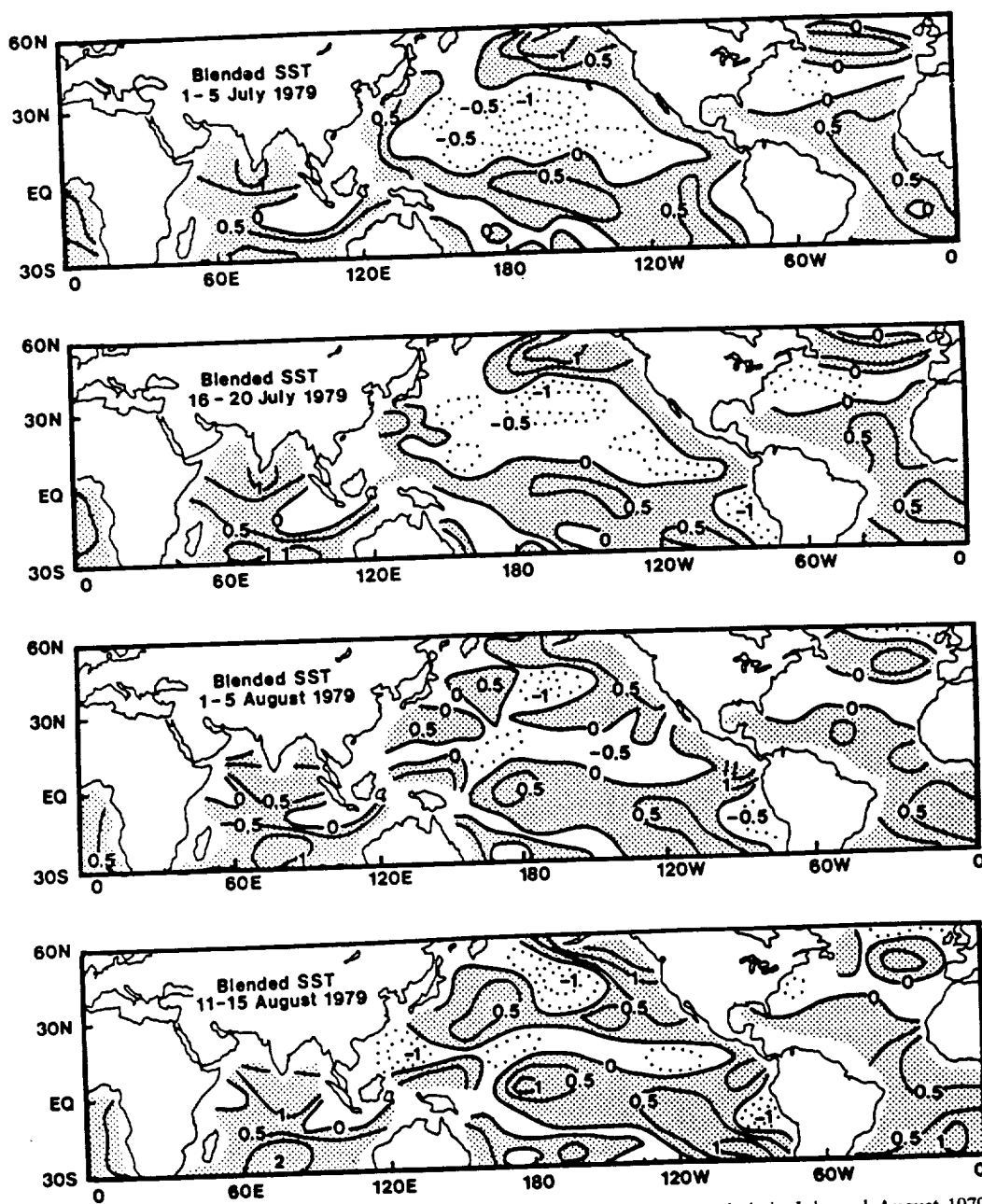
Figure 1. Blended sea-surface-temperature anomalies during four 5-day periods in July and August 1979. Contour interval is 0.5 degC. Positive anomalies are shaded.

Meteorological Center (NMC) s.s.t. climatology (Reynolds 1982) was used to compute anomalies. The patterns south of 30°S are excluded from the figure, because the climatological anomaly in this region may not be reliable (Reynolds 1983) and in any case the effect of s.s.t. anomalies south of this latitude is not expected to be as direct as that of the illustrated region. The four periods are chosen to be roughly 10-days apart to describe the s.s.t. variations during the simulation period. Since the daily fields are

8

obtained by linear interpolation of the monthly fields, an inherent smoothing of the fields may obscure time variations of s.s.t.s. However, it may be suggested that the anomaly pattern during July is stable, and its time change very gradual. The pattern is characterized in the northern hemisphere by a large area of negative anomaly in the mid Pacific with positive anomalies to the north and south. The negative anomaly area in the mid Atlantic is small, and positive areas to the north and south dominate the Atlantic. Despite the possible oversmoothing of the s.s.t. variations, there are noticeable changes from the July to August pattern. In August the large negative area in the mid Pacific becomes small and fragmental, and the positive areas are enlarged and strengthened. In the Atlantic the negative and positive areas are both weakened in August.

Distinct blocking episodes during the simulation period are identified in Eurasia and the eastern Pacific with the observed northern hemisphere circulation. They are listed in Table 1 for the identified periods, the subperiods of reinforcement, and the primary longitudinal locations in the 46–66°N belt. The observed blocking episodes are compared

TABLE 1. OBSERVED BLOCKING EPISODES DURING THE SIMULATION PERIOD
1 JULY–15 AUGUST 1979

Period	Subperiod	Primary location (46–66°N)
Eurasia:		
1–6 July		(90–120°E)
6–26 July	6–10 July	(10–90°E)
	11–15 July	(10–90°E)
	16–20 July	(30–100°E)
	21–26 July	(75–140°E)
31 July–4 August		(90–130°E)
8–13 August		(0–40°E)
10–15 August		(75–120°E)
Eastern Pacific:		
3–6 July		(150–90°W)
13–17 July		(140–100°W)
24 July–15 August	24–28 July	(150–110°W)
	29 July–1 August	(150–110°W)
	2–4 August	(150–110°W)
	5–9 August	(150–120°W)
	10–14 August	

with the blocking occurrences identified in the experiment and control run in the longitude–time diagrams of Fig. 2. Because of the localized pattern of summer blocking, identification of blocking is done manually through observation of daily 500 mb geopotential fields (see Kung and Baker 1986) rather than using an objective scheme such as performed by Kung et al. (1990). Figure 3 further illustrates the observed and simulated 500 mb circulation patterns during four selected 5-day periods when blockings occurred. Unlike the major winter blockings over the Pacific and Atlantic, which are the manifestations of zonal wave number $n = 1$ or 2 (see Kung et al. 1990), the summer blockings are more localized and have a smaller scale. This makes identification of summer blocking in the zonal wave-number domain difficult. Despite the smallness of the spatial scale, however, the periods of the blocking episodes are not necessarily shorter than those of winter blocking (see Kung and Baker 1986; Kung et al. 1990). As listed in Table 1, and shown in Fig. 2, summer blockings in the Eurasian and Pacific regions are persistent and
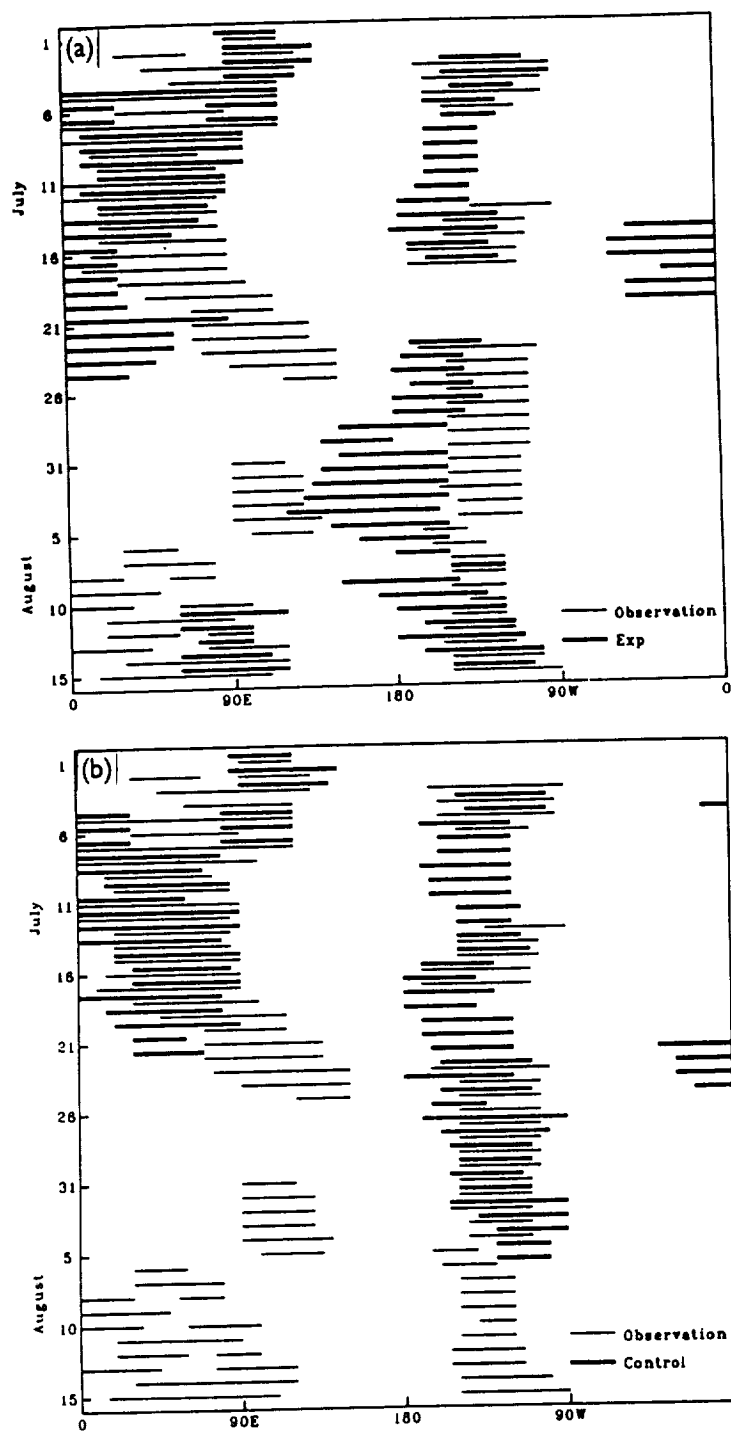
Figure 2.   Longitude–time diagram of significant ridges in the 46–66°N band of the observed and simulated circulation during the simulation period with (a) the experimental run (Exp) and (b) the control run.
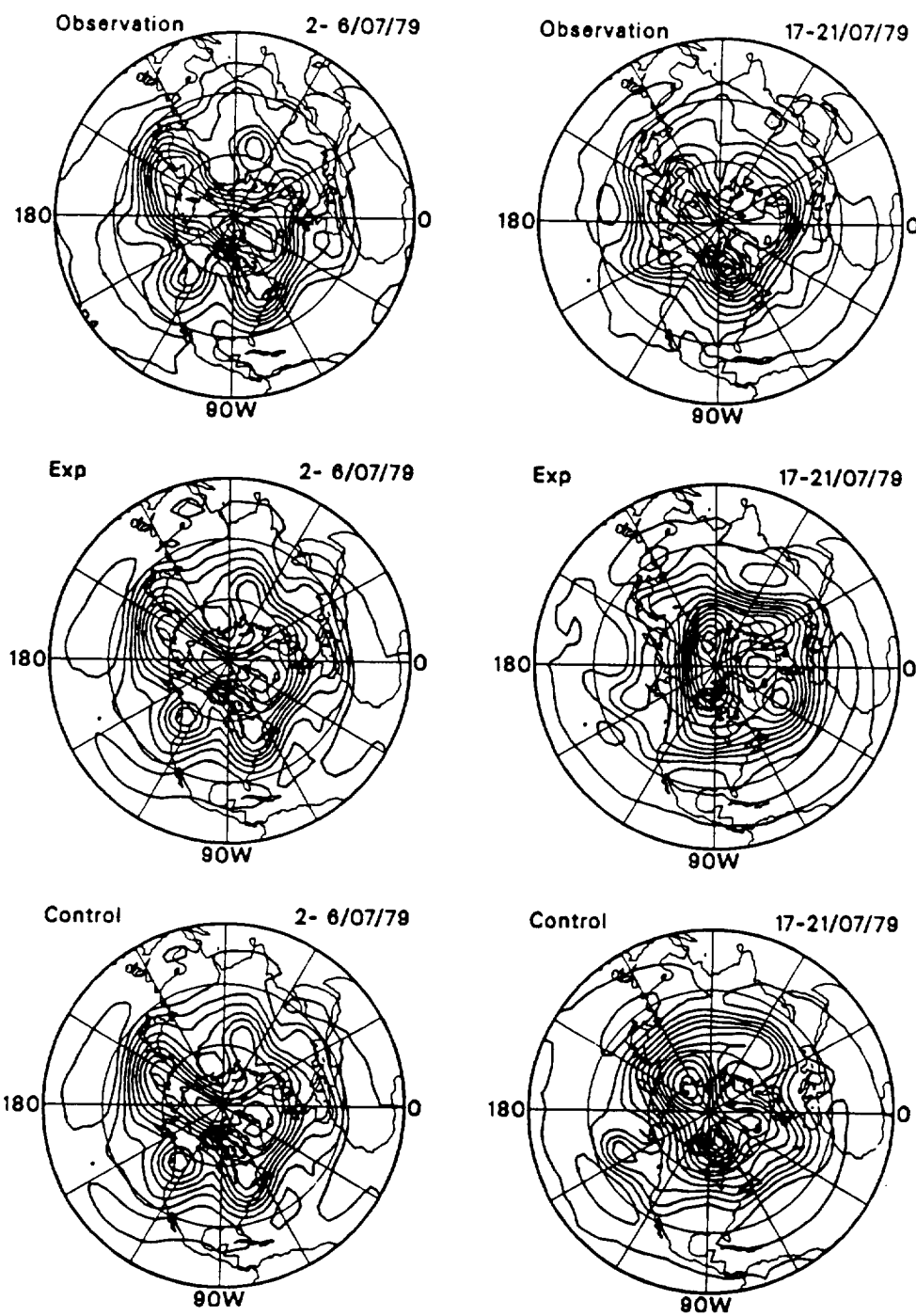
Figure 3.   Observed and simulated 500 mb circulation during four 5-day periods in July and August 1979.
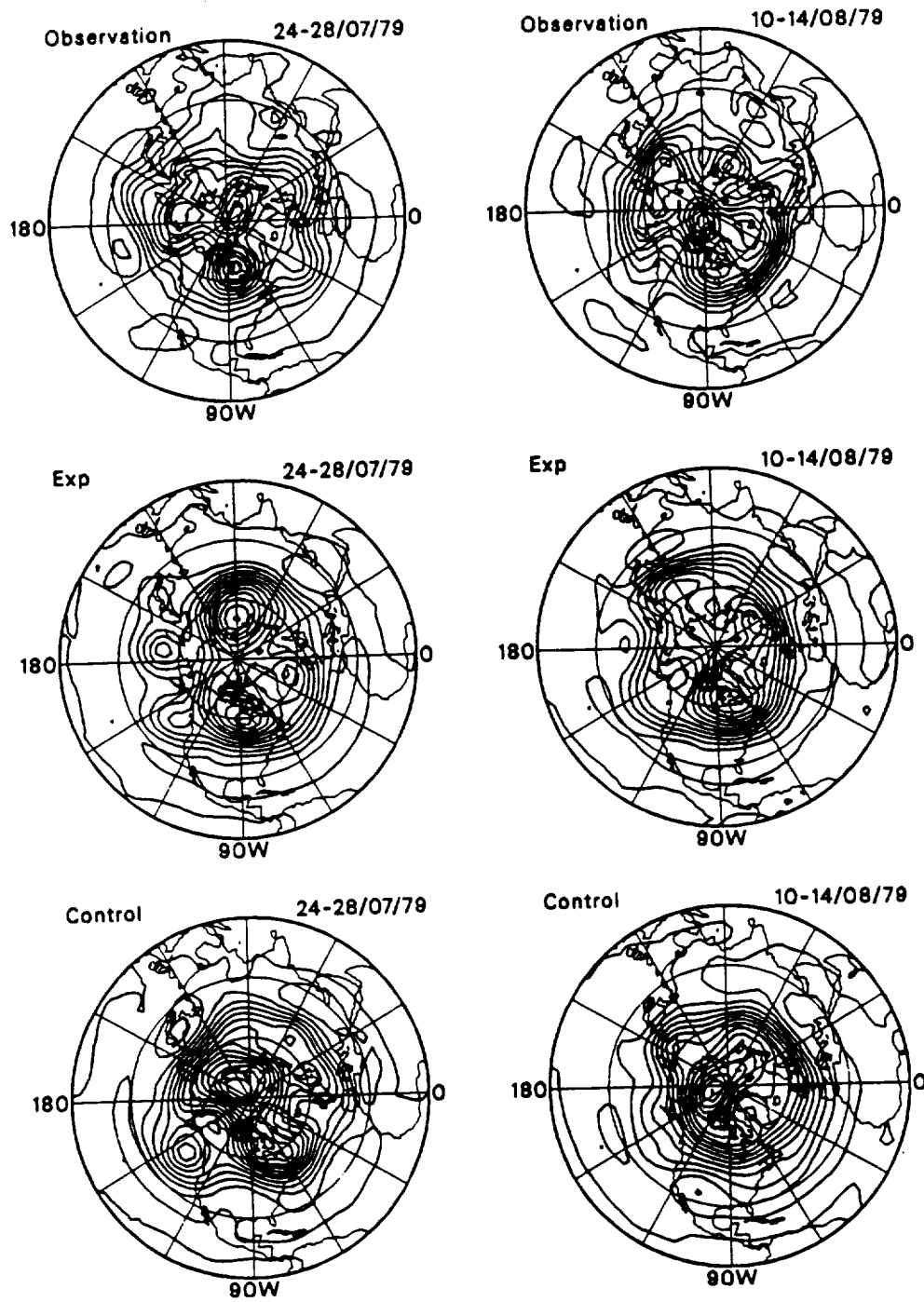
Observation 24-28/07/79

Observation 10-14/08/79

180

0

90W

Exp 24-28/07/79

Exp 10-14/08/79

180

0

90W

Control 24-28/07/79

Control 10-14/08/79

180

0

90W

Figure 3. Continued.

continually reinforced in the same general regions with only a slight shift in location. For instance, in the eastern Pacific from 23 July to 15 August, despite a small movement of the block and some weakening and revival of the system, there is, essentially, one persistent system during the later period of the simulation.

4. FORECAST SKILL

The forecast skill of the 46-day summer simulations for the experiment and control are shown in Fig. 4 for the north Pacific sector (30–86°N, 120°E–120°W) and the north Atlantic sector (30–86°N, 120–5°W) in terms of anomaly correlations of the 500 mb
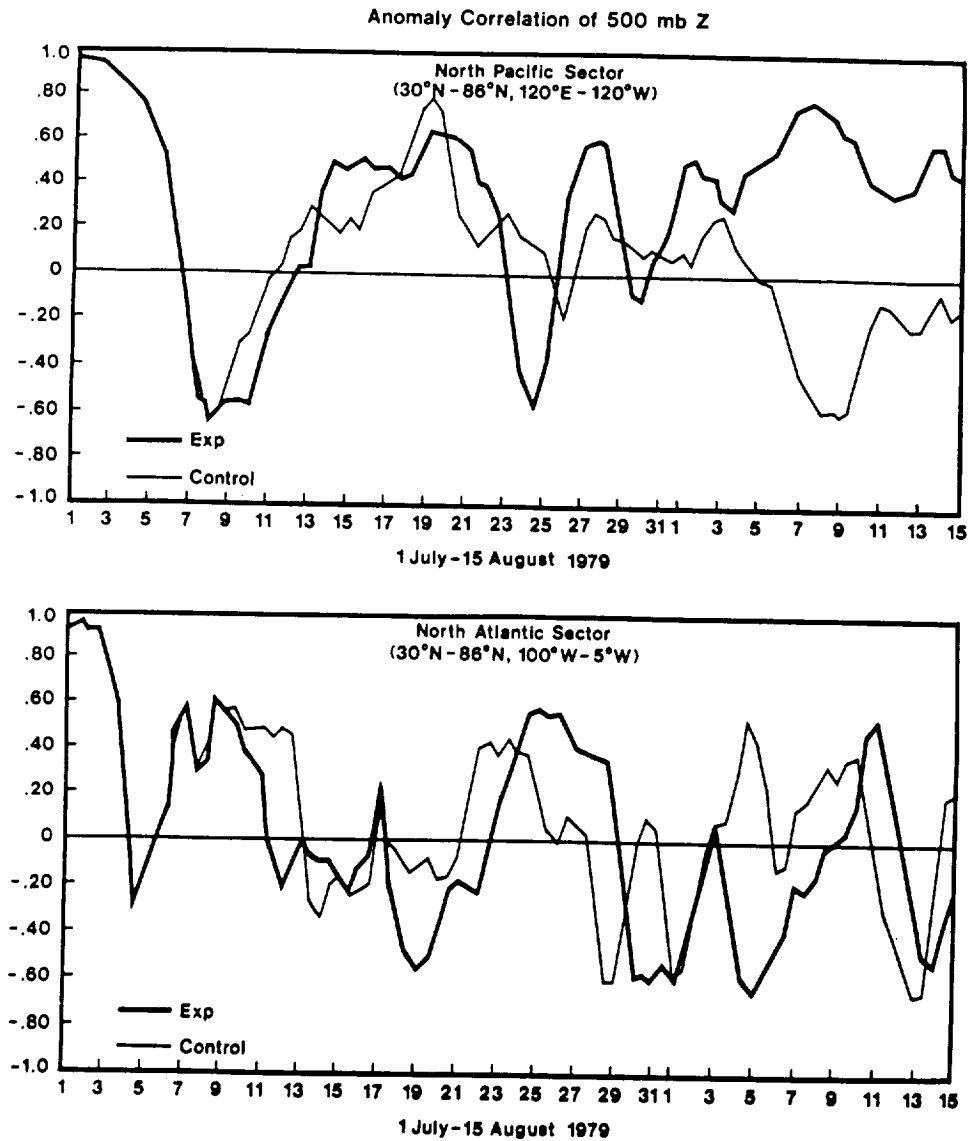

Figure 4. Anomaly correlations of the 500 mb geopotential-height field in the north Pacific and Atlantic sectors during the simulation.

13

geopotential-height field. The sectors are identical to those used in a preceding study (Kung *et al.* 1990) for the winter 30-day simulations. Both the experiment and control indicate a considerable predictability of the 500 mb pattern during early and late July in the Atlantic sector, and in mid July in the Pacific sector, when the blocking patterns are realistically simulated in respective sectors. For the last 10 days of simulation in early August, the experiment with the updated s.s.t. fields shows a very high forecast skill in the Pacific sector, whereas the forecast skill is lost in the control with climatology s.s.t.s. It is noted in Figs. 2 and 3 that the control fails to produce the persistent Pacific blocking during this period. As shown in Fig. 1, from late July to August there are changes to the s.s.t. anomaly patterns, whereas the patterns show very little change in July. The experiment updated with observed s.s.t.s during the simulation is apparently able to maintain a high forecast skill in the later stage of the 46-day simulation when the realistic eastern Pacific blocking is generated. However, the control run without the benefit of updating with observed s.s.t.s collapses, as shown by the 10–14 August control patterns (Fig. 3). It is noteworthy that, when a realistic blocking is simulated, a high forecast skill is obtained in the sector where the blockings develop, and this fact is consistent with the winter simulations as reported previously (Kung *et al.* 1990).

As the experiment and control show a striking difference in the last period of the simulation, it will be worthwhile to examine the forecast skill of this period for smaller regions. Figure 5 illustrates the 500 mb anomaly correlation in four longitudinal sectors of the northern hemisphere (30–120°E, 90°E–180°, 180–90°W and 90–40°W) from 30 to
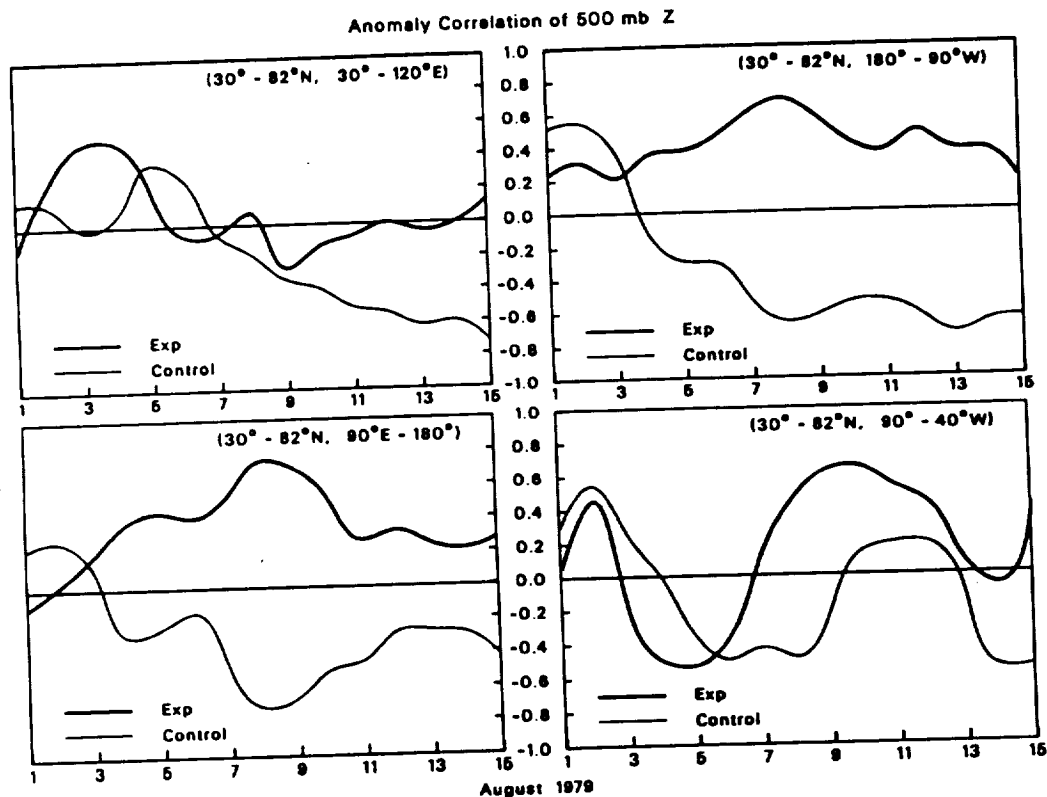

Figure 5.   Anomaly correlation of the 500 mb geopotential height in four longitudinal sectors during the last 15 days of simulation.

82°N during the last 15 days of the 46-day simulation. The high forecast skill of the experiment is most clearly observed in sectors 180–90°W and 90°E–180°. For the 180–90°W sector, we may note that the persistent summer blocking in the eastern Pacific and western North America is realistically simulated in the experiment. Some skill is also apparent in the 90–40°W sector when North America is under the influence of the Pacific blocking. In reference to the high forecast skill in the sector of 90°E–180°, it is noted that the experiment also simulated the Eurasian blocking during this period.

From Figs. 4 and 5 it is seen that the high forecast skill is associated with realistic simulation of blocking. This is also the case for the winter simulation in which the high skill in the northern hemisphere is due to the high forecast skill of planetary waves $n = 1$ and 2 (Kung et al. 1990). In the case of the summer simulation, however, the blocking episodes are localized and the association of blocking simulation and forecast skill should be sought in a smaller-scale range than that of the major winter blocking. Figure 6 compares the error kinetic energy of long waves $n = 1–7$ in simulations and persistence. The error kinetic energy is defined as the mean-square error of the simulated 500 mb wind from the observed wind or, in the case of persistence errors, by the mean-square difference between the initial and observed wind. For $n = 1–4$ the error kinetic energy of simulations is generally larger than that of persistence, implying that there is no appreciable forecast skill of long waves in the summer simulation. However, the error kinetic energy of the experiment and control, particularly that of the experiment, becomes smaller than that of persistence for $n = 5$, 6 and 7 but becomes large again for shorter wave numbers to be comparable with that of persistence. It appears that the scale range of summer blocking occurrences contribute to the forecast skill of the summer simulations.

Since the appearance of summer blocking is localized, the small error kinetic energy of the mid and short waves in the simulation should be related to the blocked area. The local error kinetic energy in six longitudinal strips (30–120°E, 120°E–180°, 180–90°W, 90–40°W, 40°W–0° and 0–30°E) in the latitudinal band of 30–82°N is shown in Fig. 7. Examination of Fig. 7, with respect to the times and locations of simulated blockings (Figs. 2 and 3), indicates that the small error kinetic energy (i.e. the high forecast skill) of the simulations is found in the regions of confluence in the downstream of realistically simulated blockings. The relatively low forecast skill in the blocked area is caused by a slight shift of the simulated blocking in areas of low error kinetic energy, although a realistic simulation of blocking has been achieved in an overall sense. By combining longitudes of the downstream area and the blocked area, a realistic simulation of summer blocking, such as the August eastern Pacific blocking, implies a high forecast skill over nearly half of the northern hemisphere in the mid and high latitudes.

5. Concluding Remarks

The summer simulation experiment using the high-resolution GLA GCM with realistic ocean surface temperatures was able to generate persistent blocking events in Eurasia and the eastern Pacific during the 46-day period from 1 July to 15 August 1979. The generation of summer blocking episodes appears, at least in part, to be due to the heating at the surface boundary over both the oceanic and continental areas. The control run with the s.s.t. climatology failed to produce such blockings in the later portion of the simulation. It is shown that there is considerable forecast skill in the area of the blocking circulations, particularly in the confluence area downstream. It appears that, with the updated s.s.t.s, the simulation of realistic summer blocking episodes in the northern hemisphere seems possible, at least for a one-and-a-half month period, with a
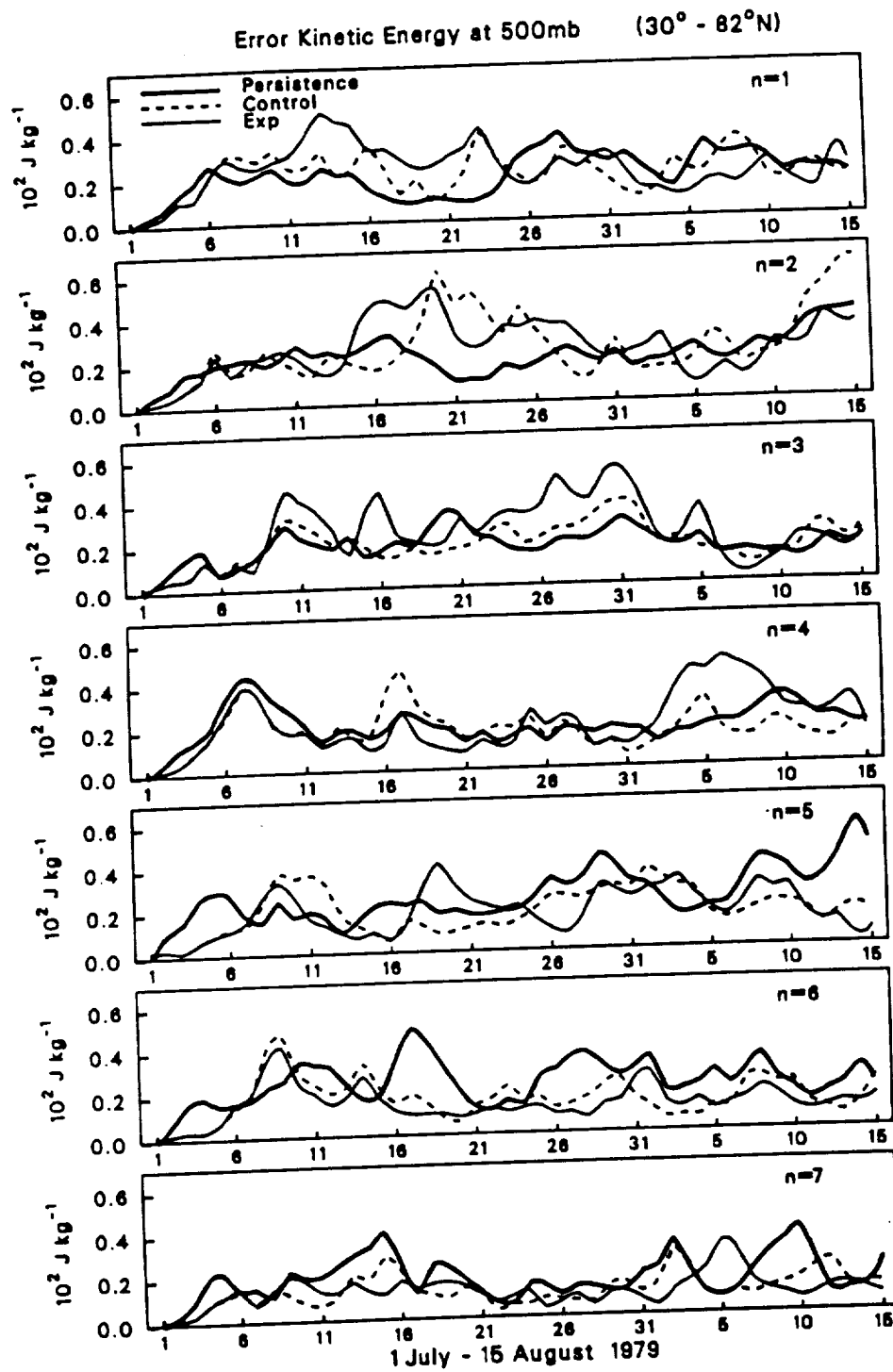
15

Figure 6. The 500 mb error kinetic energy for wave number $n = 1$–7 during the simulation period for persistence and the control and experimental runs.
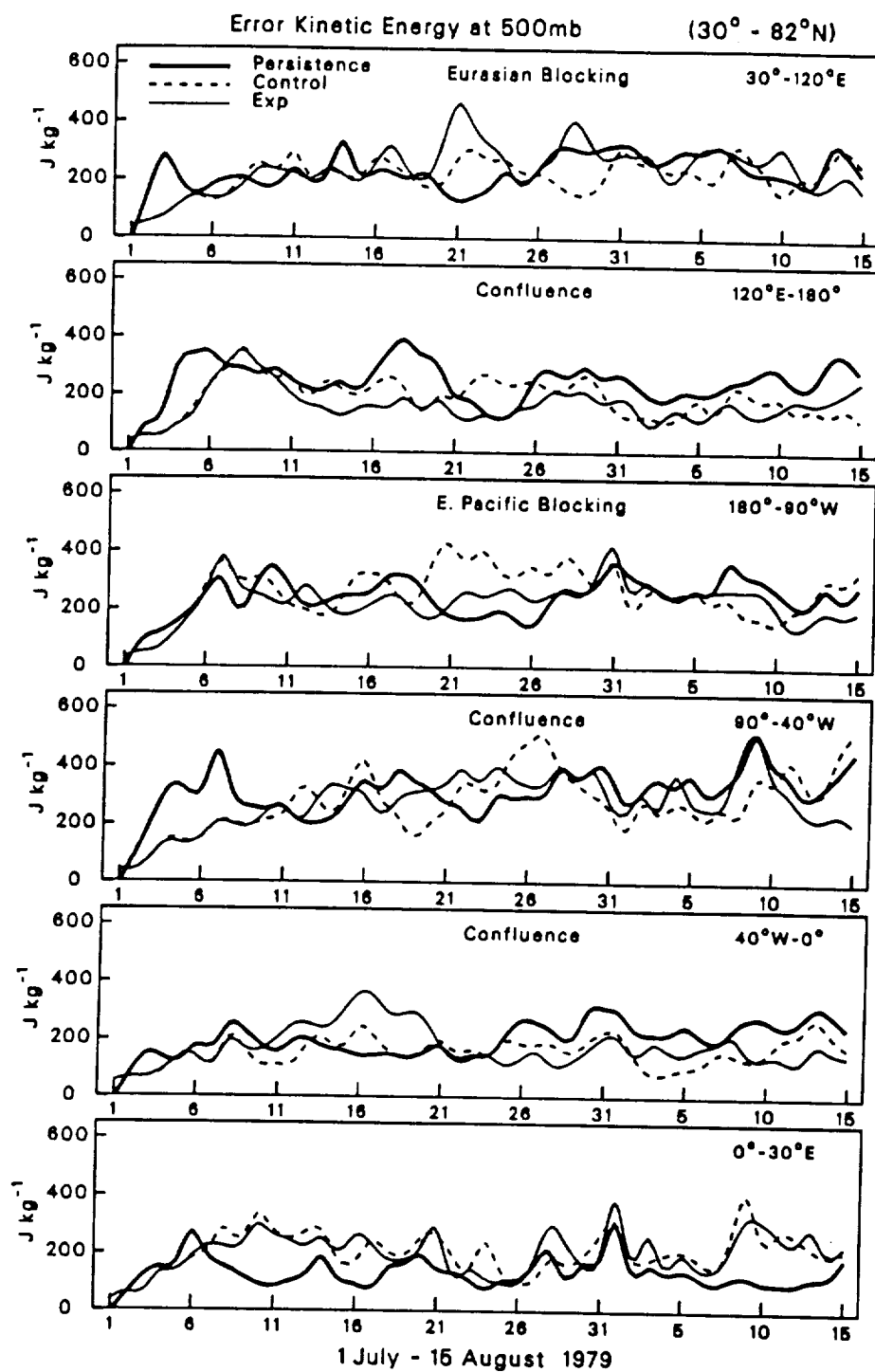
16

Figure 7.　The 500 mb local error kinetic energy in six longitudinal sectors for persistence and the control and experimental runs.

17

high forecast skill when the blocking pattern develops or is reinforced. Simulation beyond this period has not yet been attempted.

We assume that the skillful predictions of blocking episodes during July in both the experiment and control may have been helped by the improved initial data, implying that initial conditions include proper energy sources available. Nevertheless, this experiment involved only one initial state, and the results should not be generalized. As shown in Palmer's (1988) study, the variability in prediction skill is strongly related to fluctuations in the Pacific/North American mode of frequency variability. The generality of the reported simulation and the energetics of processes involved in blocking simulation are being investigated in a continuation of the study, and will be reported in future articles.

REFERENCES

Kalnay, E., Balgovind, R., Chao, W., Edelmann, D., Pfaendtner, J., Takacs, L. and Takano, K.   1983   'Documentation of the GLAS fourth-order general circulation model.' NASA Tech. Memo 86064. (NTIS N8424028)

Kalnay-Rivas, E., Bayliss, A. and Storch, J.   1977   The fourth-order GISS model of the global atmosphere. *Beitr. Phys. Atmos.*, **50**, 299–311

Kung, E. C. and Baker, W. E.   1986   Spectral energetics of the observed and simulated northern hemisphere general circulation during blocking periods. *J. Atmos. Sci.*, **43**, 2792–2812

Kung, E. C., DaCamara, C. C., Baker, W. E., Susskind, J., Park, C.-K.   1990   Simulation of winter blocking episodes using observed sea surface temperatures. *Q. J. R. Meteorol. Soc.*, **116**, 1053–1070

Palmer, T. N.   1988   Medium and extended range predictability and stability of the Pacific/North American mode. *Q. J. R. Meteorol. Soc.*, **114**, 691–713

Reynolds, R. W.   1982   'A monthly averaged climatology of sea surface temperatures.' NOAA Tech. Report NWS 31 (Available from NOAA, National Meteorological Center, Washington, D.C.)

                              1983   A comparison of sea surface temperature climatologies. *J. Climatol. Appl. Meteorol.*, **22**, 447–459

Susskind, J. and Reuter, D.   1985   Retrieval of sea surface temperature from HIRS/MSU. *J. Geophys. Res.*, **90**, 11602–11608

Susskind, J., Rosenfield, J., Reuter, D. and Chahine, M. T.   1984   Remote sensing of weather and climate parameters from HIRS/MSU on TIROS-N. *J. Geophys. Res.*, **89**, 4677–4697

Tracton, M. S., Mo, K., Chen, W., Kalnay, E., Kistler, R. and White, G.   1989   Dynamical Extended Range Forecasting (DERF) at the National Meteorological Center. *Mon. Weather Rev.*, **117**, 1604–1635

Tribbia, J. J. and Baumhefner, D. P.   1988   The reliability of improvements in deterministic short-range forecasts in the presence of initial state and modelling deficiencies. *Mon. Weather Rev.*, **116**, 2276–2288

18

4.2 Long-range forecasting of the northern hemisphere circulation with numerical-dynamical and empirical-regression models

Ernest C. Kung, Jonq-Gong Chern, Joel Susskind* and Ming-Sen Lin**

Univ. of Missouri-Columbia, Columbia, Missouri 65211, USA *Laboratory for Atmospheres Goddard Space Flight Center/NASA, Greenbelt Maryland 20771, USA, ** Central Weather Bureau Taipei Taiwan R.O.C.

ABSTRACT

It has been established that blocking episodes often dominate the hemispherical winter circulation and local summer circulation of the northern hemisphere. A high forecast skill of the general circulation model (GCM) is recognized with the development of blocking. The major winter blockings are formed through constructive interference of traveling wave $n=1$ and stationary wave $n=2$. The former is controlled by barotropic wave-wave interaction and the latter by in situ warming over the Pacific and Atlantic. A comprehensive examination of extended range forecasting with the Goddard Laboratory for Atmospheres GCMs is offered with 31-day simulations of winter blockings and 46-day simulations of summer blocking. The importance of realistic sea surface temperatures (SSTs) in blocking simulation is revealed with the daily updating of observed SSTs during the GCM simulations.

The empirical long-range forecasting scheme at the range of 1 month to 1 year is formulated with multiple regressions for various northern hemisphere phenomena and monthly-seasonal values of temperature and precipitation. A critical examination of the forecasting experiments is offered. The forecasting of Mei-Yu in Taiwan indicates that large-scale global teleconnections can be used for long-range forecasting of regional variables with certain modifications.

1. INTRODUCTION

It is becoming increasingly clear that the development of numerical forecasting at the range of 1 month to 1 year requires the major task of constructing coupled ocean-atmosphere models. For this purpose, basic studies are imperative to obtain pertinent information on the predictability of the atmospheric general circulation model (GCM) and the role of ocean surface heating in model forecasting. Before the eventual goal of the long-range forecasting capability of the GCM is attained, however, the development of an empirical-regression scheme for practical regional forecasting is

189

19

also desirable. Actually, studies in both areas complement each other for the better physical understanding of the behavior of the atmosphere. The purpose of this paper is to highlight our recent and present effort in these two areas.

In the northern hemisphere, the winter circulation is often dominated by a sequence of blocking episodes associated with the activities of low-frequency planetary waves. The extreme anomalies of summer precipitation are often identified with summer blocking patterns. For the practical importance of the phenomena, as well as the known extended predictability associated with blocking circulation (e.g., Shukla 1981; Holloway and West 1984), we focused our GCM-related study on simulation of blocking. Since the generally preferred locations of the northern hemisphere winter blocking (i.e., the North Pacific and Atlantic) are decided by the land-sea contrast and topography, it may be postulated that interannual variations of blocking patterns are mainly controlled by sea surface temperatures (SSTs) through heat release in the ocean-atmosphere interaction. Further, the response of the GCM to SST anomalies in blocking simulation may generate pertinent information for the development of the joint ocean-atmosphere model. In Section 2 of this article, the analysis of winter blocking circulation is presented in the zonal wavenumber domain in reference to prevailing SST anomalies. Sections 3 and 4 discuss the long-range simulation of winter and summer blocking episodes with the GCM in reference to initial data and SST anomaly field.

The empirical-regression approach on the basis of teleconnection is presented in Section 5. The quantities experimented in forecasting include the Indian summer monsoon, and monthly temperature and precipitation in the middle latitude locations. Currently a forecasting experiment of the Southeastern Asian monsoon (Mei-Yu), in Taiwan, is in progress. Special problems associated with regional scale long-range forecasting, such as for Taiwan Mei-Yu, are presented for examination.

2. BLOCKING CIRCULATION IN THE WAVENUMBER DOMAIN

Early in the study of the general circulation, Saltzman (1959) proposed that large-scale quasi-stationary flow systems are maintained by a non-linear barotropic transfer of kinetic energy from smaller cyclone-scale disturbances which have baroclinic energy sources. More recently, diagnostic studies (e.g. Murakami and Tomatsu 1965, Paulin 1970) identified blocking phenomena with large-scale baroclinic conversion. However, Hansen and Sutera (1984), by contrasting the blocking and non-blocking periods, reported the significance of nonlinear wave-wave interactions to support the kinetic energy of blockings. Egger et al. (1986) pointed out that the traveling weather system interacts with the block. Hansen and Chen (1982), in studying a case of Atlantic blocking, found that this block was forced by the nonlinear interaction of intense baroclinic synoptic-scale waves with barotropic ultralong waves.

In our early study (Kung and Baker 1986), the spectral energetics of the northern hemisphere

circulation during winter of the First GARP (Global Atmospheric Research Program) Global Experiment (FGGE) year was investigated with gridded analyses of observational data and parallel simulation experiments. The gridded analyses and simulation experiments utilized NASA Goddard Laboratory for Atmospheres (GLA) 4°latitude x 5°longitude coarse resolution model (see Kalnay et al. 1983) with climatological SSTs. The study has shown that the characteristic energetics features associated with the blocking situations in the northern hemisphere can be described in terms of the barotropic nonlinear wave-wave interaction $L(n)$ and baroclinic conversion $C(n)$ where n is the zonal wavenumber. The pronounced single winter blocking is developed and maintained by $L(1)$ from the kinetic energy source in n=3-10. In the case of the double blocking, both $L(1)$ and $L(2)$ support the development of blocking with $L(2)$ as the largest source. The source of kinetic energy at n=3-10 is maintained by the abundant baroclinic conversion $C(n)$ from the available potential energy in this spectral range.

A general description of energy transfer in the general circulation for blocking development is reported by Tanaka and Kung (1988) on three-dimensional normal mode functions. Figure 1 shows the temporal variations of barotropic (m=0 where m is the vertical index) and baroclinic (m=3-10) energies in the zonal mean motion (m=0), ultralong waves (n=1-2) and synoptic waves (n=3-15) over the northern hemisphere during the FGGE winter. The time variation of the zonal baroclinic energy (n=0, m=3-10) indicates clear energy peaks at 16 and 28 December and 9 January
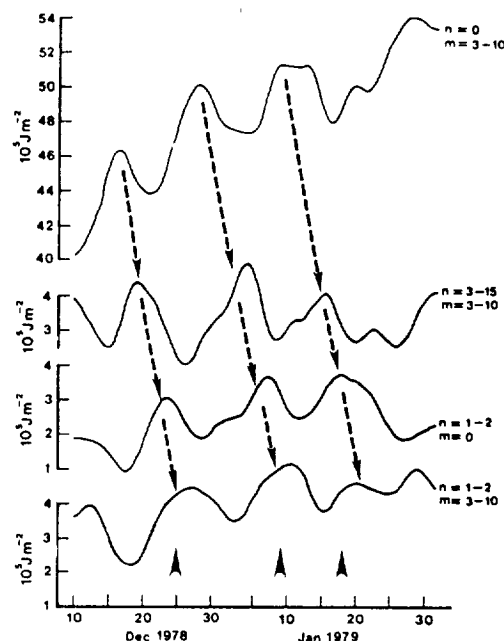

Fig. 1   Time change of barotropic (m-1) and baroclinic (m-3-10) energies for zonal mean motion (n=0), ultralong waves (n=1-2), and synoptic waves (n=3-15) over the northern hemisphere from 10 December 1978 through 31 January 1979. Appearances of typical Rex blockings are marked by arrows over the time axis.   From Tanaka and Kung (1988).

superimposed on the seasonal trend. There are subsequent increases of baroclinic energy of synoptic waves (n=3-15, m=3-10) in the time series through a process of baroclinic instability. The time lag is about 5 days.   The time variation of synoptic-scale barotropic energy

$(n=3-15, m=0)$ is not shown in the figure but it is almost in phase with the baroclinic energy. The barotropic energy of ultralong waves $(n=1-2, m=0)$ increases three days later through the wave-wave interaction of kinetic energy, the process required for amplification of ultralong waves to form the blocking. The peaks of $(n=1-2, m=0)$ are identified with the most intensified pattern of blockings, as marked in the figure. After the full development of the blocking (i.e., after reaching the mature stage of the blocking), the baroclinic energy of ultralong waves peaks. The time series in Fig. 1 further reveals evidence of the upscale energy cascade from synoptic-scale waves to planetary waves. Also, as shown in Kung and Baker (1986), under the developed blocking situation the meridional heat transport increases dramatically, and this apparently leads to the peak of the baroclinic energy of ultralong waves in the mature blocking stage.

Confirming that the blocking can be linked to both baroclinic and barotropic types of wave activities, the monthly circulation patterns of the northern hemisphere winter were analyzed with daily observations of the 500 mb field and monthly sea surface temperature (SST) analyses during 34 winter seasons from 1955 to 1989 by DaCamara et al. (1992). The blocking index I at longitude λ is evaluated by

$$I(\lambda) = Z(\lambda, 62°N) - Z(\lambda, 42°N)$$

where Z is the 500 mb geopotential height. This index was originally introduced by Lejenäs and Økland (1983) and used in Kung et al. (1989, 1990) with modifications. Positive values of I indicate the existence of a quasi-meridional dipole which is formed by a high-pressure cell poleward and a low-pressure area equatorward. The quasi-meridional dipole is a characteristic shared by both diffluent (Rex-type, see Rex 1950) and meridional (Ω-shaped) blockings. Additional scans are also made for cases of tilted orientation of meridional dipoles and cases of blocking partially out of the chosen latitudinal band. Pacific and Atlantic are the two regions of preferred winter blocking activities in the northern hemisphere. The single dominant blockings in the Pacific and Atlantic are identified by PAC and ATL. The concurrent occurrences of blocking in the Pacific and Atlantic during the same general period constitute the double blocking, and are identified by DBL.

Examination of SST anomalies in three subperiods, of approximately ten years, reveals that the anomaly patterns of these subperiods are quite different and can be associated with dominant flow patterns of the subperiods. The SST anomalies during the subperiods are shown in Fig. 2. In the subperiod 1955-1966, ATL and DBL show high frequencies of occurrences, and the Pacific and Atlantic both show generally warm SSTs. The SST pattern of this subperiod may approximate a composite of ATL and DBL types of SST anomalies strongly leaning toward DBL type due to large SST anomalies during DBL. The subperiod 1967-1978, with high frequency of ATL and NBL, shows a general cooling pattern with a moderate intensity, and the pattern should satisfy the SST conditions for ATL and NBL types of flow. The PAC flow has the highest frequency during the subperiod 1979-1989. The strong
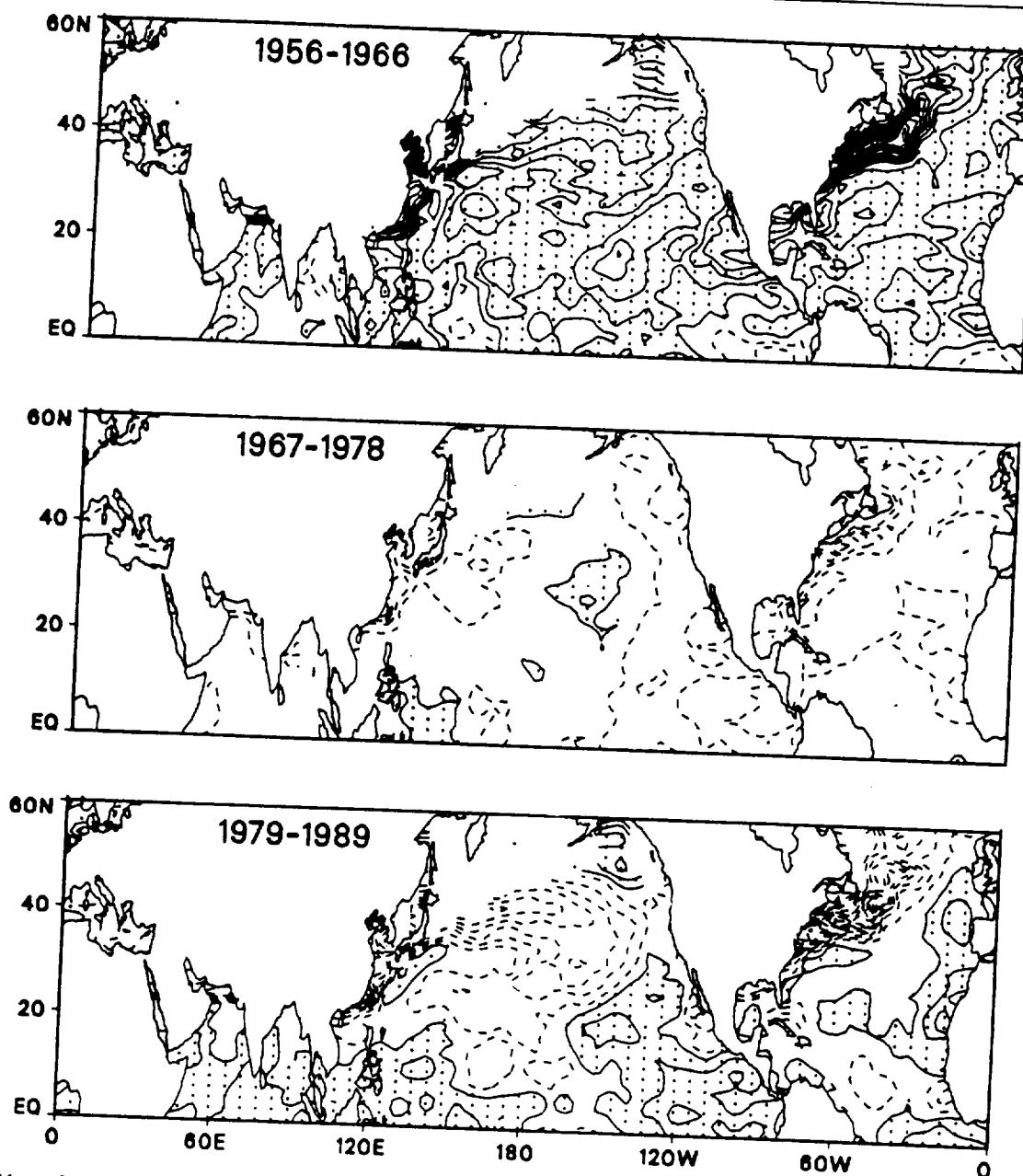
Fig. 2   Anomaly fields of winter SSTs during three subperiods with contour intervals of 0.2°C.   Zero and positive anomalies are indicated by continuous lines, and negative anomalies by broken lines.   Regions of positive anomalies are stippled.   From DaCamara, Kung, Baker, Lee and Corte-Real (1992).

cooling in the north Pacific and northwest Atlantic during this subperiod should approximate that of the PAC category.

To explore the association of winter blocking with SST anomalies in the zonal wavenumber domain, Kung et al. (1992) selected twelve major blocking episodes for examination from the same 1955-1989 period. These episodes include four cases for each category of Pacific (PAC), Atlantic (ATL) and double blocking

(DBL), and manifestations of the blocking flow pattern are examined in terms of the geopotential height and associated anomaly fields at 500 mb. These episodes are chosen for their prominence and persistence but it should be noted that by no means are they special cases. As a matter of fact, the characteristics shown by these episodes are typical of winter months in the northern hemisphere. Of 108 winter months of the 34-year period, we document only 26 months
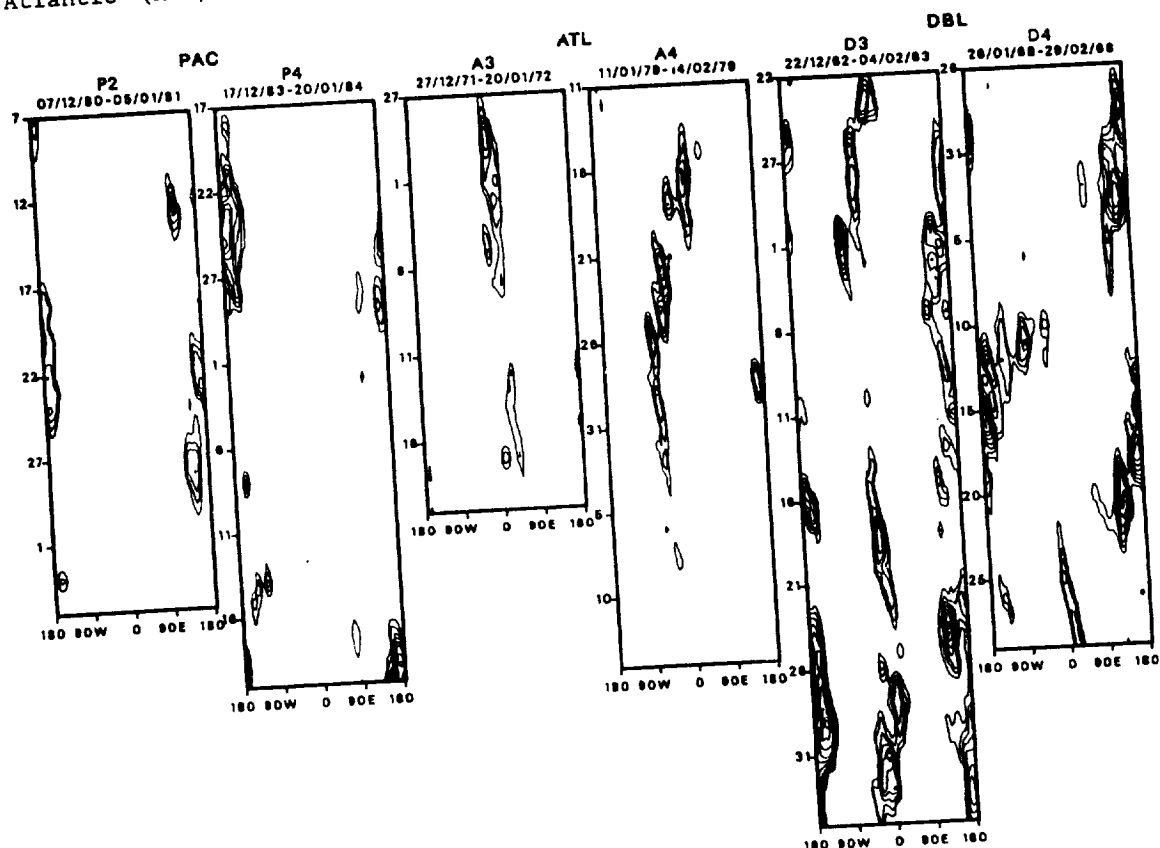

Fig. 3   Time-longitude plots of blocking index for 0 and positive values with contour interval of 50 m. From Kung, DaCamara and Susskind.

without noticeable blocking activities. All other months are under the dominance or influence of one of these three types of blocking. Each episode is a dominant and often recurring circulation pattern during the period. The lengths of the periods identified for these episodes are from 25 days to 45 days. Figure 3 shows the time-longitude plots of the daily blocking index for two episodes in each category. It appears that the double blocking events are more intense and persistent than single blockings. However, the Pacific and Atlantic components of double blocking events are not exactly in phase with certain time lags between maxima in the Pacific and Atlantic. This may suggest involvement of traveling planetary waves. It is interesting to note that the persistent blocking episodes involve the recurrence of blocking patterns in the same general locations during the period of episodes, strongly suggesting the existence of prevailing boundary conditions in terms of SST anomalies that favor the development of blocking.

As the wave-wave interaction of kinetic energy is associated with the amplification of planetary waves, it is pertinent to explore the constructive interference among planetary waves for the development of a major winter blocking. The interference of $n=1$ and 2 is confirmed with all episodes selected in this study. Figure 4 demonstrates, for one episode in each of three blocking categories, the 500 mb trough-ridge diagrams for $n=1$ and 2 in the 54°-70°N band. It is noteworthy that the primary locations of major blocking episodes during the course of blocking development are

the longitudinal segments where $n=1$ and 2 interfere constructively. The positions of $n=2$ maximum amplitude stay approximately the same in the general area of 0° and 180° throughout the winter, although the strength of the wave is subject to time variation. On the contrary, the phase angle and amplitude of $n=1$ are both variable, showing that $n=1$ travels slowly around the northern hemisphere. When the traveling $n=1$ constructively interferes with the stationary $n=2$, the major blocking develops. If $n=1$ is relatively weak and $n=2$ is strong, $n=2$ is responsible for creating the double blocking pattern. This is the case of DBL shown in Fig. 4. It is also noteworthy that weakening and redeveloping blocking in the same blocking episodes correspond well with the periodic weakening and amplifying of $n=1$ and 2.

Anomalies of 500 mb Z and SST are averaged for four episodes in each blocking category, and shown in Fig. 5 for the area between 20° and 60°N. Because the northern boundary of the area in the figure is 60°N, the positive anomalies of Z in the higher latitudes are only partially shown for blocking episodes. Yet the sharp contrast of positive Z anomalies in the north and negative anomalies in the south are well recognized in the Pacific for PAC, in the Atlantic for ATL, and in both Pacific and Atlantic for DBL. In Fig. 5, it is evident that PAC episodes are associated with the generally cool SST anomalies in the middle-latitude Pacific and western Atlantic. For ATL episodes, the negative anomalies of SST are found in the middle-latitude Atlantic and eastern Pacific. However, the negative anomalies found in the
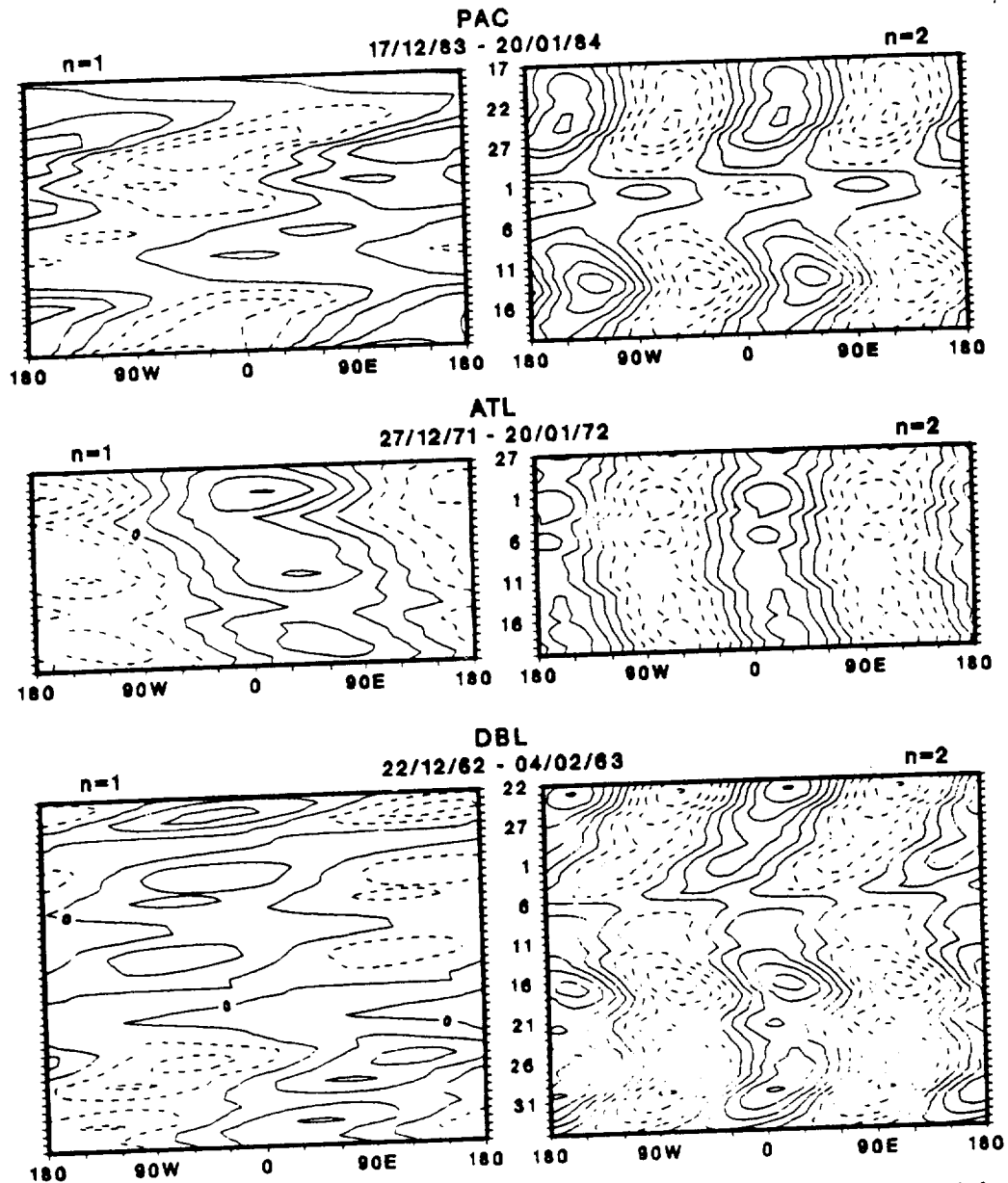
PAC
17/12/83 - 20/01/84

ATL
27/12/71 - 20/01/72

DBL
22/12/62 - 04/02/63

Fig. 4   Trough-ridge diagrams of n=1 and 2 in the 54°-70°N band with 500 mb Z during typical blocking episodes of PAC, ATL and DBL. The contour interval is 50 m, and negative contour lines are dashed. From Kung, DaCamara and Susskind (1992).
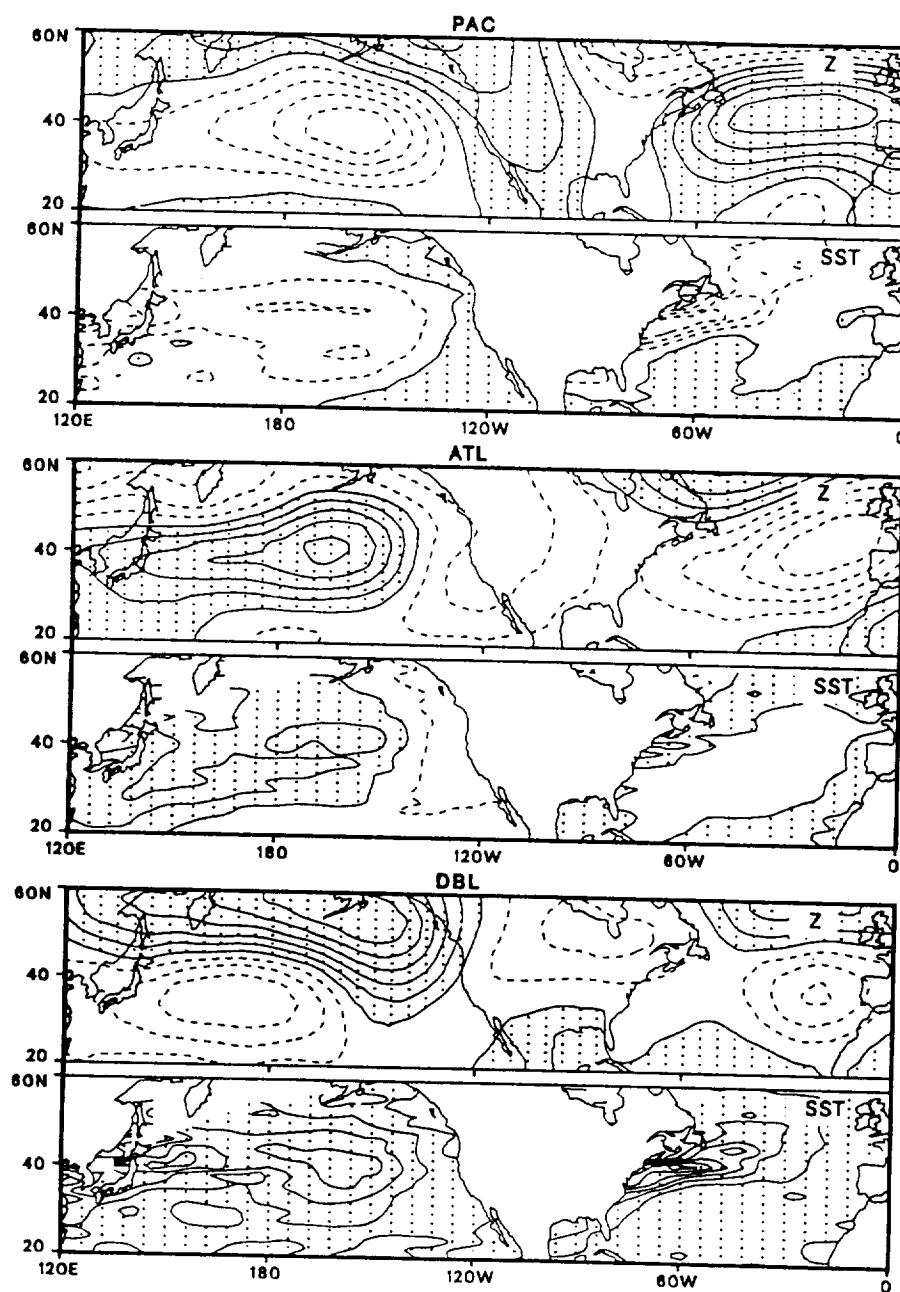
26

Fig. 5   Anomaly patterns of 500 mb Z and SST for composites of episodes for PAC, ATL and DBL. The contour interval is 50 m for Z and 0.5°C for SST. Negative contour lines are dashed. From Kung, DaCamara and Susskind (1992).

average pattern for ATL are not as distinct as the negative anomalies for PAC. Although SST anomalies of individual ATL episodes are as distinct as those of PAC episodes, the location of the Atlantic cooling is more variable than for PAC episodes, making the average pattern less distinct. Comparing the PAC and ATL episodes, it is evident that a general cooling in the Pacific and Atlantic favors the development of major single blocking in the Pacific. When the cooling is limited to the Atlantic and part of the Pacific, with a warm sector in the Pacific, a single blocking is likely to develop in the Atlantic.

The SST anomalies of DBL in Fig. 5 show definite warm SST patterns in most areas of the Pacific and Atlantic. This sharply contrasts with SST anomaly patterns in PAC and ATL situations, where the cool SSTs are associated with dominant single blocking. It is noted with Fig. 4 in the preceding discussion that the double blocking situation is developed and maintained by the stationary $n=2$. The dominant $n=2$ should be supported by the stationary baroclinic energy source and we confirm that there is no barotropic energy available for $n=2$ through nonlinear wave-wave interaction. The warm SSTs associated with DBL thus indicate that the double blockings are developed with in situ warming of the northern hemisphere circulation. The cold SSTs associated with PAC and ATL then can be interpreted to favor the nonlinear wave-wave interaction to maintain the traveling $n=1$ that couples existing $n=2$ to form the single blocking pattern. Therefore, the distinct energetics difference in single and double blocking patterns emerges. The double blocking pattern

is baroclinic in nature whereas the single major blocking depends on the barotropic nonlinear process of energy input. Because of the long characteristic time of SST variation and consequent persistence of blocking pattern, the study of blocking in relation to SST anomalies is relevant in the long-range forecasting of the northern hemisphere winter circulation.

3. LONG-RANGE SIMULATION OF WINTER BLOCKING

In our earlier study by Kung and Baker (1986), the simulation of blocking by coarse resolution GLA GCM with a climatology SST only produced a weak Pacific blocking for January 1979. The failure of the model to amplify $n=1$ to produce a pronounced blocking is attributed to the lack of $L(1)$ in the simulated circulation. The simulated winter circulation shows a strong baroclinic conversion at the whole spectral range, particularly in planetary waves $n=1$, 2 and 3. However, these are only associated with the formation of a weak blocking, and the eddy kinetic energy in the planetary-scale range cascades down to the short-wave range through wave-wave interaction.

In the following study by Kung et al. (1989), four numerical simulations of the global atmosphere for January 1979 were analyzed to study the energetics of blocking formation. Both coarse and high resolution (2°x2.5°) GLA GCMs were employed with GLA and Geophysical Fluid Dynamics Laboratory (GFDL) initial datasets. All simulations continued to use the climatology SST for January. Among four simulations that were examined, those by high resolution GCM tended to generate

28

realistically strong blocking with compatible energetics, as in the observed blocking episode. It is also noted that the simulation with the GLA initial data was able to amplify n-1 to produce the second blocking in the Atlantic in late January following the first one in the Pacific. The simulations by coarse resolution were failures. Apparently, the coarse resolution model resulted in a downscale energy cascade preventing a proper upscale input at n-1.

As a logical next step, the January 1979 global simulations were repeated by Kung et al. (1990), with the SST anomaly field updated during the model integration. Both the coarse and high resolution GLA GCM are employed with the GLA initial dataset. A simulation discussed

above (Kung et al. 1989), which was performed with the high resolution GCM utilizing GLA initial conditions, is used as the control run to examine the SST updating simulations. The SST field is provided by a blended analysis of in situ (ship and buoy) and satellite-retrieved data. The SST data retrieved from satellite radiances were obtained by the multichannel technique of Susskind and Reuter (1985) using the high resolution infrared sounder and the microwave sounding unit on Tiros-N. The approach at GLA is fundamentally different from the current operational approach at the National Environmental Satellite data and Information Service in that the surface and atmospheric conditions are determined from the radiative transfer equations with an iterative

TABLE I

Three simulation experiments and the control run of the January 1979 global atmosphere with GLA GCM, and blocking episodes identified in the observed and simulated Northern Hemisphere circulation (after Kung et al. 1990):

Run	GCM grid (latitude x longitude)	1/1/79 0000 GMT initial data	Blocking period (day/mo/year)
Observation	——	——	3/1-14/1/79 12/1-29/1/79
Exp A	4°x5°	GLA	3/1-16/1/79 27/1-30/1/79
Exp B	2°x2.5°	GLA	3/1-16/1/79 18/1-31/1/79
Exp C	2°x2.5°	GFDL	7/1-14/1/79 16/1-25/1/79
Control	2°x2.5°	GLA	3/1-12/1/79 21/1-25/1/79 28/1-30/1/79

Observation

Exp-A

90E

90E

180

0

180

0

90W

90W

21-25 Jan 79

26-30 Jan 79

Exp-B

Exp-C

90E

90E

180

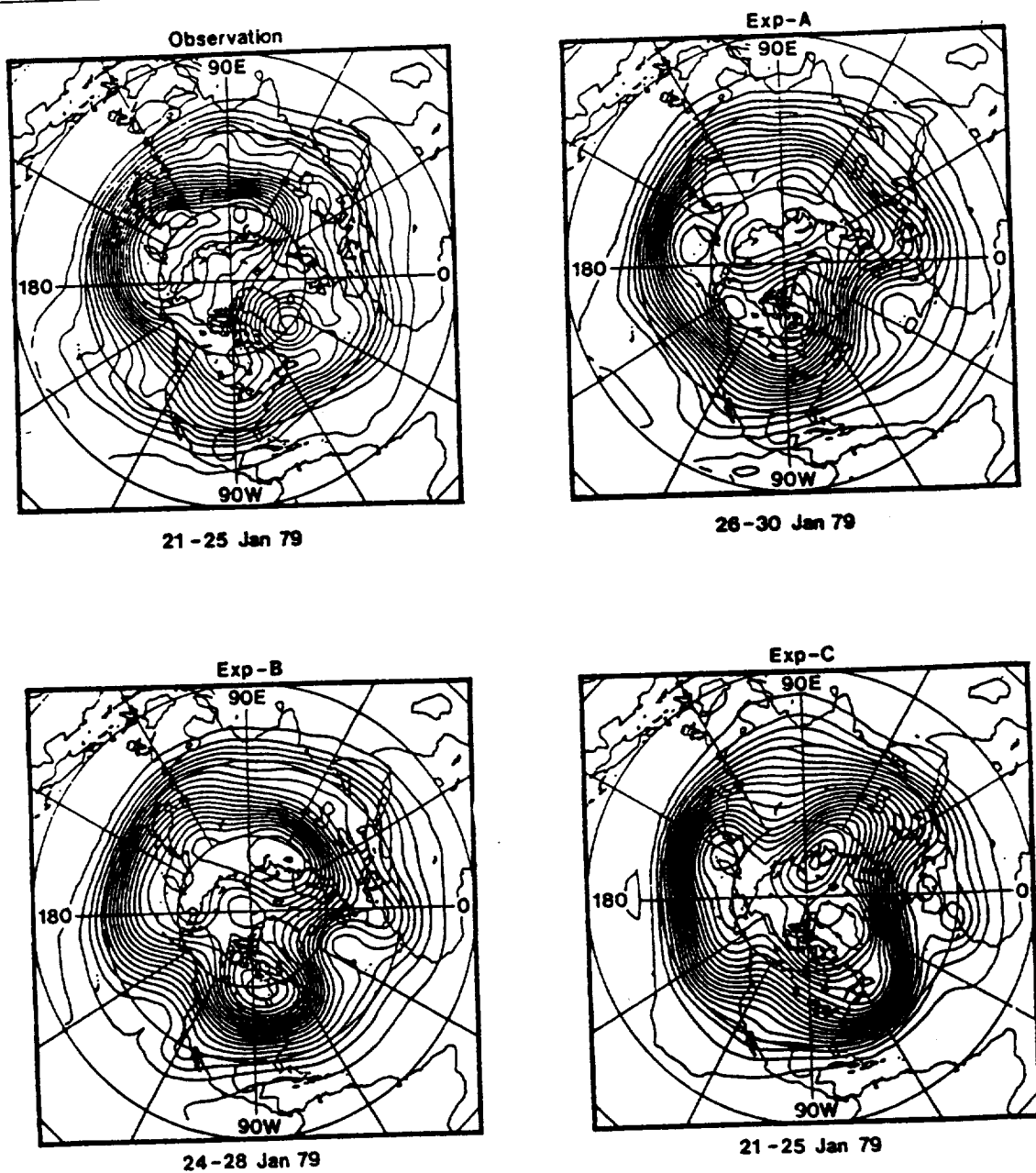0

180

0

90W

90W

24-28 Jan 79

21-25 Jan 79

Fig. 6   Observed and simulated 500 mb circulation for a 5-day period of
the developed second blocking in the Atlantic during January 1979 experiment.
From Kung, DaCamara, Baker, Susskind and Park (1990).

scheme. The basic retrieval system and analysis technique are detailed in Susskind et al. (1984) and Susskind and Reuter (1985). The monthly mean field of the in situ and satellite retrieved data are blended to the 4°x5° grid by solving Poisson's equation, subject to appropriate internal and external boundary conditions. This technique is similar to the operational blend analysis used at the National Meteorological Center (NMC) (Reynolds 1988).

For the GCM experiments, daily gridded SST fields were obtained by linear interpolation of the monthly mean blended fields, assuming that the observed monthly means are located in the middle of each month. The assumption is valid due to the smallness of time variation in the SSTs during winter months. Three simulation experiments involved in this series of study and the control run are listed in Table I with the identified blocking period. It is noted that the high resolution version of the GCM used in Experiments B and C is identical to the coarse resolution version in respect to physical parameterizations.

Comparing the simulated 500 mb circulations with the observed circulation during a 5-day period of the developed Pacific blocking (first blocking), Exp B shows the closest blocking pattern to the observation, both in the shape and the location of the block. The general pattern of the entire northern hemisphere circulation also is much better in Exps B and C than in Exp A. During a similar 5-day period of the second blocking in the Atlantic (Fig. 6), Exp B again shows a blocking pattern in closest agreement to the

observation, although the development of the Atlantic blocking is delayed for several days in the simulation. Exp C produced a dipole structure. However, the blocking is dislocated to the east, the jet is more zonal, and the blocking period is shorter than in Exp B and the observation (see Table I). Exp A, using the coarse resolution GCM, indicates the formation of the Atlantic blocking, but the occurrence is substantially delayed and the amplitude and longitudinal extent of the blocking are also limited.

Examination of simulation blocking episodes apparently indicates that the simulation by a high resolution GCM, using a realistic SST field as a boundary condition, is capable of generating a second major blocking event. As clarified in Kung et al. (1989), the high resolution GCM is able to realistically produce the first (Pacific) blocking episode through the upscale kinetic energy input into the ultralong waves by the wave-wave interaction. Since the development of blocking immediately follows the initialization of the GCM, we may assume the existence of an adequate amount of spatially distributed baroclinic energy (see Tanaka and Kung 1988) within the initial data. For the second (Atlantic) blocking event toward the end of the simulation period, however, the required source of baroclinic energy must be provided by some other means. This may suggest that the realistic ocean surface heating has provided an adequate baroclinic energy source during the simulation, producing a realistic second blocking even after the effects of initialization are presumably lost.

To examine the forecast skill

31

of the simulations, the anomaly correlations of the 500 mb geopotential field in the North Atlantic sector (30°-86°N, 100°-5°W) are presented in Fig. 7 for Exps A and B and the control run. The anomaly correlation of Exp B can be seen to represent the group of high resolution simulations with Exps B and C. The figures show that following the initial state, there is high forecast skill for all three simulations in the Atlantic sector. Although the skill scores drop in mid-January, toward the end of January the relatively high skill of Exp B becomes apparent with the development of a realistic Atlantic blocking. Exp A shows some insignificant skill at the end of

January associated with a rather limited blocking with the coarse resolution GCM. Throughout the simulation period, Exp B exhibits a relatively high anomaly correlation, while the control run, without a realistic SST field, shows a marked deterioration toward the end of the month.

The forecast skill of ultralong waves may be examined by separating zonal wavenumbers $n-1$ and 2 from other wavenumbers in the error growth of geopotential height and error kinetic energy during the simulation period. The former is expressed in terms of a root-mean square error in the 500 mb geopotential height field and the latter in terms of a mean-square error in the 500 mb wind
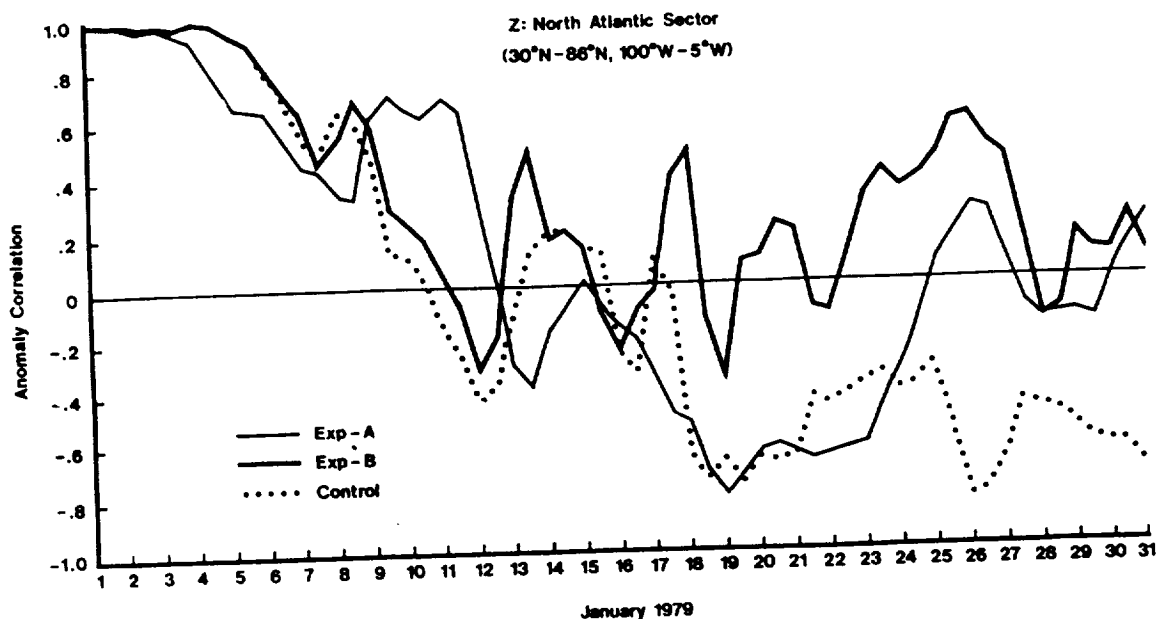

Fig. 7   Anomaly correlations of the 500 mb geopotential field in the North Atlantic sector during the January 1979 simulation experiments. From Kung, DaCamara, Baker, Susskind and Park (1990).

field. Both are taken in the 38°-70°N latitudinal band, and it is indicated that the ultralong waves ($n=1-2$) in all of the simulations show high skill relative to the persistence up to 17-18 days. Beyond that, Exps B and C, using the high resolution GCM, still show good skill toward the end of the month. However, for shorter waves of $n=3-10$, the forecast skill is only recognizable for the initial 7-10 days of the simulation. Clearly the improved blocking simulation with the realistic SST field, particularly the generation of the second blocking event in the Atlantic toward the end of the one-month period, is for the improved prediction of the ultralong waves.

Although the improved blocking simulation has resulted from the use of a realistic heating field, we cannot determine in this study if it is due to the improved initial field of SSTs, their realistic time variations during the simulation, or their combined effect. This may be studied in an additional series of simulations with various initial times. It is important to note that only one initial state (1 January 1979) is involved in this series of simulations. As such, the results can not be generalized. If the results of future blocking simulations indicate the importance of updating SSTs during the model integration, then one possible conclusion would be that a coupled ocean-atmosphere model is critical for significantly improving extended-range forecast skill. Another view would be that in these simulations, the upper limit of what would be possible with a coupled ocean-atmosphere model is tested, since updating the observed SSTs during the

atmospheric model integration may imply a correct ocean model SST prediction.

4. LONG-RANGE SIMULATION OF SUMMER BLOCKING

Following the preceding simulation of winter blocking during January 1979, experiments have been performed by Kung et al. (1992) for a 46-day summer period from 1 July to 15 August 1979, to simulate summer blocking. The summer simulation also utilized the same high resolution GLA GCM. During the simulation, SST anomalies were updated daily with observations. A parallel control run used climatology SSTs in lieu of observed SSTs.

The SST anomalies in Fig. 8 and the persistent blocking patterns of the eastern Pacific in the later half of the simulation period in Fig. 9 seem to indicate that the summer blocking in the eastern Pacific is also associated with the positive SST anomalies in the eastern Pacific. The warming persisted and magnified during this period, while the blocking is strengthened. As the scale of summer blocking is smaller than that of winter blocking, it is consistent with the finding of DaCamara et al. (1992) that the smaller blocking tends to be more baroclinic in nature. This _in situ_ association of warm SST anomaly patch and persistent summer blocking may well suggest that the realistic simulation of the August eastern Pacific blocking in the experiment is for the updating of SSTs during the model integration. The control run with the climatology SST failed to generate this blocking for the lack of realistic surface heating. It is also shown that there is a
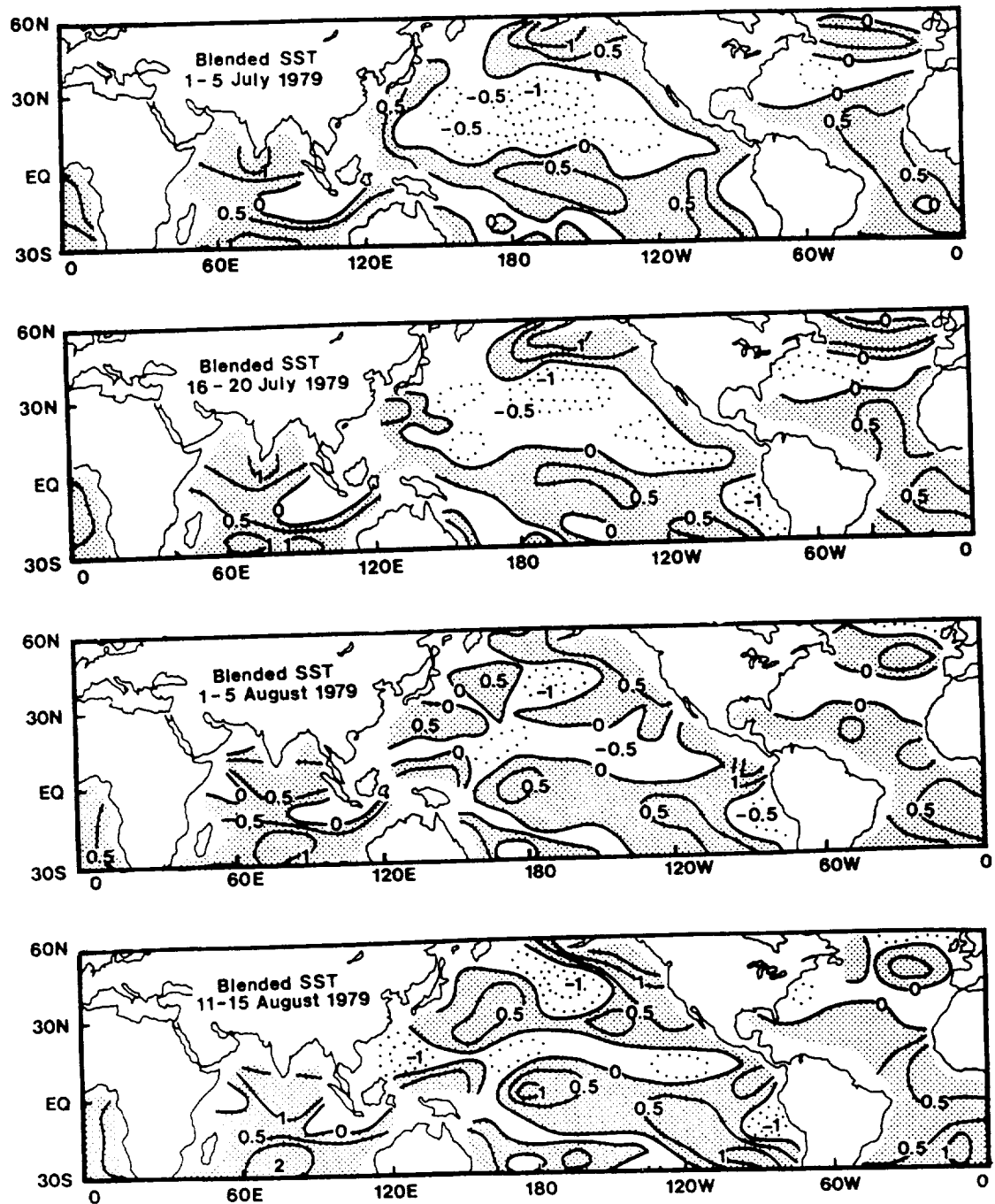
Fig. 8   Blended SST anomalies during four 5-day periods in July and August
1979. Contour interval is 0.5°C. Positive anomalies are shaded. From Kung,
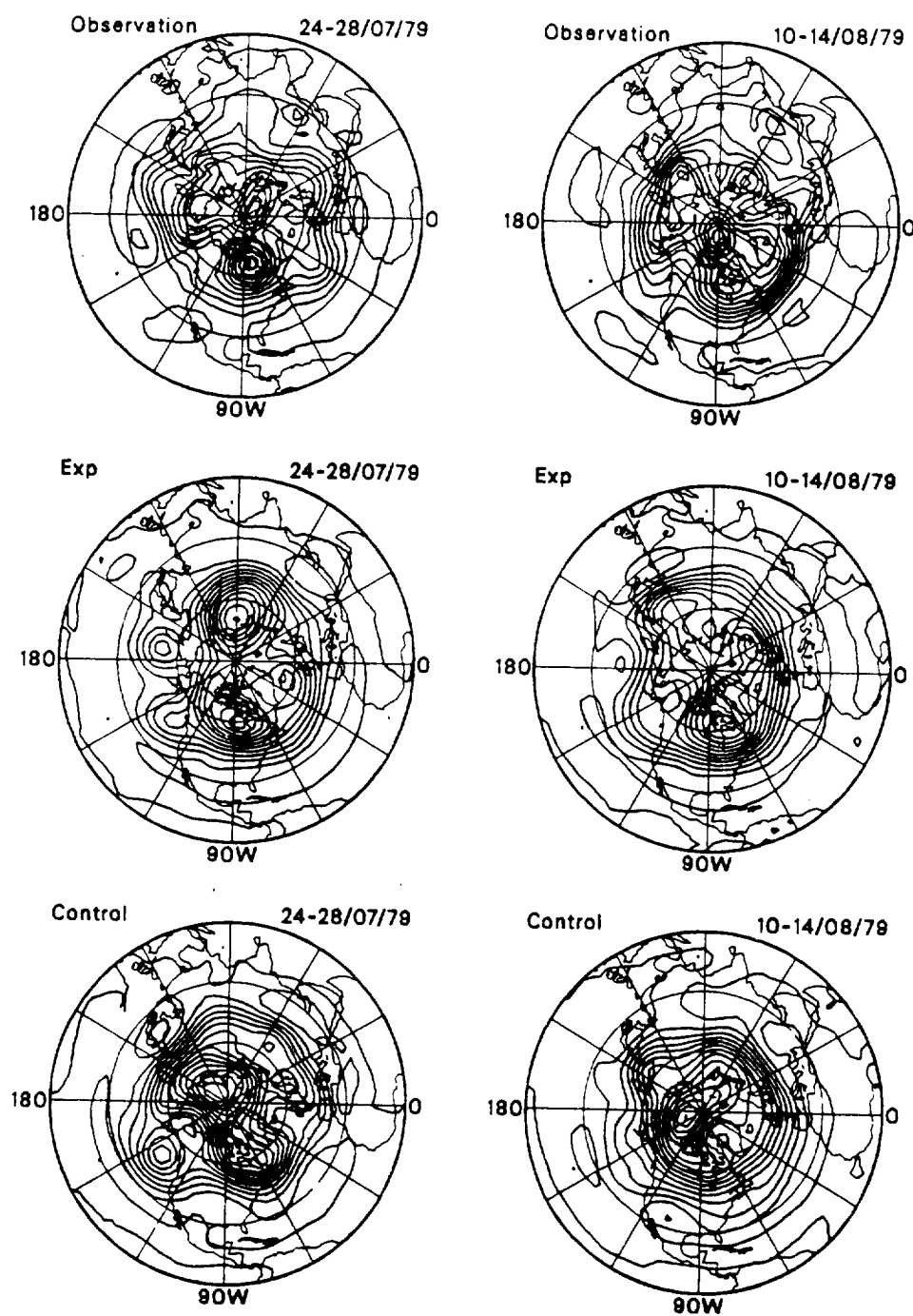Min, Susskind and Park (1992).

34

Fig. 9   Observed and simulated 500 mb circulation during two 5-day period;
near the end of 45-day simulations. From Kung, Min, Susskind and Park (1992)

considerable forecast skill in the area of summer blocking circulation, particularly in the confluence area of the downstream. Simulation beyond this period has not yet been attempted.

5. EMPIRICAL-REGRESSION FORECASTING

Regression forecasting on the basis of teleconnection is important since it does not base itself on the extrapolation of time series, which assumes some steady state or steady trend of variations. It is an application of synoptic analysis in the long-range frame. It implicitly relates the physical processes, known or not yet known, to the future state of the atmospheric circulation beyond

the deterministic range of the current GCM forecasting. Thus, as stated by Hastenrath (1985) the success of regression forecasting depends on the successful identification of effective predictors, which is difficult due to physical processes not yet well known. It also should be noted that the operational mode, or the pattern of the general circulation, undergoes considerable variation in a decade or two, making the established single regression useless after a certain period. Pointing to these difficulties, the logical strategy will be the use of the multiple regression approach, with predictors selected objectively from a large group of meteorological and oceanic
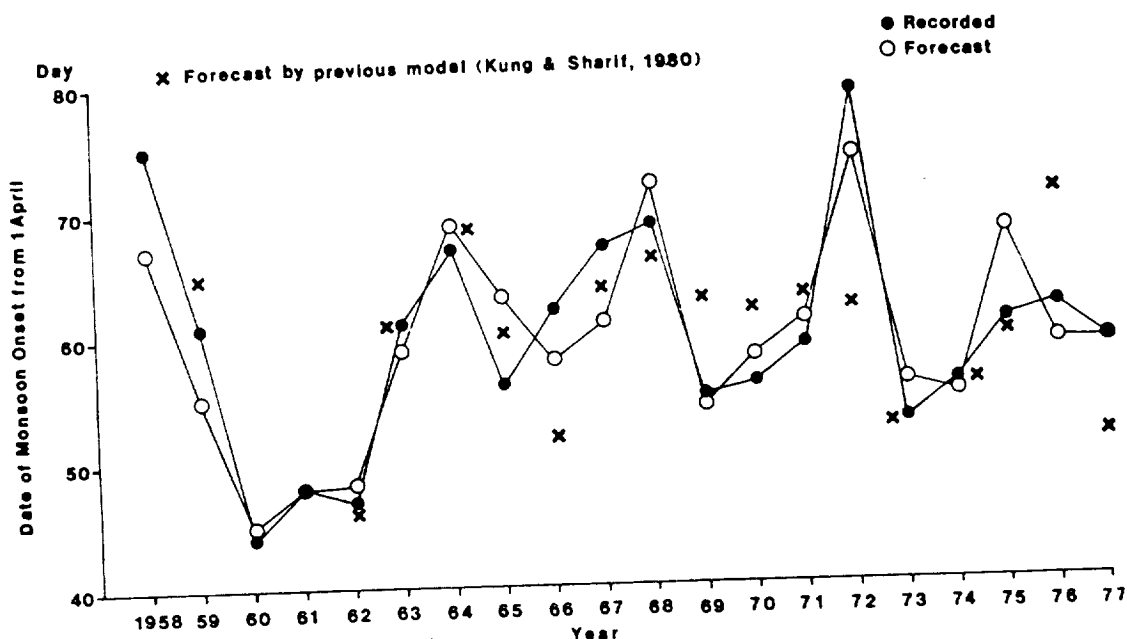

Fig. 10   Recorded and forecasted dates of the Indian summer monsoon onset on the Kerala coast. From Kung, Min, Susskind and Park (1982).

parameters.

Figure 10 demonstrates the recorded and forecasted dates of the Indian summer monsoon on the Kerala coast, by Kung and Sharif (1980, 1982). In their 1980 study, 8 predictors were utilized, but they are all from the April mean upper air parameters over the forecast point. In the 1982 study, only 5 predictors were utilized, but they were objectively selected from January to April mean upper air parameters over India and Australia, SSTs of the Indian region, and precipitation in Eurasia (representing the snowcover). A marked improvement in the 1982 study compared to the 1980 study is obvious. The forecast gaps of 1966, 1969, 1972 and 1977 in the 1980 study were resolved in the 1982 study. The contrast of these two sets of forecasts from 1958 to 1977 clearly indicates the importance of identifying useful predictors, also demonstrating the validity of our objective method to select predictors from the large pool of meteorological and oceanic variables.

Similar experiments were performed by Kung and Tanaka (1985) to forecast monthly temperature and precipitation with antecedent upper air parameters and SST with a modified scheme of multiple regression. Parameters in both the northern and southern hemispheres were employed. The scheme uses five predictors with the database for the period 1963-1983. The scheme chooses the first predictor on the basis of cross-correlation between the predictand and variables for the general regression:

$$y = a_0 + a_1 x_1 + a_2 x_2 + \cdots a_n x_n$$

where a is the regression

coefficient, x is the predictor and n is the number of predictors, and $n = 5$ in this case. The selection of the predictors and fitting of the regression coefficients are performed simultaneously in this analysis. In order to select the first predictor x_1 from m possible predictors, the correlation coefficient between y and x, $r(y, x_i)$, is computed in a time series with each of m possible predictors. The first predictor x_1 is then selected by

$$Max[r^2(y, x_i), i = 1, 2, \cdots, m],$$

i.e., the correlation coefficient of x_1 gives the maximum $r^2(y, x_1)$ among the computed m correlation coefficients. After selection of x_1, a simple regression is formed by the least squares fitting,

$$y = a_1 x_1 + \varepsilon_1$$

where ε_1 is the first residual component and $r(x_1, \varepsilon_1) = 0$.

The second predictor x_2 is selected by examining the correlation between the residual ε_1 and the possible predictors remaining:

$$Max[r^2(\varepsilon_1, x_i), i = 1, 2, \cdots, m-1].$$

The first residual, ε_1, is then regressed linearly on x_2 as

$$\varepsilon_1 = a_2 x_2 + \varepsilon_2$$

where ε_2 is the second residual and $r(x_2, \varepsilon_2) = 0$. a_2 is determined by the least squares method again. After the selection of predictors x_1 through x_n, the regression coefficients a_0 through a_n, are recomputed with a conventional method of the multiple regression.

This scheme is formulated so

37

July Ts in Northeastern U.S.
(Forecast with February Data)

● Recorded
○ Forecasted

YEAR
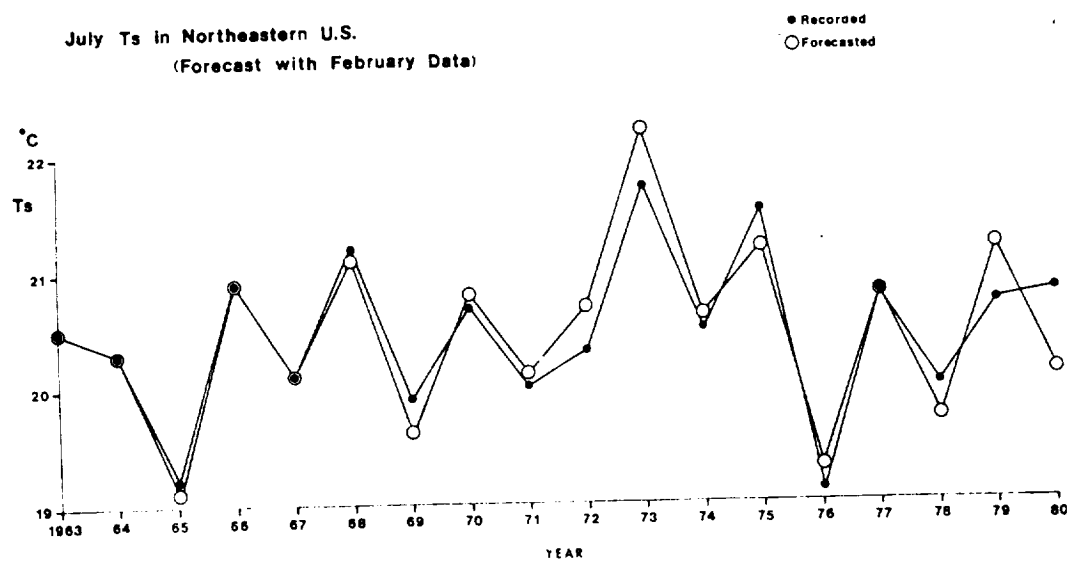
Correlation between forecasted and recorded surface temperature

○ Significant at 95% level
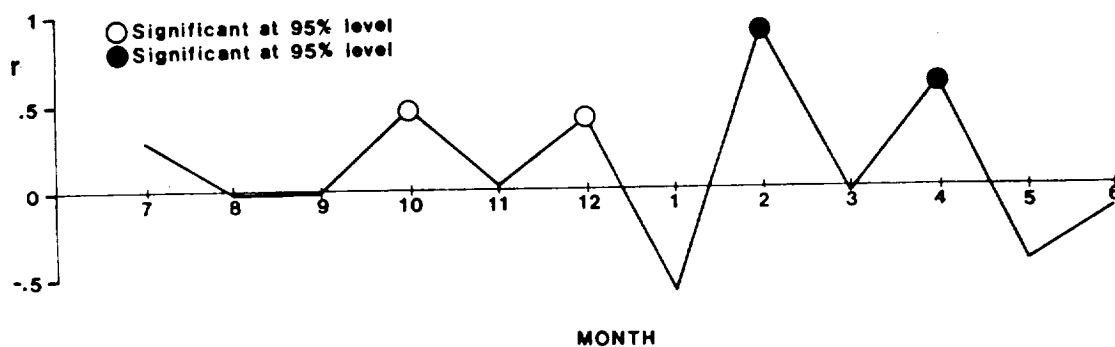● Significant at 95% level

MONTH

Fig. 11   Forecast experiment of July surface temperature in the northeastern United States. From Kung and Tanaka (1985).

38

that the regression residuals are minimized with the fewest possible predictors. The collinearity among predictors is effectively reduced even though the correlation among selected meteorological parameters may not be zero. It is also noted that the successive regression with residuals is applied only for the selection of predictors. Since the regression coefficients are computed after the selection is completed, the present scheme is a multiple regression scheme in the conventional sense. The comparison of the regression coefficients with those obtained during the selection, shows that their difference is negligibly small. This indicates the validity of the present scheme. In Kung and Tanaka (1985) the scheme gives a lead time of predictors a two to eleven month period preceding predictands, minimizing the collinearity among predictors.

An example of high forecast skill in this series of study is shown in Fig. 11, forecasting July temperatures in the northeastern United States. The correlation coefficient between the recorded and forecasted temperature is 0.92, and the mean square error $0.3°C$. It is also noted in the lower half of Fig. 11 that the correlation between the forecasted and recorded values is not necessarily the highest immediately preceding the event. In this series of experiments, as illustrated in Fig. 12, it is suggested that the forecasting on the basis of a simple predictor is inadequate, and that the use of five predictors seems sufficient. In the experiments, the predictors are selected independently every year without involving the forecast year's data. However, in most cases, the same predictors are
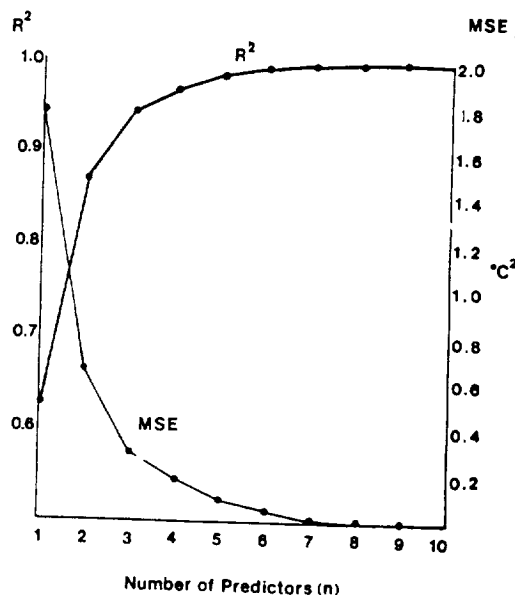

Fig. 12 Coefficient of multiple determination and mean square error as functions of number of predictors in predicting January surface temperature in the northeastern United States. From Kung and Tanaka (1985).

selected from the large pool of variables.

Through our model and empirical forecast experiments, the importance of SSTs as predictor is well recognized by the better forecasts which result when the SSTs are involved. The release of latent heat from the ocean surface is the major source of energy input to the atmosphere, and the variations in location and amount of energy input essentially determine the deviations of the general circulation from the average pattern. Many important

works exist in this area (e.g. Bjerknes 1969; Kawamura 1986; Namias 1959, 1976; Rowntree 1972). We have pursued the problem with specific interest in establishing large-scale teleconnections between predictands and SST predictors.

In Park and Kung (1988), we examined the first two principal components of the North American summer temperature field, and have shown that they have considerable prognostic value. It is noteworthy that the summer temperature of the midwestern to eastern part of North America is solely determined by the first component. Through the teleconnection of the principal components and preceding SST field, it appears that the thermal fields over the North Pacific in the preceding winter and spring are closely related to the North American temperature in the following summer. As shown in Fig. 13, the negative anomalous SST departures in the central North Pacific precede the higher summer temperature in the Midwest, and the positive departures precede the lower summer temperature. The signal of anomalous SST departures appears in the fall and reaches its maximum in the winter and spring. As this is an interesting relationship previously uncovered, it also should be pointed out that the relationship may offer a convenient way to obtain a quick outlook of the coming seasons.

The El Niño-Southern Oscillation (ENSO) is known as a global phenomenon whose influence is often detected in quasi-stationary waves as well as in the related synoptic-scale weather events in the extratropical latitudes during the northern hemisphere winter. Although Chen (1982) indicated that the forced Rossby mode is weak or absent during the northern hemisphere summer, the signal of ENSO was detected in the North American summer temperature in our study, suggesting that the influence of El Niño on the general circulation persists beyond the winter half of the year. It is unlikely, however, that El Niño has a direct influence on the atmospheric circulation in the northern hemisphere summer at times when the anomalous tropical ocean surface condition is modified. Instead of direct influence, the ocean-atmosphere interaction, such as in the Aleutian region and the central North Pacific in the transition seasons, is closely related to El Niño, possibly playing a role in determining the downstream temperature pattern over North America in the subsequent summer.

Our present multiple regression scheme, as described in this section and detailed by Kung and Tanaka (1985), is also being applied to the forecasting of localized phenomena. For example, Kinoshita (1989) successfully predicted the recess of Southeastern Asian monsoon (Mei-Yu or Bai-u) with the scheme. At present, a collaborative investigation is in progress with the Central Weather Bureau, Taiwan, R.O.C. to develop forecasting schemes for Mei-Yu and seasonal rainfall in Taiwan. Since our preceding studies of empirical forecasting, the database has been expanded to include upper air and SST data from 1955 to present, and we may experiment forecasting beyond the defined data period. For instance, if we formulate regression equations with a 20-year database, we may forecast from 1975 to present without involving the forecast year during the data period. The forecast
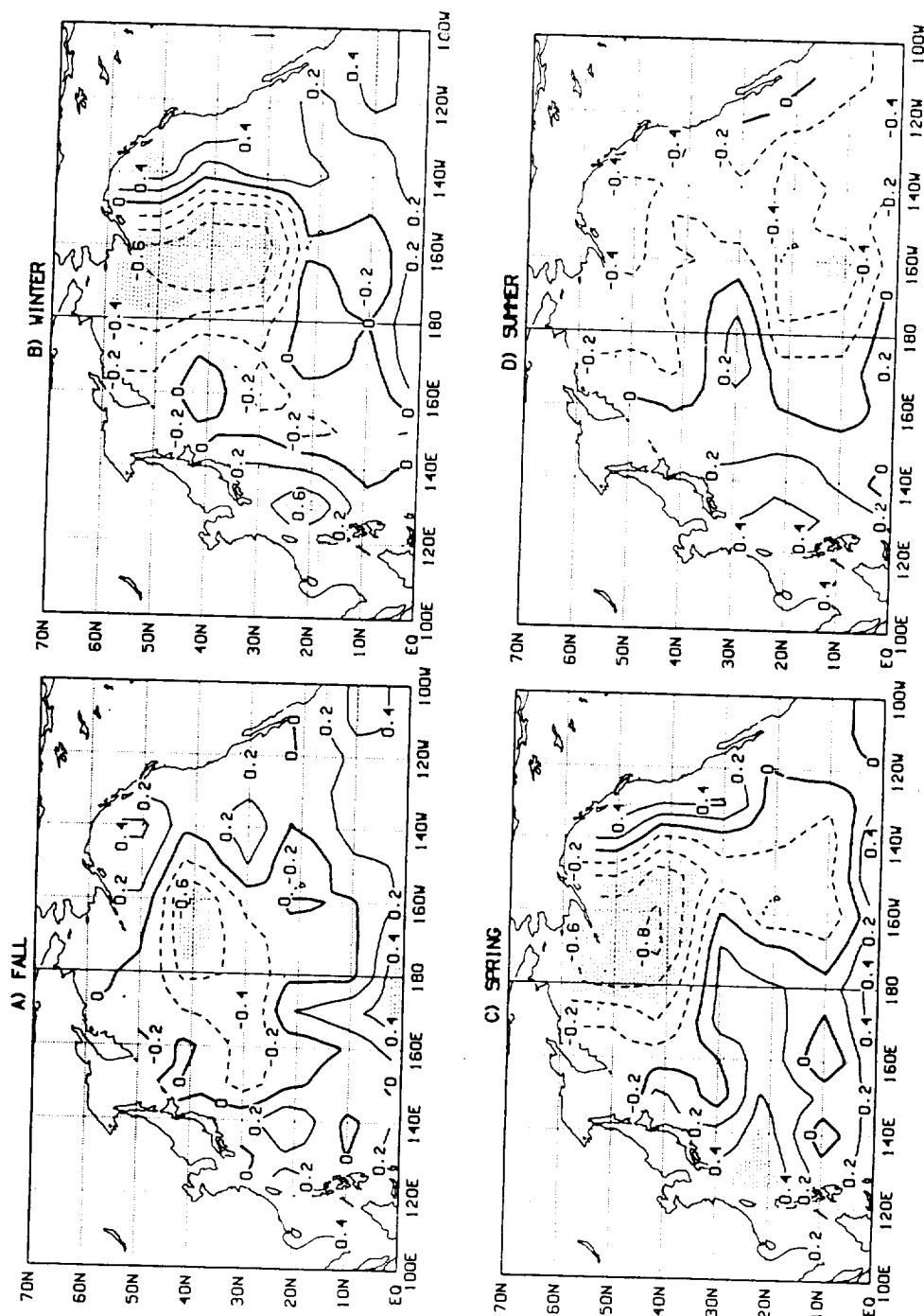
Fig. 13   Cross-correlation between the seasonal SST anomalies and the first component of the North American summer temperature. Shaded areas indicate correlations exceeding the 95% level of significance. Isopleths are drawn for each 0.2. From Park and Kung (1988).

experiment is thus a completely independent experiment in reference to basic regression analysis.

Our ongoing study shows that the regression scheme may be applied in the restricted-area phenomena in Taiwan so long as the phenomena are part of large-scale systems, which is the case for Mei-Yu and seasonal

rainfall. However, it also has become clear that there are considerable noises of local origin affecting the regression forecast. The noises seemingly result, at least in part, from the interaction of large-scale and local-scale (subsynoptic and meso scale) effects and it is imperative that the

TABLE II

Summary results of 1990 Mei-Yu forecast in Taiwan with real-time monthly global data from October 1989 to February 1990. Forecasted values represent averages of single-regression forecasts at various points. Dates of the onset and recess are the day from April 1.

Predictor		Forecast			
		Onset date	Recess date	Period (days)	Rainfall (mm)
Oct 1989	700 mb T	46.5	77.6	31.5	480
	500 mb Z	48.0	79.7	34.5	447
	SST	49.5	77.3	31.2	454
Nov 1989	700 mb T	51.0	76.7	30,3	452
	500 mb Z	49.0	79.0	30.0	499
	SST	48.5	76.0	28.8	485
Dec 1989	700 mb T	45.3	___(a)	34.4	437
	500 mb Z	46.3	78.7	34.0	356
	SST	49.7	81.8	27.0	471
Jan 1990	700 mb T	47.5	___(a)	36.8	494
	500 mb Z	46.8	85.0	37.5	481
	SST	___(b)	___(b)	___(b)	___(b)
Feb 1990	700 mb T	50.0	___(a)	29.5	385
	500 mb Z	51.0	___(a)	30.3	483

Notes:
(a) No regression was given for weak cross-correlation.
(b) SST data were not used for January and February 1990 because the datasets were not prepared.
(c) Official records of 1990 Taiwan Mei-Yu at Taipei are:
Onset 48
Recess 79
Period 32 days
Rainfall 420 mm

forecasting scheme be properly adjusted to suit the local situations. Our study indicates that, except for years of abnormal Mei-Yu (i.e. very early or late onset, drought, etc.) the set of single regression may be utilized effectively if many data points are used independently and the cross-correlations are properly updated every year. The real-time forecast of 1990 normal year was thus successfully carried out, but the abnormal 1991 Mei-Yu (late onset, short period) needed a multiple regression of three predictors. Table II shows the results of 1990 real time forecast with antecedent real-time data from October 1989 to February 1990; each value in the

table representing the average of single regression forecasts at points where strong teleconnections are observed between predictands and monthly values of predictors. The official records of Mei-Yu at Taipei are the onset May 18 (Day 48 from April 1), recess June 18 (Day 79), period 32 days, and total rainfall 420 mm. Thus the forecasts are very close to the actual observation. In the table it is noted that these independent real-time forecasts with successive monthly data are very consistent and prediction is possible from fall.

Table III compares the 1990 and 1991 real-time forecasts for Mei-Yu onset with single regression and 3-term multiple regression. The

TABLE III

1990 and 1991 real-time forecast of Mei-Yu onset in Taiwan by single and 3-term multiple regressions with monthly data of preceding October, January and March. Sample size is the number of regression equations for predictors at various locations, and SD the standard deviation of the forecast within the sample.

Month of real-time data		Single regression		3-term regression	
		1990	1991	1990	1991
October	Sample	13	13	13	13
	Mean	47.5	32.7	47.7	44.8
	SD	1.3	14.3	2.8	5.2
January	Sample	25	25	25	25
	Mean	46.6	53.7	47.8	50.7
	SD	2.6	23.8	1.6	4.8
March	Sample	12	12	6	6
	Mean	47.2	55.7	46.9	57.0
	SD	2.3	15.2	4.5	3.2
Total	Sample	50	50	44	44
	Mean	47.1	50.9	47.6	49.5
	SD	2.1	18.6	2.7	6.0

Mei-Yu Period Forecast
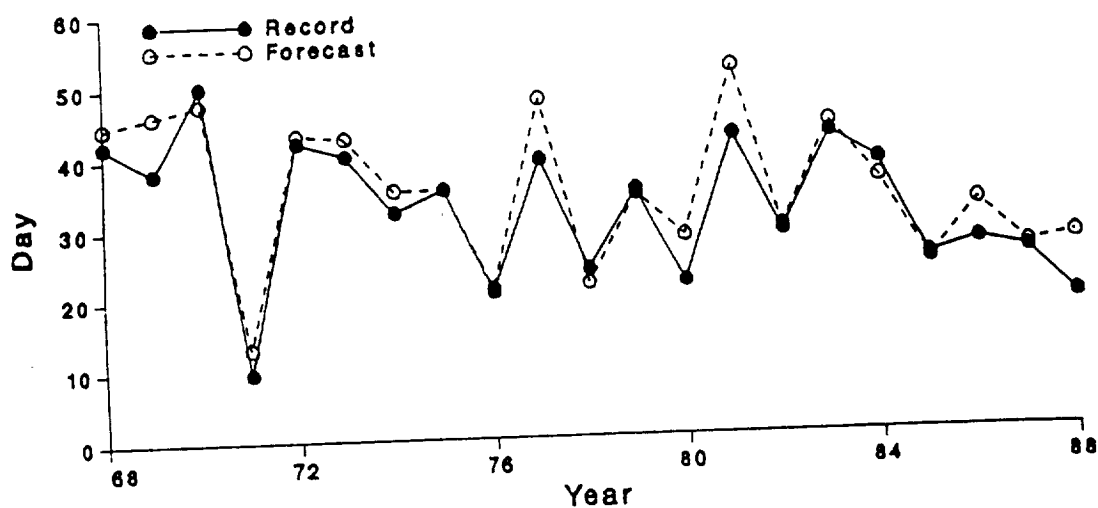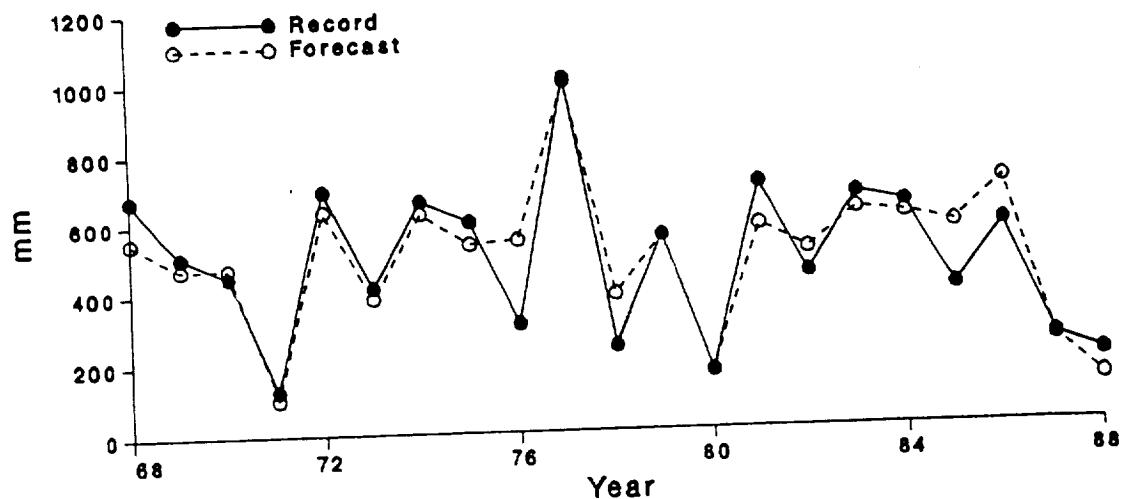

Mei-Yu Rainfall Forecast

Fig. 14   Mei-Yu multiple regression forecasts for the period (days) and total rainfall in Taipei from 1968 to 1988. Datasets for regressions are for 10-year periods preceding the forecast years.

results of single regression forecasting are disturbed in 1991, as affirmed by the large standard deviations in 1991 among independent regression forecasts. However, the standard deviations are only slightly larger for multiple regression in 1991 than in 1990 when multiple regression is used. It may suggest the general applicability of the multiple regression scheme in both normal and abnormal years. It is likely that in the abnormal year, the operational mode of the general circulation deviates from the normal prevailing pattern, making the single regression less useful. However, when the multiple regression is utilized, the possible change of the operational mode is already incorporated in the selection of multiple predictors.

Figure 14 illustrates the results of forecast experiments for Mei-Yu period and rainfall from 1968 to 1988 with January predictors. Observational data in January of the forecast year are used as the real-time data. The 3-term multiple regressions are estimated with a 10-year database, and used for three successive years. Thus each year's forecasts are done with three independently obtained sets of regression, each set representing a group of multiple regressions at different grid points of strong cross-correlations. The best value among three sets of regressions for each year is plotted in the figure. The levels of departure among forecasts are indicated in Table III. The figure clearly demonstrates the utility of multiple regressions.

6. REMARKS

Our recent efforts in extended-range numerical model forecasting and empirical long-range forecasting have been reviewed in this paper. The model forecasting research is focused on the blocking simulation in the northern hemisphere winter and summer. The blocking appears to possess considerable predictability and thus useful forecast skill in the model integration for at least one and one-half months. At present, the study continues with specific interest in the response of simulation to updated SST fields during the model integration. The study is intended to obtain essential information regarding the feasibility of constructing the joint ocean-atmosphere model.

The study in empirical forecasting for the range of 1 month to 1 year is progressing in the regression forecast of seasonal rainfall in Taiwan. The study is intended to provide viable information to apply the hemispherical teleconnections to localized predictands. We intend to formulate a generally applicable procedure for operational regression forecasting in a general setting in the northern hemisphere.

Central Weather Bureau (CWB81-3M-03). We are indebted to Director General C.Y. Tsay and the Forecast Center of Taiwan Central Weather Bureau for their support in conducting the collaborate forecasting experiment for Taiwan region. The technical assistance of Ms. Karen Blahnik is sincerely appreciated.

REFERENCES

Bjerknes, J., 1969. *Mon. Wea. Rev.*, 97, 163-172.

Chen, W.Y., 1982. *Mon. Wea. Rev.*, 110, 808-823.

DaCamara, C.C., Kung, E.C., Baker, W.E., Lee, B.C. and Corte-Real, J.A.M. 1992. *Beit. Phys. Atmosph.*, 65, (In Press).

Egger, J., Metz W. and Müller, G.M. 1986. *Adv. Geophys.*, 29, 183-198.

Hansen, A.R. and Chen, T.C. 1982. *Mon. Wea. Rev.*, 108, 1146-1165.

Hansen, A.R. and Sutura, A. 1984. *Tellus*, 36A, 52-63.

Hastenrath, S. 1985. *Climate and Circulation of Tropics*, R. Reidel Publishing Co., 455 pp.

Holloway, G. and West, B.J. (Eds.) 1984. *Predictability of Fluid Motions*, American Institute of Physics, 612 pp.

Kalnay-Rivas, E., Bayliss, A. and Storch, J. 1977. *Beitr. Phys. Atmos.*, 50, 299-311.

Kawamura, R. 1984. *J. Meteor. Soc. Japan*, 62, 910-916.

Kinoshita, N. 1989. *Tenki*, 36, 83-87.

Kung, E.C. and Baker, W.E. 1986. *J. Atmos. Sci.*, 43, 2792-2812.

Kung, E.C., DaCamara, C.C., Baker, W.E., Susskind, J. and Park, C.-K. 1990. *Quart. J. Roy. Meteor. Soc.*, 116, 1053-1070.

Kung, E.C., DaCamara, C.C. and Susskind, J. 1992. Unpublished Manuscript, Department of Atmospheric Science, University of Missouri, Columbia, Missouri.

Kung, E.C., Min, W., Susskind, J. and Park, C.-K. 1992. *Quart. J. Roy. Meteor. Soc.*, 118, 351-363.

Kung, E.C., Tanaka, H.L. and Baker, W.E. 1989. *Mon. Wea. Rev.*, 117, 2019-2040.

Kung, E.C., and Sharif, T.A. 1980. *J. Appl. Meteor.*, 19, 370-380.

Kung, E.C., and Sharif, T.A. 1982. *J. Meteor. Soc. Japan*, 60, 672-681.

Kung, E.C., and Tanaka, H. 1985. *J. Meteor. Soc. Japan*, 63, 619-631.

Lejenäs, H. and Økland, H. 1983. *Tellus*, 35A, 350-362.

Murakami, T., and Tomatsu, K. 1965. *J. Meteor. Soc. Japan*, 43, 73-89.

Namias, J. 1959. *J. Geophys. Res.*, 64, 631-646.

Namias, J. 1976. *Mon. Wea. Rev.*, 104, 1107-1121.

Park, C.-K. and Kung, E.C. 1988. *J. Meteor. Soc. Japan*, 66, 677-690.

Paulin, G. 1970. *Mon. Wea. Rev.*, 98, 795-809.

Rex, D. 1950. *Tellus*, 2, 196-211.

Reynolds, R.W. 1988. *J. Climate*, 1, 75-86.

Rowntree, P.R. 1972. *Quart. J. Roy. Meteor. Soc.*, 98, 290-321.

Saltzman, B. 1957. *J. Meteor.*, 14, 513-523.

Shukla, J. 1981. *J. Atmos. Sci.*, 38, 2547-2572.

Susskind, J. and Reuter, D. 1985. *J. Geophys. Res.*, 90, 11602-11608.

Susskind, J., Rosenfield, J., Reuter D. and Chahine, M.T. 1984. *J. Geophys. Res.*, 89, 4677-4697.

Tanaka, H.L. and Kung, E.C. 1988. *J. Atmos. Sci.*, 45, 3723-3736.

4.3
Prominent Northern Hemisphere Winter Blocking Episodes and Associated Anomaly Fields of Sea Surface Temperatures

Ernest C. Kung[1], Joel Susskind[2], and Carlos C. Dacamara[3]

[1] *Department of Soil & Atmospheric Sciences,*
University of Missouri-Columbia Columbia, Missouri, U.S.A.
[2] *Laboratory for Atmospheres, Goddard Space Flight Center/NASA*
Greenbelt, Maryland, U.S.A.
[3] *Department of Physics, Faculty of Science, University of Lisbon,*
Lisbon, Portugal.

TAO office: P.O. Box 23-59, Taipei, Taiwan, R.O.C.

47

Prominent Northern Hemisphere Winter Blocking Episodes and Associated Anomaly Fields of Sea Surface Temperatures

ERNEST C. KUNG[1], JOEL SUSSKIND[2] and CARLOS C. DACAMARA[3]

ABSTRACT

From a 34-year data period, twelve major winter blocking episodes in the northern hemisphere are selected for examination: four episodes for each category of Pacific, Atlantic and double blocking. It is shown that the single blockings in the Pacific or Atlantic are formed through constructive interference of the traveling zonal wave of $n=1$ and stationary wave of $n=2$. The $n=1$ is supported by the energy input through the nonlinear wave-wave interaction, and the $n=2$ by in situ warming over the Pacific and Atlantic. The concurrent double blocking in the Pacific and Atlantic are formed by the stationary $n=2$ when the traveling $n=1$ is weak. The negative anomaly fields of sea surface temperatures in the Pacific and Atlantic are associated with the single blocking in the Pacific and Atlantic. On the contrary, the positive anomalies in both the Pacific and Atlantic are associated with concurrent Pacific and Atlantic blockings, indicating the baroclinic nature of the double blocking.

1. INTRODUCTION

The winter circulation in the northern hemisphere is often dominated by a sequence of blocking episodes in the Pacific and Atlantic regions in association with the activities of low-frequency planetary waves. It is noted that a considerable forecast skill exists for such persistent large-scale anomaly patterns (see Shukla, 1981; Holloway and West, 1984; Kung et al., 1990), making the study of winter blocking particularly important. A major concern in this area of study has been the transition of the extratropical circulation from states dominated by transient synoptic-scale disturbances to the low-frequency regimes dominated by quasi-stationary planetary waves, and the maintenance of an established blocking pattern.

---

[1] Department of Soil and Atmospheric Sciences, University of Missouri-Columbia Columbia, Missouri, U.S.A.

[2] Laboratory for Atmospheres, Goddard Space Flight Center/NASA Greenbelt, Maryland, U.S.A.

[3] Department of Physics, Faculty of Science, University of Lisbon, Lisbon, Portugal.

Despite the known difficulty in precisely defining the blocking phenomena, the general characteristics of quasi-stationary ridges of blocking circulation are well recognized, and a wealth of literature exists on the subject since the early studies of Elliot and Smith (1949), Berggren *et al.* (1949), Rex (1950) and others. More recent development in this area was reviewed in Saltzman *et al.* (1986). During a blocking period, distinct obstruction of the northern hemisphere westerlies is apparent in and around the block. However, from the viewpoint of the major blocking, it is not a local system. As shown by many in recent years (e.g., Hansen and Chen, 1982; Hansen and Sutera, 1984; Kung and Baker, 1986; Kung *et al.*, 1990; Saltzman et al., 1986; Tanaka, *et al.* 1986; Vakalyuk, 1985), the diagnosis in the zonal spectral domain is an effective approach to reveal essential mechanisms involved in growth and maintenance of blocking patterns.

There have been diverging opinions on the energetics nature of blocking among researchers. Saltzman (1959), in his early study of the general circulation, proposed that the large-scale quasi-stationary systems are maintained by a nonlinear barotropic transfer of kinetic energy from smaller cyclonic-scale disturbances which have baroclinic energy sources. Diagnostic studies by Hansen and Chen (1982), Murakami and Tomatsu (1965), Paulin (1970) and others identified blocking phenomena with large-scale baroclinic conversion. However, Hansen and Sutera (1984), by contrasting the blocking and nonblocking periods, reported the significant wave-wave interactions to support the kinetic energy of blocking. From the vorticity consideration, Green (1977), Illari (1984), Shutts (1983) and others also demonstrated that the synoptic-scale eddy forcing supports the formation of blocking. Our preceding studies of observed and simulated blocking episodes (Kung and Baker, 1986; Kung *et al.*, 1989) revealed that the development of northern hemisphere winter blocking is associated with the nonlinear wave-wave transfer of kinetic energy from synoptic-scale disturbances to planetary waves. For observed blocking episodes during December 1978 and January 1979, Tanaka and Kung's (1988) energetics diagnosis in three-dimensional normal mode expansion depicted an ordinary transfer of energy from the zonal baroclinic component to the barotropic component of planetary waves via synoptic scale conversion. Kung *et al.* (1990) further demonstrated that a high resolution general circulation model is capable of producing two successive realistic blockings in the Pacific and Atlantic through one winter month in January 1979 if the sea surface temperature (SST) field is updated daily with observations during the model integration.

As blockings are a group of quasi-stationary circulation patterns of similar synoptic appearance, but likely of different causes and mechanisms involved, it is reasonable to find diverging diagnostic results among various case studies. To approach a problem of complexity such as blocking, both the case study and long-term climatological analysis are necessary. In our preceding work (DaCamara *et al.*, 1991) monthly circulation patterns of the northern hemisphere were analyzed with daily 500 mb field and monthly sea surface temperature (SST) anomaly field during 34 winter seasons from 1955 to 1989. All 102 monthly circulations were classified into 5 categories of patterns according to dominant blocking activities of the month: Pacific blocking, Atlantic blocking, double blocking, sequential blocking and no blocking. It appeared that, on the gross average, the Pacific, Atlantic and double blocking dominated winter circulation and can be associated with characteristic SST anomaly field in the Pacific and Atlantic. However, by taking the gross averages of the long-term period, variability among different cases can be easily masked. Thus a parallel case study of the same time period is highly desirable.

In this study, prominent major blocking episodes are the focus of our attention. Twelve major winter blocking episodes are selected from the daily analyses of 500 mb flow from 1956

to 1989: four episodes for each category of Pacific, Atlantic and double blocking. Through examination of prominent cases, this study attempts to distinguish the characteristics of these blockings in their development and maintenance. Manifestations of the blocking flow pattern are examined in terms of the geopotential height and associated anomaly fields. Activities of planetary waves are examined by trough-ridge diagrams, kinetic energy and its wave-wave interaction to provide energy input at zonal wavenumber n=1 and 2. The patterns of associated SST anomaly fields are then considered in terms of energy source for in situ baroclinic conversion and wave-wave interaction. It is noted that this is a case study and not an ensemble analysis, although twelve cases are more than the number of cases usually treated in most case studies. We are not attempting a composite climatological analysis of numerous blocking episodes during a long-term period. Such an attempt would be difficult, since various causes and thus various mechanisms may be involved in many cases of developing blocking. Rather, we would like to examine characteristics of major episodes in three categories of blocking development which show common prominent appearances in each category.

2. DATASETS AND SCHEME OF ANALYSIS

Datasets utilized in this study include the daily northern hemisphere geopotential height at 500 mb (Z) in December, January and February from December 1955 to February 1989, and monthly SST analyses for the same period. The Z fields are obtained from the daily National Meteorological Center (NMC) octagonal grid analyses at 1500 GMT from 1955 to 1957, and 1200 GMT for the rest of the period. The octagonal grid analyses are edited and bilinearly interpolated to a $4° \times 5°$ latitude-longitude spherical grid from 18°N to 90°N. The wind fields are computed using the geostrophic approximation, and their Fourier transforms are obtained at latitude circles 4° apart. Monthly SST analyses are acquired from the Comprehensive Ocean Atmosphere Data Set (Slutz *et al.*, 1985) for the period 1956-1979, and NMC real-time analyses (Reynolds, 1988) for the period 1970-1989. Consistency of both analyses is verified for the overlapping period, and a complete time series of 1956-1989 is generated at the $2° \times 2°$ grid. The Z and SST anomalies at each grid point are computed in reference to the 34-year mean value of the month.

A blocking is recognized when the blocking index I at longitude λ is greater than 50m along a longitudinal sector:

$$I(\lambda) = Z(\lambda, 62°N) - Z(\lambda, 46°N)$$

This index was originally introduced by Lejenäs and Økland (1983) and used in Kung *et al.* (1989,1990) with minor modifications. Positive values of I indicate the existence of a quasi-meridional dipole which is formed by a high-pressure cell poleward and a low-pressure area equatorward. The quasi-meridional dipole is a characteristic shared by both diffluent (Rextype, see Rex, 1950) and meridional (Ω-shaped) blockings. In the additional scan for cases of tilted orientation of meridional dipoles and cases of blocking partially out of the chosen latitudinal band, $Z(\lambda \pm 5°, 62°N)$ is substituted for $Z(\lambda, 62°N)$ in computing the blocking index I. The blocking identified by I is verified by manual inspection of the flow pattern. Pacific and Atlantic are the two regions of preferred winter blocking activities in the northern hemisphere. The single dominant blockings in the Pacific and Atlantic are identified by PAC and ATL in this paper. The recurrence of blocking in the Pacific and Atlantic during the same general period constitute the double blocking, and are identified by DBL.

The kinetic energy at wavenumber n, K(n), and the nonlinear transfer of kinetic energy from wavenumber m to wavenumber n, L(n,m), are evaluated in reference to planetary wave activities. Evaluation of K(n) is described in Saltzman (1957) and our previous studies (e.g., Kung and Baker, 1986). The term L(n,m) for an open system, defined by two latitudinal walls and two isobaric surfaces, explicitly incorporates the fluxes across the boundary of the domain. Its evaluation is discussed by Kanamitsu (1980), Kanamitsu *et al.* (1972), and Tsay and Kao (1978). The evaluation in this study follows their formulation (see DaCamara *et al.*, 1991) and is detailed in Dacamara (1991). Since our analysis is based on the single level data at 500 mb, the vertical flux term is not involved in computation.

3. BLOCKING EPISODES AND PATTERNS OF CIRCULATION

Twelve major blocking episodes are selected from the daily analyses of 500 mb flow for the 34-year data period. They include four episodes, each in three categories: PAC, ATL and DBL. These episodes are identified in this paper as P1, P2, P3, P4 for PAC; A1, A2, A3, A4 for ATL; and D1, D2, D3, D4 for DBL. Table 1 lists periods, subperiods, primary locations, and short descriptions of development for each of twelve episodes. Of 108 winter months of the 34-year period, we document only 26 months without noticeable blocking activities (DaCamara *et al.*, 1991). All other months are under the dominance or influence of one of these three types of blocking. Episodes chosen in this study show prominent patterns of blocking circulation. However, they are chosen for their prominence and persistence to study their distinguished characteristics with least interference of secondary features.

As described in Table 1, each episode is a dominant and often recurring circulation pattern during the period. The lengths of periods identified for these episodes are from 25 days to 45 days. Figure 1 shows the time-longitude plots of the daily blocking index for all twelve episodes examined in this study. Initiation, development, decaying and re-enforcement of blocking are identified by manual examination of such time-longitude diagrams. Some subjective judgement is inevitable in identification, but as shown in Figure 1, identification is straightforward. A new blocking occurrence is generally recognized when the contour lines are not connected. It is shown in Figure 1 that the winter blockings in the Pacific and Atlantic are formed over the oceanic area, although they may extend into the continental area. From both Figure 1 and Table 1 it appears that the double blocking events are more intense and persistent than single blockings. However, the Pacific and Atlantic components of double blocking events are not exactly in phase with certain time lags between maxima in the Pacific and Atlantic. This may suggest involvement of traveling planetary waves. It is interesting to note that the persistent blocking episodes involve the recurrence of blocking patterns in the same general locations during the period of episodes. This may suggest the existence of prevailing boundary conditions that favor the development of blocking. The SST anomaly patterns will be examined in this regard later in this paper.

Figures 2, 3 and 4 are the 10-day mean circulation patterns and anomaly fields of Z between 20°N and the pole, for each episode of PAC, ATL and DBL when the blockings are fully developed. The prominence of the Pacific blocking in the northern hemisphere circulation is apparent in Figure 2. As the blocking dominates in the Pacific, the Atlantic is occupied by basically zonal flow. In the Pacific, the anomaly field is characterized by a sharp contrast of negative anomaly area in the south and positive area in the north. During the Atlantic blocking, the patterns in the Pacific and Atlantic are reversed (see Figure 3). During the double blocking the characteristic flow patterns and associated anomaly fields are seen

in both the Pacific and Atlantic. However, examining Figures 2, 3 and 4, it is evident that the regions of blocking activities and contrast of positive and negative anomalies are more extensive in the Pacific than in the Atlantic. If the formation of winter blocking is to be related to SST anomaly pattern, this seems reasonable, since the oceanic area of the Pacific is much more extensive than that of the Atlantic.

Table 1. Selected major episodes of Pacific, Atlantic and double blocking.

Case	Period (day/mo/yr) and Number of days	Subperiod (day/mo)		Primary Location in 42-62°N	Description
P1	22/12/77 –20/1/78 (30days)	22–26/12 27/12–15/1 16–20/1		180–120°W 180–120°W 180–120°W	Developing Rex blocking Fully developed Rex blocking Decaying Omega blocking
P2	7/12/80 –5/1/81 (30days)	7–11/12 12–16/12 17–31/12 1–5/1	(1) (2)	150°E–150°W 150°E–120°W 150°E–120°W 120°E–180° 150°E–150°W	Identifiable Rex blocking Decaying ridge Fully developed Rex blocking Slowly retrograding from (1) to (2) Inverted Omega blocking
P3	27/12/82 –30/1/83 (35days)	27–31/12 1–10/1 11–15/1 16–20/1 21–25/1 26–30/1		180–120°W 150°E–150°W 150°E–150°W 120–90°W 180–120°W 120–90°W	Developing Omega blocking Fully developed Rex blocking Decaying Omega blocking Developing Omega blocking Fully developed Omega blocking Decaying Omega blocking
P4	17/12/83 –20/1/84 (35days)	17–21/12 22–26/12 27–31/12 1–5/1 6–10/1 11–15/1 16–20/1		180–120°W 180–120°W 180–120°W 120–90°W 180–120°W 180–120°W 180–120°W	Omega blocking Fully developed Rex blocking Decaying ridge Developing ridge Developing Omega blocking Fully developed Omega blocking Decaying Omega blocking
A1	26/1– 24/2/66 (30 days)	26–30/1 31/1–4/2 5–14/2 15–19/2 19–24/2		30°W–30°E 60°W–0° 60°W–0° 60°W–0° 60°W–0°	Developing ridge Developing Omega blocking Fully developed Rex blocking Omega blocking Decaying ridge
A2	31/1– 24/2/69 (25 days)	31/1–4/2 5–14/2 15–19/2 19–24/2		60°W–0° 60°W–0° 90–30°W 90–30°W	Developing Rex blocking Fully developed Rex blocking Fully developed Omega blocking Decaying ridge
A3	27/12/71 –20/1/72 (25 days)	27/12–10/1 11/1–15/1 16–20/1		30°W–30°E 30°W–60°E 0–60°E	Fully developed Rex blocking Fully developed Rex blocking Fully developed Rex blocking
A4	11/1– 14/2/79 (35 days)	11–15/1 16/1–4/2 5–14/2	(1) (2)	60°W–0° 60°W–0° 90–30°W 60°W–0°	Developing ridge Fully developed Rex blocking Slowly retrograding from (1) to (2) Fully developed Omega blocking

Table 1. (Continued.)

D1	6/1– 4/2/57 (30 days)	6–10/1	(1) (2)	180–120°W 30°W–30°E	Omega blocking developing in both (1) and (2)
		11–20/1	(1) (2)	180–120°W 30°W–30°E	Fully developed Rex blocking in both (1) and (2)
		21–30/1	(1) (2)	180–120°W 0–60°E	Omega blocking in both (1) and (2)
		31/1–4/2	(1) (2)	180–120W 0–60°E	Decaying Omega blocking in both (1) and (2)
D2	7/12/61 –5/1/62 (30 days)	7–11/12	(1) (2)	180–120°W 30°W–30°E	Developing Omega blocking in both (1) and (2)
		12–21/12	(1) (2)	150°E–150°W 0–60°E	Fully developed Omega blocking in both (1) and (2)
		22–26/12	(1) (2)	120°E–180° 90–60°W	Fully developed Rex blocking in both (1) and (2)
		27–31/12	(1) (2)	120°E–180° 60°W–0°	Omega blocking in both (1) and (2)
		1–5/1	(1) (2)	150°E–150°W 60°W–0	Decaying ridges in both (1) and (2)
D3	22/12/62 –4/2/63 (45 days)	22–26/12	(1) (2)	180–120°W 30°W–30°E	Omega blocking in both (1) and (2)
		27/12–10/1	(1) (2)	150°E–150°W 60°W–0°	Fully developed Rex blocking in (1) and (2)
		11–25/1	(1) (2)	180°–120°W 30°W–30°E	Omega blocking in (1) and Rex blocking in (2)
		26–30/1	(1) (2)	180–120°W 60°W–0°	Fully developed Omega blocking in both (1) and (2)
		31/1–4/2	(1) (2)	150°E–150°W 60°W–0°	Rex blocking in (1) and Omega blocking in (2)
D4	26/1– 29/2/68 (35 days)	26–30/1	(1) (2)	180°–120°W 30°W–30°E	Developing Omega blocking in (1) and developing ridge in (2)
		31/1–4/2	(1) (2)	120°E–180° 60°W–0°	Rex blocking in (1) and Omega blocking in (2)
		5–9/2	(1) (2)	120–90°W 60°W–0°	Omega blocking in both (1) and (2)
		10–19/2	(1) (2)	120–90°W 60°W–0°	Rex blocking in both (1) and (2)
		20–29/2	(1) (2)	120–90°W 30°W–30°E	Omega blocking in (1) and Rex blocking in (2)

Under the dominance of a single blocking in the Pacific or Atlantic, the amplification of the planetary wave n=1 is most obvious in the northern hemisphere circulation (Figures 2 and 3), whereas the amplification of n=2 occurs in the double blocking circulation (Figure 4). This situation may permit the treatment of major winter blockings in the zonal wavenumber domain despite their traditional, synoptic treatment as local manifestations. As the wave-wave interaction of kinetic energy is associated with the amplification of planetary waves, it is pertinent to conjecture that the constructive interference among planetary waves may be a factor for the development of a major winter blocking. Austin (1980) reported that n=1 and 2 tend to interfere constructively in the Atlantic sector, and n=2 and 3 interfere in the Pacific sector. In our preceding study (Kung et al., 1990), it was suggested that during the development of a Pacific blocking in January 1979, n=1 and 2 came in place at the location
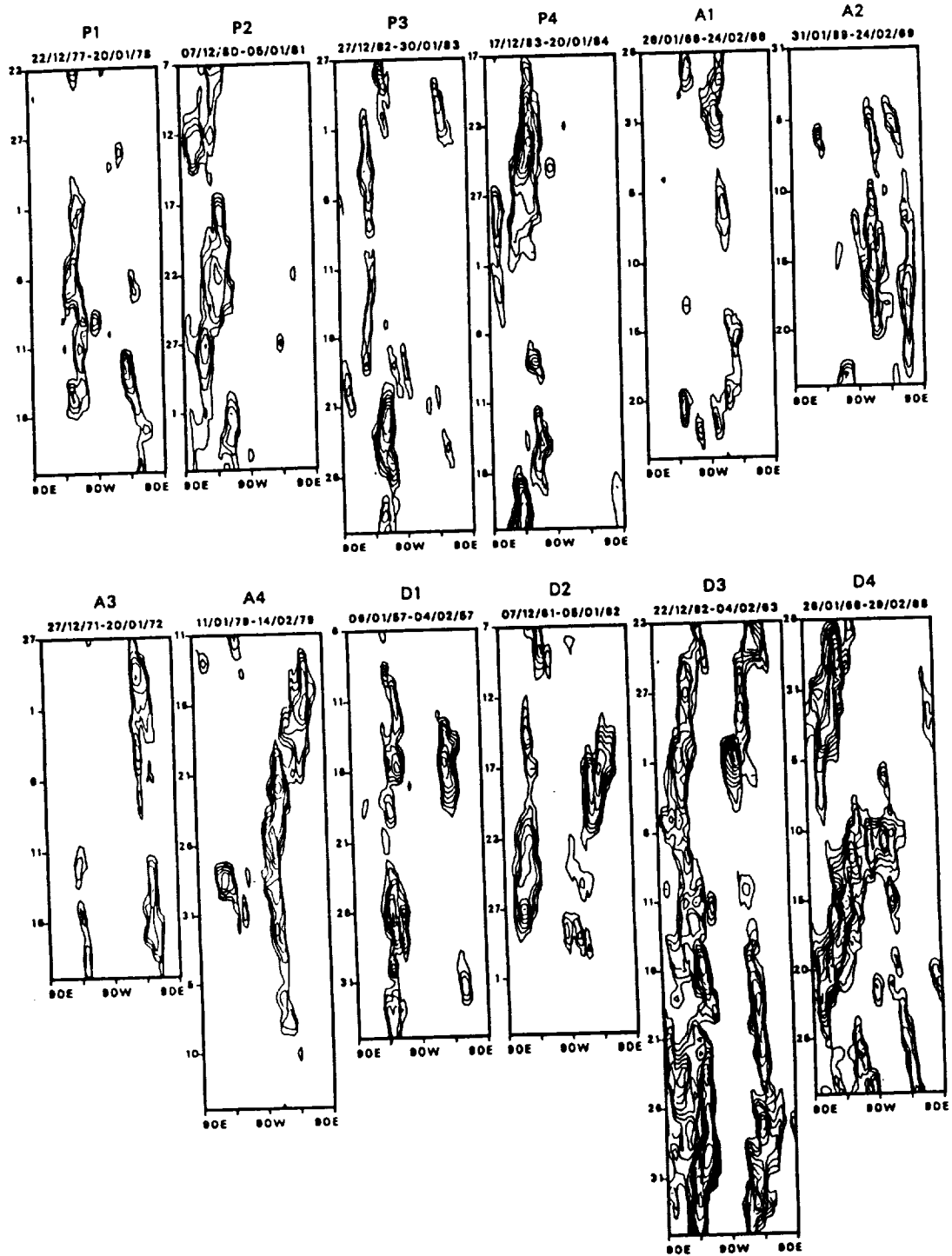
Fig. 1. Time-longitude plots of blocking index for 0 and positive values with contour interval of 50 m.
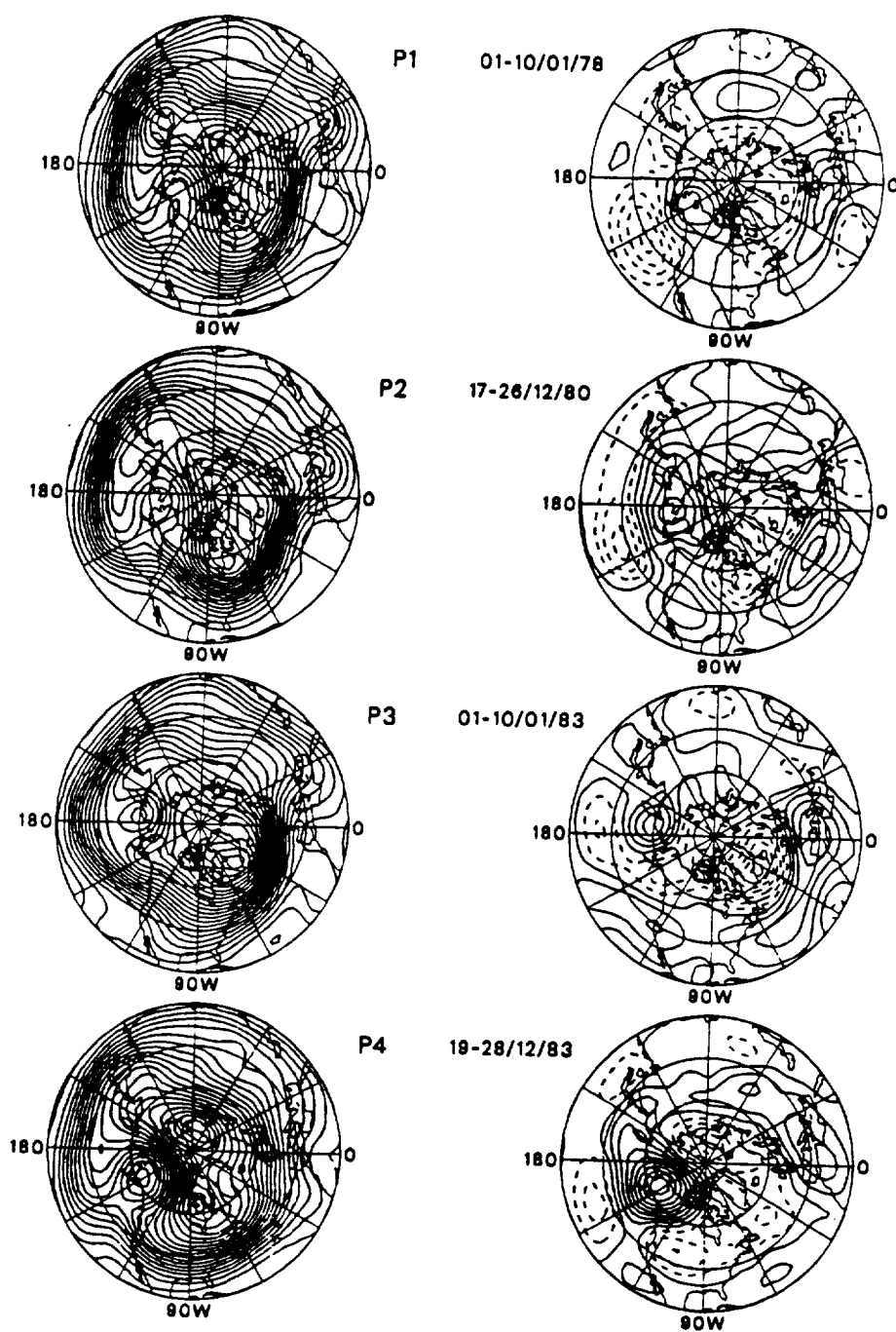
Fig. 2. Patterns of 10-day mean 500 mb circulation and anomaly fields of Z from 20° to 90°N during the fully developed episodes of PAC. The contour interval is 50 m and negative contour lines are dashed.
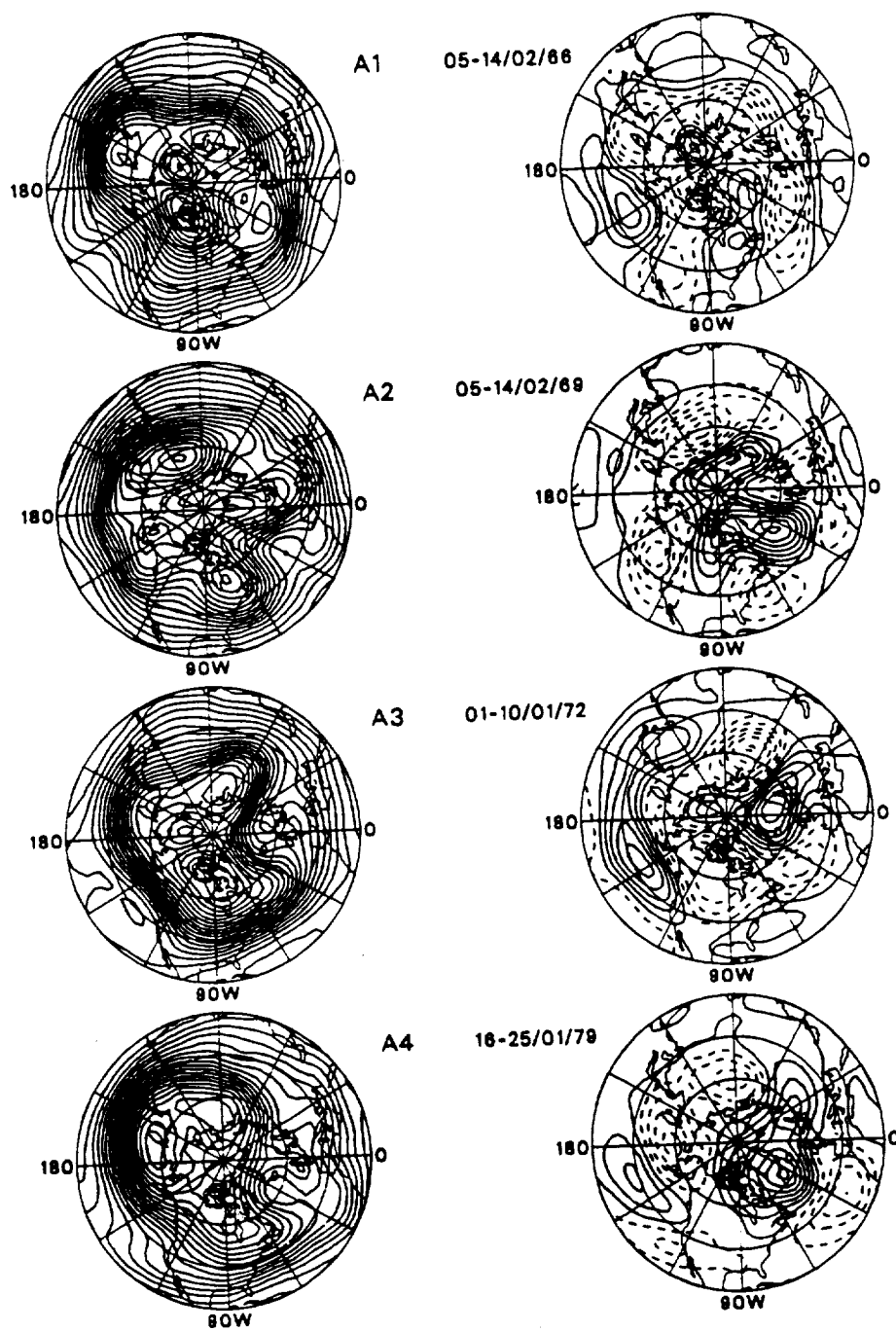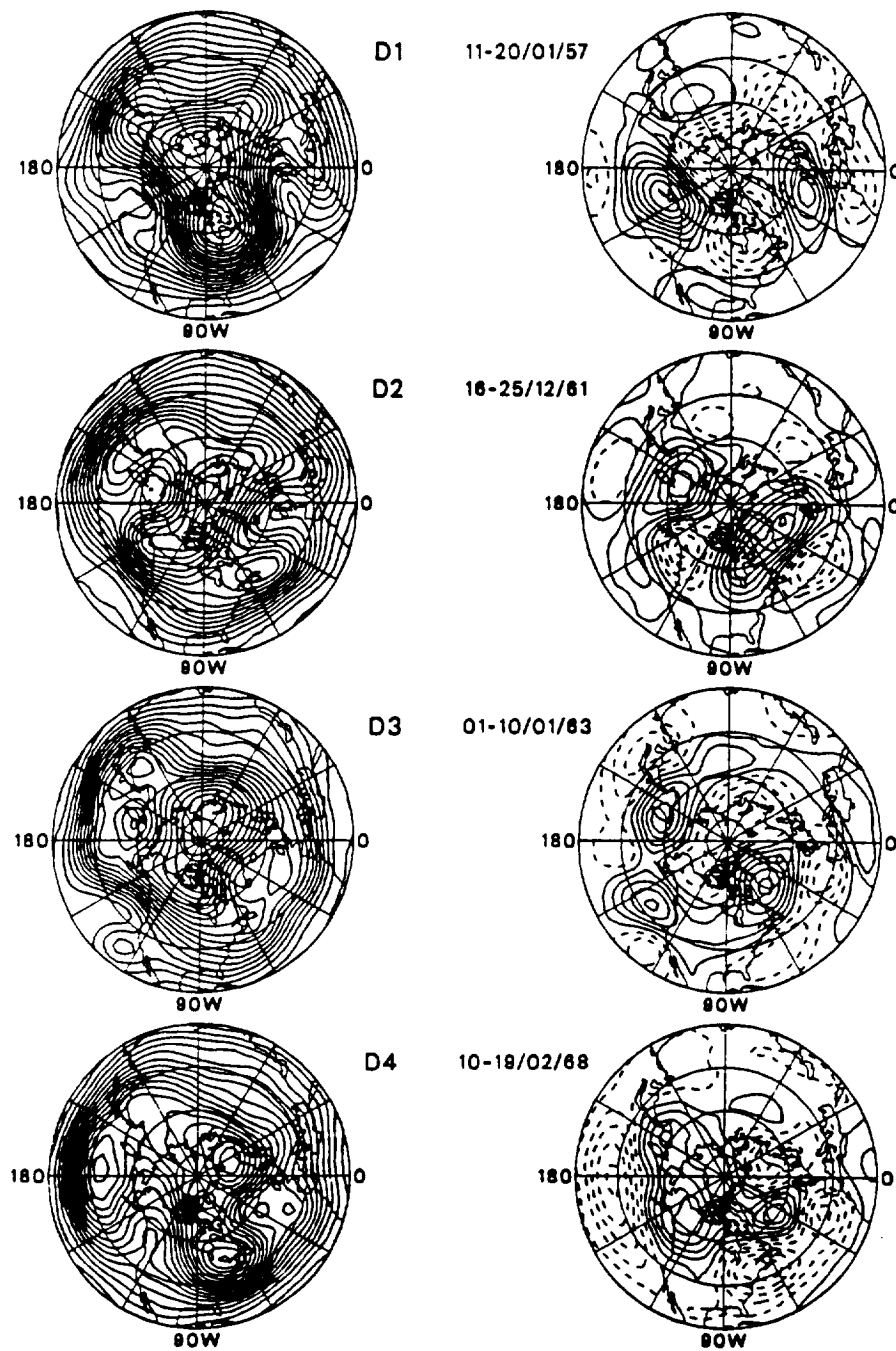
A1   05-14/02/66

A2   05-14/02/69

A3   01-10/01/72

A4   16-25/01/79

Fig. 3. As in Figure 2, but for ATL.

D1　　11-20/01/57

D2　　16-25/12/61

D3　　01-10/01/63

D4　　10-19/02/68

Fig. 4. As in Figure 3, but for DBL.

of the block. Toward the end of the same month the interference of n=1 and 2 in the Atlantic was identified with the development of a major Atlantic blocking.

The interference of n=1 and 2 is confirmed with all episodes selected in this study. Figure 5 demonstrates for one episode in each of three blocking categories the 500 mb trough-ridge diagrams for n=1 and 2 in the 54°-70° band. Although the blocking index is defined between 46° and 62°N to account for the general pattern of circulation, the 54°-70°N
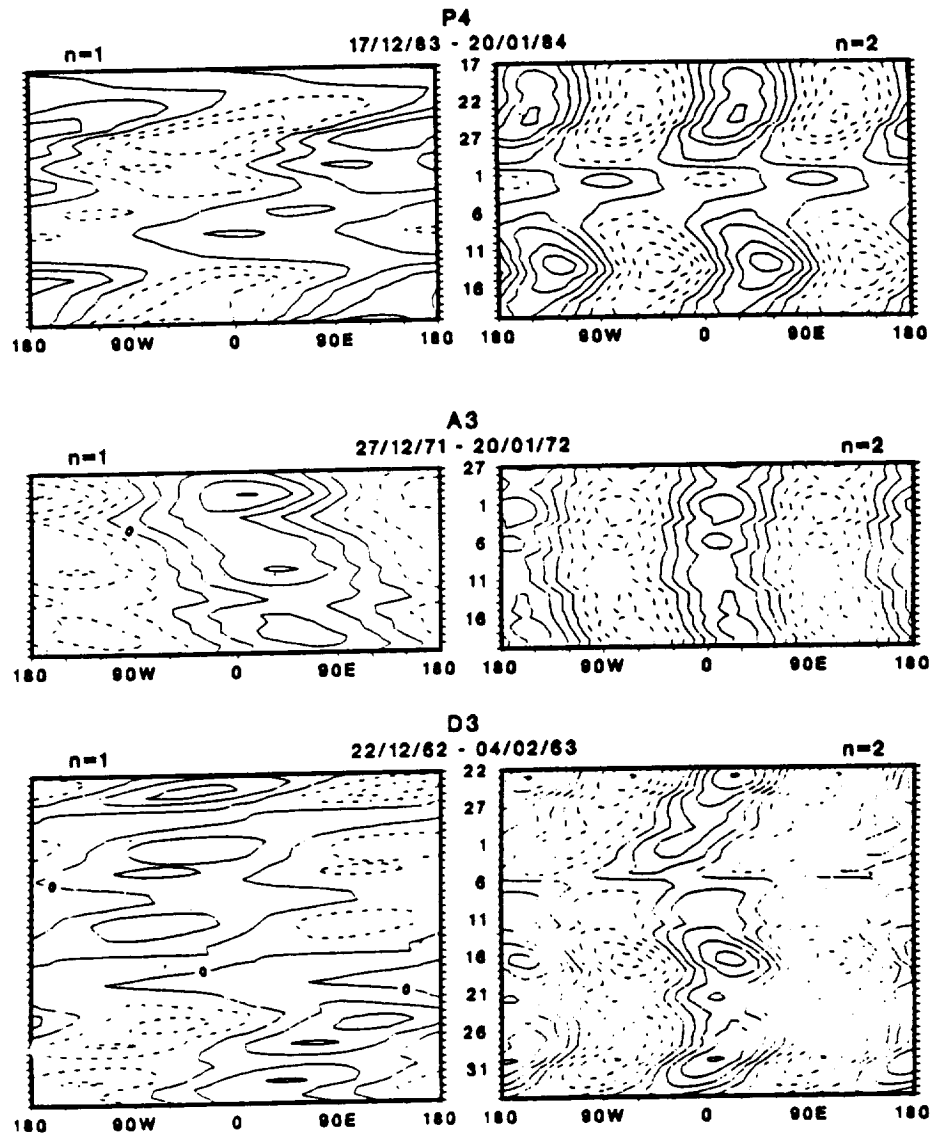
Fig. 5. Trough-ridge diagrams of n=1 and 2 in the 54°-70°N band with 500 mb Z during blocking episodes of P4 (PAC), A3 (ATL) and D3 (DBL). The contour interval is 50 m, and negative contour lines are dashed.

58

band is used in this application because it is the latitudinal band in which the blocking pattern is maximized. It is noteworthy that the primary locations of major blocking episodes (as indicated in Table 1) during the course of blocking development are the longitudinal segments where n=1 and 2 interfere constructively. Madden (1983) found that the interferences of stationary and traveling waves of the same longitudinal scale cause time variations in the large-scale circulation. It is noted in Figure 5 that the positions of n=2 maximum amplitude stay approximately the same in the general area of $0°$ and $180°$ throughout the winter, although the strength of the wave is apparently subject to time variation. On the contrary, the phase angle of n=1, in addition to the amplitude, is variable, indicating that n=1 travels slowly around the northern hemisphere. It is seen here that, when the traveling n=1 constructively interferes with the stationary n=2, the major blocking develops. If n=1 is relatively weak and n=2 is strong, n=2 is responsible for creating the double blocking pattern, as is the case of D3 shown in Figure 5. It is also noteworthy that weakening and redeveloping blocking in the same blocking episodes, as identified in Table 1, correspond with the periodic weakening and amplifying of n=1 and 2.

A comprehensive energetics description is not the purpose of this paper. Neither is it possible with the dataset of this study to compute energy transformations, except for nonlinear interactions at the 500 mb level. Thus only the kinetic energy K and nonlinear transfer L are presented in Figures 6 and 7 to describe characteristic meridional distribution of K(n) for n=1,2 and 3 for PAC, ATL, and DBL episodes and associated L(n,m) in reference to n=1. The characteristics of circulation are first observed by K(n) as kinetic energy and represent the strength of circulation. Examination of L(n) is pertinent for blocking cases, since the development and maintenance of blocking are closely associated with the nonlinear transfer of kinetic energy, which provides the barotropic energy source (Kung and Baker, 1986; Kung *et al.*, 1989). As shown in Figure 6, K(1) of PAC is most pronounced among the three categories of blocking, and is also least unstable from episode to episode. For ATL, K(1) is less pronounced than for PAC, which is consistent with the observation that the Pacific blocking is more dominant than the Atlantic blocking (see Figures 2 and 3). For DBL episodes, K(2) is most pronounced among planetary waves, as expected from the dominance of the n=2 pattern.

The L(1), the input of kinetic energy to n=1 from all other waves, and L(1,2), the input of kinetic energy from n=2 to n=1, are most pronounced for PAC, as seen in Figure 7. This indicates that the traveling n=1 (see Figure 5) has its source at n=2 in forming the Pacific blocking. In the case of DBL, n=1 is also maintained by n=2 through L(1,2), but the magnitude of K(1) is much less than for PAC. For ATL the barotropic energy source of n=1 is not at n=2. An earlier case study of an ATL episode by Kung and Baker (1986) shows that during the development stage of an atlantic blocking n=1 is supported by nonlinear interaction with synoptic scales smaller than n=3. It is also noted in this study, though not shown in Figure 7, for all three categories of blocking situation the wave-wave energy input into n=2 is very small: negative for PAC and ATL and only slightly positive for DBL. Thus the energy source at n=2 should come from the baroclinic conversion, both for the maintenance of n=2 itself and in support of transformation to n=1.

4. SEA SURFACE TEMPERATURE ANOMALIES AND BLOCKING

From the foregoing discussion of planetary wave activities, it may be questioned if the three categories of major winter blocking are associated with different types of energetics forcing. It is generally recognized that the SST anomaly fields exercise a major control over
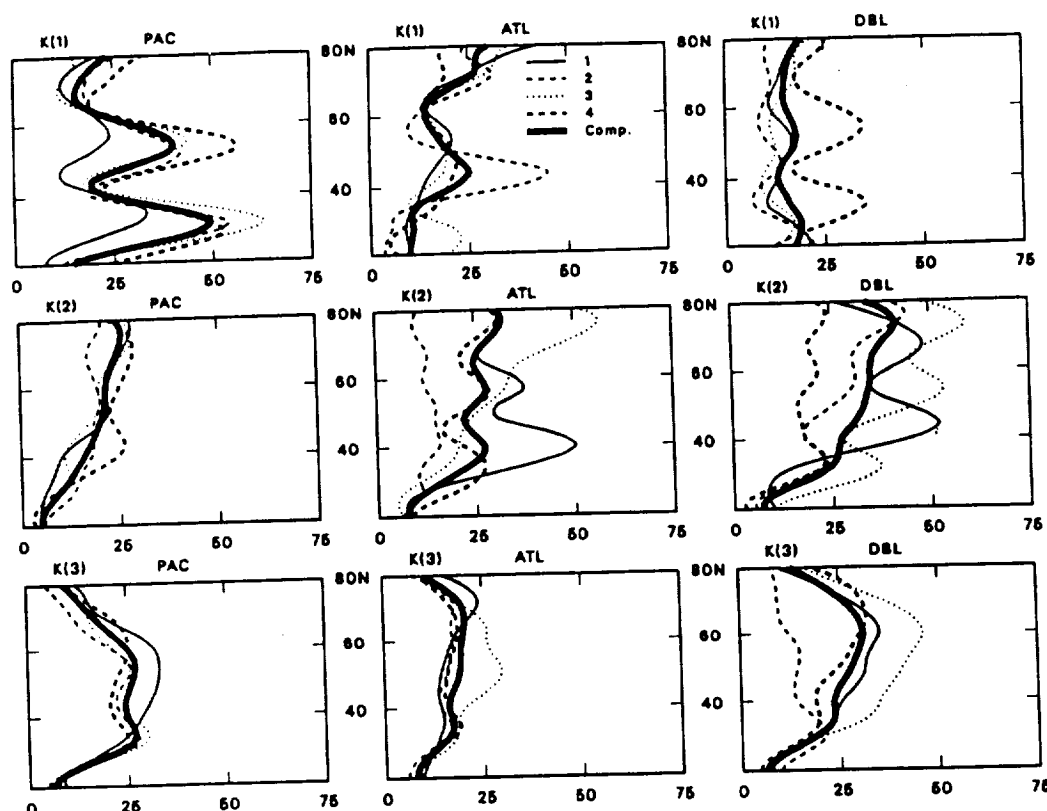
Fig. 6. Meridional distributions of kinetic energy K(n) for n=1, 2 and 3 in units of m^2s^{-2} for four episodes and their mean for PAC, ATL and DBL.

the winter circulation through heat release in the ocean-atmosphere interaction (e.g., Kung et al., 1990; Namias, 1959, 1978; Wallace et al., 1990). The patterns of SST anomalies are examined in reference to the major blocking episodes in this study.

Anomalies of Z and SST are averaged for four episodes in each blocking category, and shown in Figure 8 for the area between 20° and 60°N. Blocking area includes both the positive area of Z anomalies in higher latitudes and negative area in lower latitudes. Because the northern boundary of the area in the figure is 60°N, the positive anomalies of Z in the higher latitudes are only partially shown for blocking episodes (see Figures 2,3, and 4). Yet the sharp contrast of positive Z anomalies in the north and negative anomalies in the south are well recognized in the Pacific for PAC, in the Atlantic for ATL, and in both Pacific and Atlantic for DBL. It is noted that the areas of blocking both in the Pacific and Atlantic tend to appear in lower latitudes for DBL than for PAC and ATL.

In Figure 8, it is evident that PAC episodes are associated with the generally negative SST anomalies in the middle-latitude Pacific and western Atlantic. For ATL episodes the negative anomalies of SST are found in the middle-latitude Atlantic and eastern Pacific. However, the negative anomalies found in the average pattern of ATL in Figure 8 are not as distinctive as the negative anomalies for PAC. Yet, as shown in Figure 9, SST anomalies of individual ATL episodes are as distinct as those of PAC episodes. As the location of the
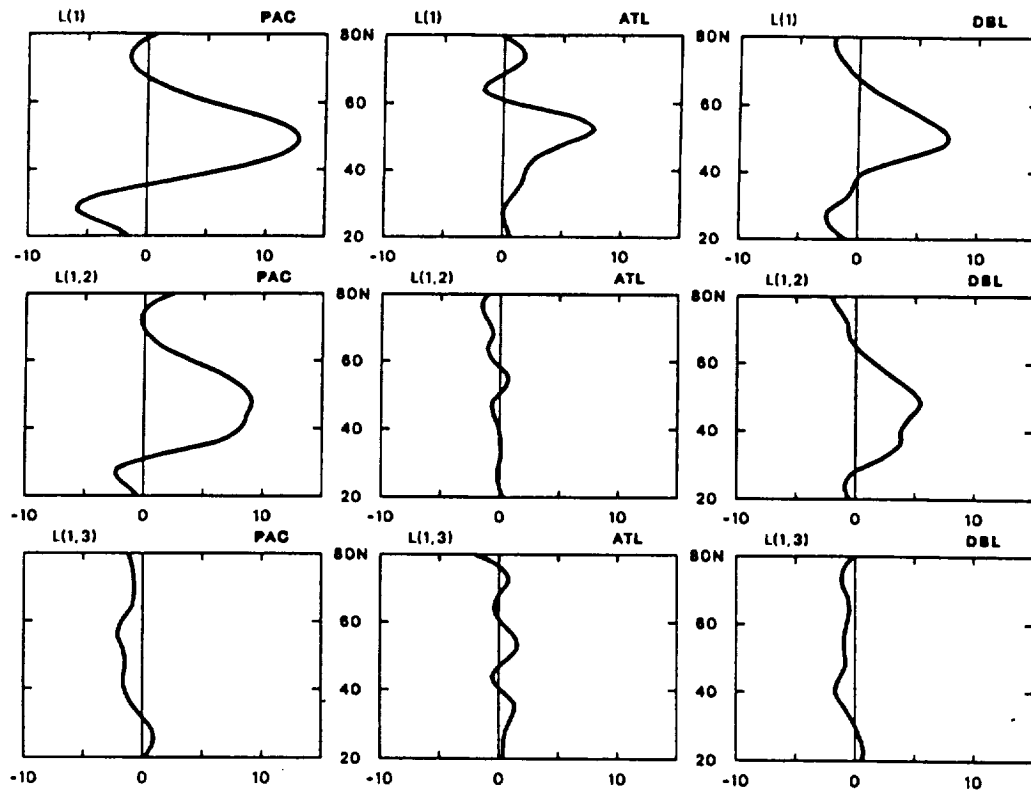
Fig. 7. Meridional distributions of kinetic energy input at n=1 by nonlinear wave-wave interaction L(1), and its component from n=2 and 3, L(1,2) and L(1,3), in units of $10^{-5} m^2 s^{-3}$ for composites of PAC, ATL and DBL.

negative Atlantic SST anomalies is more variable than for PAC episodes, the average pattern becomes less distinct. This seems to be related with the fact that the circulation pattern of ATL episodes is more variable than that of PAC episodes, as evident in the circulation patterns of Figures 2 and 3 and latitudinal distributions of K(1) and K(2) in Figure 6. Comparing the PAC and ATL episodes, it is apparent that general negative SST anomalies in the Pacific and Atlantic favor the development of major single blocking in the Pacific. When the negative pattern is limited to the Atlantic and part of the Pacific, with positive anomalies in the Pacific, a single blocking is likely to develop in the Atlantic.

The SST anomalies of DBL in Figures 8 and 9 show definitive positive patterns in most areas of the Pacific and Atlantic. This is a sharp contrast with SST anomaly patterns in PAC and ATL situations where the negative SST anomalies are associated with dominant single blocking. It is noted in the preceding section that the double blocking situation is developed and maintained by the stationary n=2 (Figure 5). The dominant n=2 should be supported by the baroclinic energy source since no barotropic energy is available for n=2 through nonlinear wave-wave interaction. The positive SST anomalies associated with DBL indeed indicate that the double blockings are developed with in situ warming of the northern hemisphere
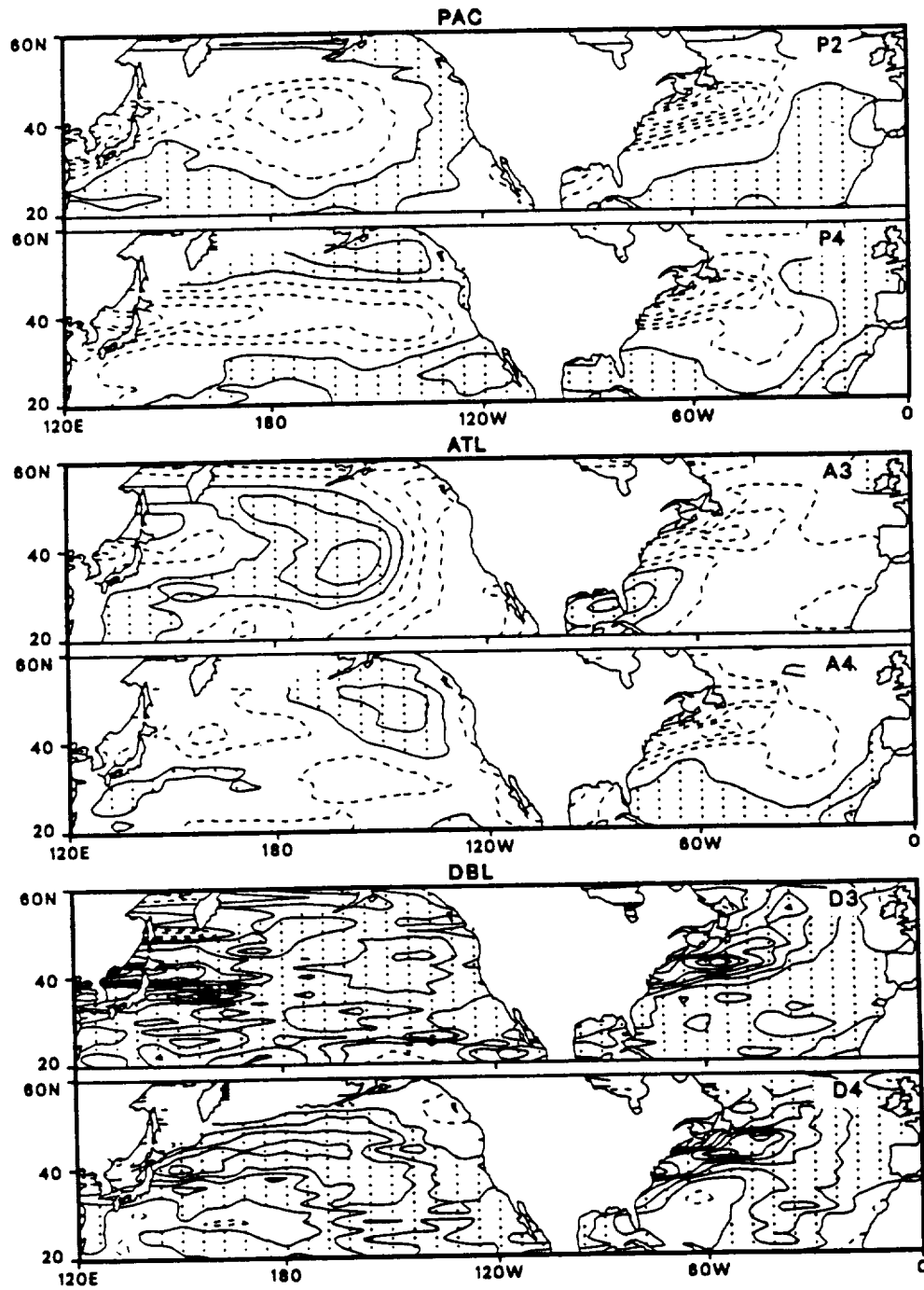
Fig. 8. Anomaly patterns of 500 mb Z and SST for composites of episodes for PAC, ATL and DBL. The contour interval is 50 m for Z and 0.5°C for SST. Negative contour lines are dashed.

62
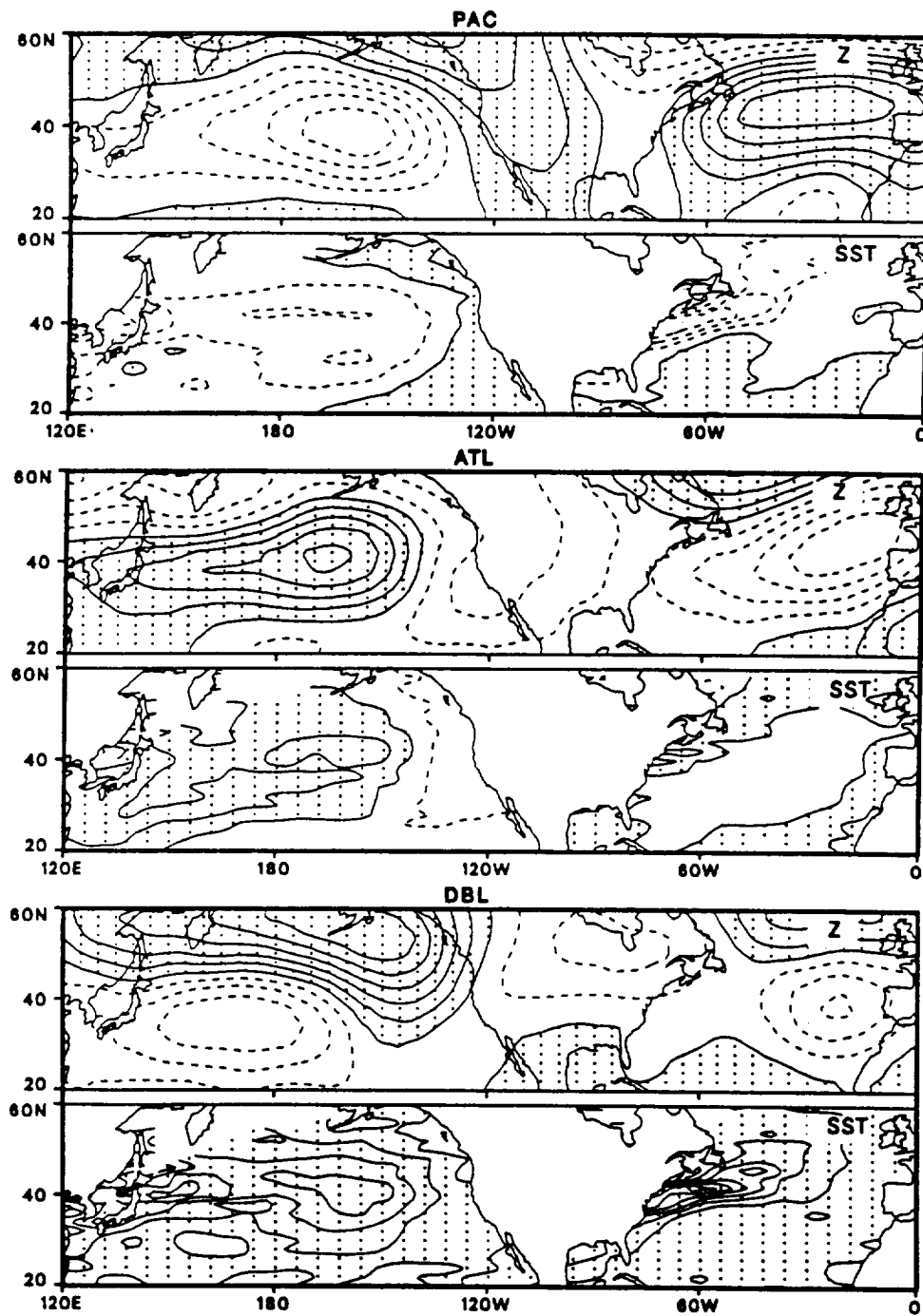
Fig. 9. Anomaly patterns of SST associated with blocking episodes of PAC (P2 and P4), ATL (A3 and A4) and DBL (D3 and D4). The contour interval is 0.5°C, and negative contour lines are dashed.

circulation. The negative SST anomalies associated with PAC and ATL then can be interpreted to favor the nonlinear wave-wave interaction to maintain the traveling n=1 that couples existing n=2 to form a single blocking pattern. The distinct energetics difference of single and double blocking patterns shown by these cases are interesting. The prominent double blocking pattern is baroclinic in nature whereas the occurrence of single major blocking depends on the barotropic nonlinear process of energy input.

5. CONCLUDING REMARKS

Because of the long characteristic time of SST variation and consequent persistence of blocking pattern, the study of blocking in relation with SST anomalies may have relevance in the long-range forecasting of the northern hemisphere winter circulation. With twelve prominent blocking episodes during the 34-year data period, this study has shown that the major single blockings in the northern hemisphere winter circulation are developed in the Pacific or Atlantic trough constructive interference of traveling n=1 and stationary n=2. The former is supported by the nonlinear wave-wave interaction of kinetic energy, and the latter by the in situ warming over the Pacific and Atlantic. The double blockings situation in the Pacific and Atlantic is formed by n=2 when the traveling n=1 is weak. These planetary wave activities are seemingly associated with the accompanying SST anomaly patterns during these major blocking episodes. The negative SST anomalies of the Pacific and Atlantic are associated with PAC and ATL, whereas the in situ warming in both the Pacific and Atlantic is associated with DBL.

For the purpose of focusing on prominent major blocking situations, the approach taken in this study is that of case examination with only twelve major blocking episodes. As such, the results discussed only apply to major blocking episodes studied in this paper, and cannot be generalized to other blocking circulations. However, the results of this case study may offer useful information in considering the formation and maintenance of the northern hemisphere winter blockings. At present, a composite diagnosis of all winter blocking episodes during the 1956-1991 period is in progress in terms of planetary wave activities and will be reported subsequently.

REFERENCES

Austin, J. G. 1980: The blocking of middle latitude westerly winds by planetary waves. *Quart. J. Roy. Meteor. Soc.,* **106**, 327-350.

Berggren, R., B. Bolin, and C. G. Rossby, 1949: An aerological study of zonal motion, its perturbation and breakdown. *Tellus,* **1**, 14-37.

64

DaCamara, C. C. 1991: Planetary wave activities and energetics in the Northern Hemisphere winter circulation, Ph. D. thesis, 105 pp, University of Missouri-Columbia, (Available from UMI Dissertation Services, 300 N. Zeeb Rd., Ann Arbor, MI 48106-1346).

DaCamara, C. C., E. C. Kung, W. E. Baker, B.-C. Lee, and J. A. M. Corte-Real, 1991: Long term analysis of planetary wave activities and blocking circulation in the Northern Hemisphere winter. *Beit. Phy. Atmos.*, **64**, 285-278.

Elliot, R. D., and T. B. Smith, 1949: A study of the effects of large blocking highs on the general circulation in the Northern Hemisphere. *J. Meteor.*, **6**, 67-85.

Green, J. S. A. 1977: The weather during July 1976: Some dynamical considerations of the drought, *Weather*, **32**, 120-126.

Hansen, A. R., and T. C. Chen, 1982: A spectral energetics analysis of atmospheric blocking. *Mon. Wea. Rev.*, **108**, 1146-1165.

Hansen, A. R., and A. Sutera, 1984: A comparison of the spectral energy and enstrophy budgets of blocking versus nonblocking periods. *Tellus*, **36A**, 52-63.

Holloway, G., and B. J. West, (Eds.) 1984: Predictability of Fluid Motions. American Institute of Physics, 612 pp.

Illari, L. 1984: Diagnostic study of the potential vorticity in a warm blocking anticyclone. *J. Atmos. Sci.*, **41**, 3518-3526.

Kanamitsu, M. 1980: Some climatological and energy budget calculations using the FGGE III-b analyses during January 1979. Dynamic Meteorology, L. Bengtson, M. Ghil, and E. Källen, Eds., Springer-Verlag, N. Y., 263-361 .

Kanamitsu, M., T. N. Krishnamurti, and C. Depradine, 1972: On scale interactions in the tropics during Northern summer. *J. Atmos. Sci.*, **29**, 698-706.

Kung, E. C., and W. E. Baker, 1986: Spectral energetics of the observed and simulated Northern Hemisphere general circulation during blocking periods. *J. Atmos. Sci.*, **43**, 2792-2812.

Kung, E. C., H. L. Tanaka, and W. E. Baker, 1989: Energetic examination of winter blocking simulations in the Northern hemisphere. *Mon. Wea. Rev.*, **117**, 2019-2040.

Kung, E. C., C. C. DaCamara, W. E. Baker, J. Susskind, and C.-K. Park, 1990: Simulations of winter blocking episodes using observed sea surface temperatures. *Quart. J. Roy. Meteor. Soc.*, **116**, 1053-1070.

Lejenäs H., and H. Økland 1983: Characteristics of Northern Hemisphere blocking as determined from a long time series of observational data. *Tellus*, **35A**, 350-362.

Madden, R. A. 1983: The effects of the interference of traveling and stationary waves on time variations of the large-scale circulation. *J. Atmos. Sci.*, **40**, 1110-1125.

Murakami, T., and K. Tomatsu, 1965: Energy cycle in the lower atmosphere. *J. Meteor. Soc. Japan*, **43**, 73-89.

Namias, J. 1959: Recent seasonal interactions between North Pacific waters and the overlying atmospheric circulation. *J. Geophys. Res.*, **64**, 631-646.

Namias, J. 1978: Multiple causes of the North American abnormal winter 1976-77. *Mon. Wea. Rev.*, **106**, 279-295.

Paulin, G. 1970: A study of the energetics of January 1959. *Mon. Wea. Rev.*, **98**, 795-809.

Rex, D. 1950: Blocking action in the middle troposphere and its effect upon regional climate. I. An aerological study of blocking action. *Tellus*, **2**, 196-211.

Reynolds, R. W. 1988: A real-time global sea surface temperature analysis. *J. Climate*, **1**, 75-86.

Saltzman, B. 1957: Equations governing the energetics of the larger scales of atmospheric turbulence in the domain of wavenumber. *J. Meteor.*, **14**, 513-523.

Saltzman, B., and A. Fleisher, 1959: On the maintenance of the large-scale quasi-permanent disturbances in the atmosphere. *Tellus*, **11**, 425-431.

Saltzman, B., R. Benzi, and A. G. Wiin-Nielsen, (Eds.) 1986: Anomalous Atmospheric Flows and Blocking. Vol. 29. Advances in Geophysics. Academic Press. 459 pp.

Shukla, J. 1981: Dynamical predictability of monthly means. *J. Atmos. Sci.*, **38**, 2547-2572.

Shutts, G. J. 1983: The propagation of eddies in different jet streams: Eddy vorticity forcing of blocking flow fields. *Quart. J. Roy. Meteor. Soc.*, **109**, 737-761.

Slutz, R. J., S. J. Lubker, J. D. Hiscox, S. D. Woodruff, R. L. Jenne, D. H. Joseph, P. M. Steurer, and J. D. Elms, 1985: COADS, Comprehensive Ocean-Atmosphere Data Set Release 1, 262 pp, (Available from NOAA Climate Research Program, Environmental Research Laboratories, Boulder, CO 80303).

Tanaka, H. L., and E. C. Kung, 1988: Normal mode energetics of the general circulation during the FGGE year. *J. Atmos. Sci.*, **45**, 3723-3736.

Tanaka, H., E. C. Kung, and W. E. Baker, 1986: Energetics analysis of the observed and simulated general circulation using three-dimensional normal mode expansion. *Tellus*, **38A**, 412-428.

Tsay, C.-Y., and S.-K. Kao, 1978: Linear and nonlinear contributions to the growth and decay of the large-scale atmospheric waves and jet stream. *Tellus*, **30**, 1-13.

Wallace, J. M., C. Smith, and Q. Jiang, 1990: Spatial patterns of atmosphere-ocean interaction in the northern winter. *J. Climate*, **3**, 990-998.

Vakalyuk, Y. 1985: The blocking of the middle latitude circulation: capability of its investigation based on FGGE data. *GARP Special Report*, **42**, I 90-95.

4.4 <u>Large-Scale Modes of Variations in the Global Sea</u>
<u>Surface Temperatures and Northern Hemisphere</u>
<u>Tropospheric Circulation</u>

ERNEST C. KUNG and JONQ-GONG CHERN

University of Missouri-Columbia
Columbia, Missouri 65211   USA

and

JOEL SUSSKIND

Laboratory for Atmospheres
Goddard Space Flight Center/NASA
Greenbelt, Maryland 20771   USA

April 1994

1. Introduction

It is well recognized that the ocean surface provides a major boundary forcing to the general circulation of the atmosphere through the process of ocean-atmosphere heat transfer. A systematic investigation of the sea surface temperature (SST) anomalies in reference to the tropospheric circulation is thus a desired step toward better understanding of climatic fluctuations. This study is one such attempt by means of principal component analysis to identify prevailing modes of variations in SSTs and the tropospheric circulation.

The utility of the principal components, which are also referred to as empirical orthogonal functions or eigenvectors, in analyzing the large-scale variations of the circulation field has been demonstrated by Kutzbach (1967, 1970), Kidson (1975a,b), Weare et al. (1976), Weare (1977), Barnett (1978), Heddinghaus and Kung (1980), Trenberth and Paolino (1981), Kawamura (1984, 1986), Park and Kung (1988) and others. One goal of such an analysis is to reduce a large number of variables into a manageable set of components, while retaining the maximum variance of the original variables, enabling us to concisely describe patterns of interrelationship among observed variables. In the analysis of highly correlated meteorological fields, a limited number of principal components may effectively represent the fundamental modes of variations which are highly loaded on these components. It is important to note that the empirical orthogonal functions have no predetermined forms, and only depend on the interrelationship within the dataset of analysis. Thus, they are particularly suitable to investigate anomalous fields of the general circulation, for which no known analytical form exists because of complex boundary conditions and various scales of nonlinear interactions.

In this study, pattern vectors and time coefficients are obtained for major principal components of monthly mean fields of the global SSTs and the Northern Hemisphere geopotential height Z(m) at 700, 500 and 300 mb. Variances of intra-annual seasonal variations are eliminated by defining the anomaly fields of monthly means in reference to the long-term means of individual months for the entire data period from 1955 to 1992. The characteristics of the first three components of SST fields are identified and discussed. The quality of SST data changes significantly during the data period because of the availability of satellite observations in the later years. The heterogeneity of data in time series is examined, and its elimination is considered. The intra-annual seasonal variations of SSTs are also presented with principal components of long-term means of twelve individual months. The association of SST components and Z components is studied on the basis of inter-annual variations of these components. Cross-correlations of SST components with the observed Z fields are further studied to examine the seasonal-range predictability of the tropospheric circulation in reference to SST anomalies.

2. Data and scheme of analysis

Datasets utilized in this study include monthly global SST analyses for the period of 1955-92, and daily northern hemisphere Z analyses at 700, 500 and 300 mb for the same period. Monthly SST analyses were obtained from two different sources: the Comprehensive Ocean-Atmosphere Data Set (COADS) (Slutz et al. 1985) for the period of 1955-79 and the NMC SST real-time analyses (Reynolds 1988) for the period of 1970-92. Both analyses are on 2°x 2° latitude-longitude grids, but the grid points of two analyses are staggered. The consistency of both analyses was verified for the overlapping period of 1970-79, and the COADS analysis of 1958-69 was interpolated on the grid points of the Reynolds analysis to make a complete time series of 1955-92. Missing data points in early COADS analysis were interpolated in space from the surrounding grid points. The SST data were used for the oceanic areas between 40°S to 60°N. The monthly Z fields were computed from the daily National Meteorological Center (NMC) Northern Hemisphere octagonal grid analyses at 1500 GMT from 1955-57, and at 1200 GMT for the rest of the period.

The general mathematical procedures for computation of orthogonal pattern vectors and their coefficients are as provided in Kutzbach (1967). The grid values of monthly mean fields are standardized to zero mean and unit variance so that each grid point can have normalized significance in describing the spatial variation. As stated in the introduction, the anomaly fields are obtained with respect to the multi-annual means of respective monthly mean fields for the study of inter-annual variations. This allows for the elimination of the seasonal cycle. On the other hand, the intra-annual seasonal cycle is presented by subjecting the multi-annual means of 12 individual months to principal component analysis. The variable matrix, which

70

has normalized departures from time means, is used to compute the corresponding correlation matrix, whose elements are the correlation between grid points. The eigenvectors of such a correlation matrix represent a set of normalized departure fields. The eigenvectors are not rotated in order to retain the maximum variance in the first few components (see Walsh and Richman 1981). The characteristic pattern vector is described as the eigenvector multiplied by the standard deviation of its corresponding principal component. Thus, characteristic patterns represent the simple correlations between respective components and meteorological fields.

Most of the available principal component analyses of large-scale meteorological fields indicate that the first three components are sufficient to describe the large-scale variations (e.g., Kutzbach 1970; Weare et al. 1976; Weare 1977; Park and Kung 1988). As discussed by Overland and Preisendorfer (1982), it is important to determine if the principal components obtained in the analysis are statistically significant, so that the geophysical interpretation of results will be meaningful. As shown in pattern vectors of major components (Figs. 2, 4, 5, 6 and 7), large-scale characteristic patterns are described mostly by large correlation coefficients of |0.4| to |0.8|, which are significant at the 98 to 99.9% confidence level for the time period of datasets. The higher components also show some significance in limited areas, but the level of significance in large areas drops sharply. In this paper, the discussion is limited to the first three components.

3.   Principal components of SST fields

The inter-annual variations of coefficients of 1st principal components of January and July SSTs for the period of 1955-92, as shown in Fig. 1, indicate a large gap at 1970. This phenomenon is also observed in all other months. If the SST data for the period of 1970-92 are subjected to principal component analysis, the 1st and 2nd components of the new time series match almost exactly with the 2nd and 3rd components of the original 1955-92 time series. The discontinuity of the 1955-92 data at 1970 in the 1st principal component is important as the 1st component contributes 18% of the total variance, and is larger than any other component's contribution. This gap indicates a major systematic difference of SST data before and after (including) 1970, most likely reflecting both the inclusion of satellite data and a different scheme of analysis in NMC data from that in earlier COADS records.

In this study, the original 1st component in the 1955-92 dataset is disregarded, and the 2nd, 3rd and 4th components are treated as the true 1st, 2nd and 3rd component of the 1955-92 period. The principal components to be discussed hereafter refer to the true components after elimination of the original 1st component as a systematic bias. This is justified by the near exact match of the 1st and 2nd components of the 1970-92 dataset with the 2nd and 3rd components of the 1955-92 datasets. Since we are only interested in the first few major components, small-scale variations that are associated with the original 1st component, other than the gap at 1970, do not enter into the picture and can be ignored.

Figure 2 shows the pattern vectors for the first three components of January and July SSTs, and their corresponding coefficients are shown in

72

Fig. 3. The percentage variances of the first five components out of the total 35 components, listed in Table 1, indicate a comparable contribution of the first few components with previously available principal component analyses (see citations in Section 2). The pattern vectors of the 1st components, as shown in Fig. 2, represent the largest-scale spatial variation in the Pacific and Atlantic. The variation in the northwest-southeast direction is conspicuous in the Pacific with a maximum positive area in the tropical region. The 2nd component shows a well defined positive area in the eastern tropical Pacific, which is similar to the 1st component previously obtained in the regional analyses of the Pacific SSTs (e.g., Weare 1986; Weare et al. 1976). Much of the other areas in the Pacific and Atlantic are negative, contrasting the large positive areas of the 1st component. The 3rd component shows variations in the Pacific and Atlantic in the northwest-southeast direction. The pattern vectors beyond the 3rd component show a localized, fragmental pattern, and are not included in our discussion of large-scale SST variations.

It is apparent that the pattern vectors of the 2nd component represent the El Niño-Southern Oscillation (ENSO) type of SST anomalies. Since the 1st component also has a general positive area in the central and eastern tropical Pacific, it is interesting to examine the time variations of these two components. As marked for January SSTs in Fig. 3, the prominent ENSO winters of 1957-58, 1965-66, 1972-73, 1976-77, 1982-83 and 1991-92 are characterized by the amplification of both 1st and 2nd components in phase. The combined coefficients of the 1st and 2nd components in Fig. 3 are weighted means by the respective percentage variances as listed in Table 1. In cases of the moderate to weak ENSO winters, either the 1st or 2nd component is amplified,

but not both of them in phase. The following summer of an ENSO winter is not necessarily associated with the ENSO type SST anomalies. When the 1st and 2nd principal components are reversed following the ENSO winter (see Fig. 3), the southeastern Pacific is occupied by extensive negative areas. Such is the case for July 1964, 1973, and 1988 when negative SST anomalies developed in this area.

When we subject the long-term (1955-92) SST means of the 12 months of the year to the principal component analysis, we obtain pattern vectors and time variations of coefficients as shown in Fig. 4 for the 1st and 2nd components. The variation of pattern vectors are concentrated in the tropical latitudes, and the time variations of both the 1st and 2nd components reflect the time scale of seasonal variations. Comparing the pattern vectors of 4 separate months in Figs. 2 and 5, it is seen that basic patterns of 3 principal components seem to hold throughout the year, but are subject to the seasonal changes which are not negligible in terms of strength and local modification. The intra-annual seasonal variations presented in Fig. 4 should be considered when the persistence of prevailing SST anomalies is to be projected. The pattern vectors of January and July, as shown in Fig. 2, are modified between winter and summer to exhibit spring and fall patterns, as shown in Fig. 5 for April and October.

4.   Principal components of the Northern Hemisphere circulation

Pattern vectors of the first three components of the Northern Hemisphere circulation in terms of January and July Z fields are shown in Figs. 6, 7 and 8 respectively at the 700, 500 and 300 mb levels. A similarity in pattern is observed through the troposphere from 700 mb to 300 mb, and the 2nd component shows the best similarity at all three levels with "centers of action" in the same quadrants. These centers of action are stable and dominant, and consistent with the generally recognized winter flow patterns. As the first two components of winter Z fields determine the general pattern of the winter Northern Hemisphere flow, it is also noted in Table 1 that the contribution of percentage variance in the winter flow by the 2nd Z component is much greater than those by the 2nd components in SST and summer Z. The 3rd component, among the first three components, shows the more localized patterns, which is a generally observed character of higher components in the principal component analysis.

When the July patterns are compared to the January patterns in Fig. 6-8, it is apparent that the patterns of all summer components are weakened at all levels, and the scale of dominant patterns becomes generally small. The distinguished patterns of the 2nd and 3rd components in winter become fragmented in summer with the sharpest contrast at 500 mb. However, components in summer show general consistency at different levels. The contrast between the summer and winter patterns merely reflects the difference between the dominant winter circulation and the significantly weakened summer circulation in the Northern Hemisphere.

Explicit association of physical processes with separate components of the circulation fields is beyond the scope of the principal component

analysis. However, because of the lower boundary forcing of SSTs, it is useful to examine the correlations between components of SSTs and Z fields. Table 2 lists the correlation coefficients between the first three components of SSTs in January, April, July and October, and those of monthly Z fields at 700, 500 and 300 mb during the period of 1955-92. The correlation coefficient |0.35| is significant at the 95% level, and |0.44| at the 99% level. In Table 2 it is evident that the 1st SST component is strongly correlated with the 1st Z component. The correlation is large at 300 mb and 500 mb throughout the year, particularly at 300 mb. However, at 700 mb it is limited to the winter season. In other words, the 1st components of SSTs with the Z components is more significant in the upper troposphere than in the lower troposphere. The correlation of the 2nd and 3rd SST components with Z components is generally low. Although some sporadic correlations exist in the table, they do not indicate an organized pattern of correlation. According to the correlations in Table 2, only the 1st SST component shows a significant, persistent correlation with the 1st Z component in the mid and upper troposphere.

As the 1st and 2nd SST components seem to determine the occurrence of ENSO events (Fig. 3), it will be interesting to examine if the principal components of the upper-air circulation show a specific ENSO mode as in SSTs. Figure 9 illustrates the composite 700 mb and 500 mb flow pattern and anomaly fields for the prominent ENSO January months of 1958, 1966, 1973, 1977, 1983, and 1992. The 700 mb anomaly field resembles the pattern vectors of the 2nd principal component of the January 700 mb field (Fig. 6), and the 500 mb anomaly field shows a similarity to the pattern vectors of the 3rd principal component of the January 500 mb field. It is noted, however, that the inter-annual variations of such principal components are not clearly associated with

winter ENSO occurrence. The situation is thus different from that of the time

variations of SST components in association with ENSO occurrence (see Fig. 3).

Although SSTs show a clear large-scale mode of boundary forcing in ENSO

winters, the responding upper-air circulation does not show such clear ENSO

components. The anomalous circulation patterns, as often reported for ENSO

winters, seem to be modifi-

cations to the basic field of circulation rather than dominant specific large-

scale patterns.

5. Cross-correlation patterns

In a lag-correlation analysis, Kawamura (1986) demonstrated that time coefficients of the first component of the monthly mean North Pacific SST tends to lead the 500 mb Z in the extratropical latitudes. The lead time is up to 12 months or more, depending on the month of SST. Park and Kung (1988) showed that the SST anomalies for preceding seasons in the North Pacific are closely related to the first component of surface temperatures in North America in the following summer. The latter determines the summer temperature in the midwestern and mid-Atlantic United States. It is possible that the principal components of SST fields may be useful in the long- (seasonal-) range empirical forecast.

Figures 10, 11 and 12, respectively, illustrate the cross-correlation patterns between the 1st, 2nd and 3rd principal components of January SSTs and the January, April and July anomaly fields of 500 mb and 300 mb Z. All three SST components are well correlated to the 500 mb and 300 mb Z field of the same month, January. The contour spacing is 0.2, and the correlation in the figure is significant at 90, 95, 99 and 99.5% with the coefficients of $|0.28|$, $|0.33|$, $|0.42|$ and $|0.45|$. In April, with a lead time of 3 months, all three SST components show similarities with January flow patterns. Some variations from the January patterns, particularly the strengthening of the 2nd component correlation in April is noted. The correlations become weaker and more fragmented in July, apparently reflecting the weaker and more fragmented circulation patterns of the summer. However, the centers of action as recognized in earlier months in Pacific, Atlantic, North America and Eurasia are still traceable.

78

Comparing cross-correlations of January SST components with 500 mb and 300 mb flow patterns in Figs. 10-12, it is noted that the characteristic correlation patterns, as observed with 500 mb fields, are identified in 300 mb Z fields in terms of both spatial distribution and strength of cor-relation coefficients. This suggests that the response of tropospheric circulation to SST anomaly fields is consistent in the mid and upper troposphere.

The cross-correlation patterns of the 1st, 2nd and 3rd principal components of July SSTs with the July, October and January 500 mb and 300 mb Z fields are illustrated in Figs. 13, 14 and 15. The cross-correlation patterns observed in July carry through October and January. The patterns observed in 500 mb are also clearly observed in 300 mb. One clear distinc-tion from the January SST cross-correlation is the strong correlation pattern of July SSTs with January 500 mb and 300 mb Z fields with a lead time of at least 6 months. It is also noteworthy that the cross-correlation with the January Z fields is stronger than with the October Z fields. These reflect strong winter circulation patterns, and also indicate a useful seasonal-range predictability of winter upper-air circulation patterns with the anomaly fields of summer SSTs.

6. Concluding remarks

As stated in the introduction, the purpose of this paper is to identify prevailing modes of variations in SSTs and the tropospheric circulation. The results obtained in this study offer useful information in further diagnosis of the SST and circulation fields, and also the utilities of the SST anomaly field in seasonal-range forecasting of the tropospheric circulation. The principal component analysis of monthly mean fields of the global SSTs and the Northern Hemisphere tropospheric circulation for the 38-year period as presented in this study seems to yield the following specific information:

1.   A change in the source of SST data results in a large systematic bias in a long-term SST dataset. However, the bias may be effectively corrected if an appropriate principal component is identified and eliminated from the dataset.

2.   Periods of strong ENSO correspond to both the 1st and 2nd SST components being in phase.

3.   The first few principal components of monthly SST and Z fields are sufficient to describe the SST and tropospheric circulation patterns.

4.   Basic patterns of the first three principal components of SSTs remain similar throughout the year, but are subject to seasonal changes, which are not negligible.

5.   The first SST component is strongly correlated with the first component of tropospheric Z field.

6.   Cross-correlations of SST components with the tropospheric circulation suggest a useful predictability of the tropospheric circulation in reference to SST anomalies. The lead time observed in this study is up to 6 months for the winter circulation in reference to summer SSTs.

Acknowledgments

81

REFERENCES

Barnett, T.P., 1978: Estimating variability of surface air temperature in
   the Northern Hemisphere. Mon. Wea. Rev., 106, 1353-1367.

Heddinghaus, T.K., and E.C. Kung, 1980: An analysis of climatological
   patterns of the Northern Hemispheric circulation. Mon. Wea. Rev.,
   108, 1-17.

Kawamura, R., 1984: Relation between atmospheric circulation and dominant
   sea surface temperature anomaly patterns in the North Pacific during
   the northern winter. J. Meteor. Soc. Japan, 62, 910-916.

Kawamura, R., 1986: Seasonal dependency of atmosphere-ocean interaction
   over the North Pacific. J. Meteor. Soc. Japan, 64, 363-371.

Kidson, J.W., 1975a: Eigenvector analysis of monthly mean surface data.
   Mon. Wea. Rev., 103, 177-186.

Kidson, J.W., 1975b: Tropical eigenvector analysis and the Southern
   Oscillation. Mon. Wea. Rev., 103, 187-196.

Kutzbach, J.E., 1967: Empirical eigenvectors of sea-level pressure, surface
   temperature and precipitation complexes over North America. J. Appl.
   Meteor., 6, 791-802.

Kutzbach, J.E., 1970: Large-scale features of monthly mean Northern
   Hemisphere anomaly maps of sea-level pressure. Mon. Wea. Rev., 98,
   708-716.

Overland, J.E., and R.W. Preisendorfer, 1982: A significant test for
   principal components applied to cyclone climatology. Mon. Wea. Rev.,
   110, 1-4.

Park, C.-K., and E.C. Kung, 1988: Principal components of the North American summer temperature field and antecedent oceanic and atmospheric conditions. <u>J. Meteor. Soc. Japan</u>, 66, 667-690.

Reynolds, R.W., 1988: A real-time global sea surface temperature analysis. <u>J. Climate</u>, 1, 75-86.

Slutz, R.J., S.J. Lubker, J.D. Hiscox, S.D. Woodruff, R.L. Jenne, D.H. Joseph, P.M. Steurer, and J.D. Elms, 1985: COADS, Comprehensive Ocean-Atmosphere Data Set. Release 1, 262 pp. [Available from NOAA Climate Research Program, Environmental Research Laboratories, Boulder, CO 80303.]

Trenberth, K.E., and D.A. Paolino, 1981: Characteristic patterns of variability of sea level pressure in the Northern Hemisphere. <u>Mon. Wea. Rev.</u>, 109, 1169-1189.

Walsh, J.E., and M.B. Richman, 1981: Seasonality in the associations between surface temperatures over the United States and the North Pacific Ocean. <u>Mon. Wea. Rev.</u>, 109, 767-783.

Weare, B.C., 1977: Empirical orthogonal analysis of Atlantic Ocean surface temperature. <u>Quart. J. Roy. Meteor. Soc.</u>, 103, 467-478.

Weare, B.C., A.R. Navato, and R.E. Newell, 1976: Empirical orthogonal analysis of Pacific sea surface temperature. <u>J. Phys. Oceanogr.</u>, 6, 671-678.

Table 1. Percentage variance of the first five principal components
during the period of 1955-92.

Component	SST		Z(700mb)		Z(500mb)		Z(300mb)	
	Jan.	July	Jan.	July	Jan.	July	Jan.	July
1	17.1	12.2	17.5	17.1	17.7	20.0	20.0	22.1
2	7.4	8.6	15.5	9.9	13.0	8.7	13.2	12.0
3	5.6	5.5	9.3	8.9	10.3	8.5	8.9	7.0
4	5.0	5.2	8.7	7.3	9.0	6.8	7.6	5.8
5	4.4	4.9	6.4	5.9	6.3	5.6	6.7	5.0
Total	39.5	36.4	57.4	49.1	56.3	49.6	56.4	51.9

Table 2. Correlation coefficients between principal components of monthly SSTs and principal components of monthly Z fields at 700, 500 and 300 mb during the period of 1955-92.

SST(1st)	January			April			July			October		
Z	Jan	Feb	Mar	Apr	May	Jun	Jul	Aug	Sep	Oct	Nov	Dec
700 mb												
(1st)	-.48	-.63	-.60	-.53	.25	.44	-.28	-.34	.22	-.06	-.29	.51
(2nd)	.46	.03	-.19	-.06	-.45	.24	-.27	.02	.43	.62	-.19	.09
(3rd)	-.18	.11	-.20	-.35	.40	-.24	-.04	.50	.13	.43	.31	.05
500 mb												
(1st)	-.36	-.55	.48	-.49	.43	-.61	-.45	-.45	.24	-.26	-.12	-.51
(2nd)	-.43	-.04	-.18	-.23	-.01	.24	-.08	.15	-.13	.08	-.04	.12
(3rd)	.09	-.05	-.23	-.18	-.24	-.17	.13	.13	.06	-.47	.56	.12
300 mb												
(1st)	.56	.71	.75	.65	.75	-.84	.64	.60	.61	.34	.25	.49
(2nd)	.22	-.15	.16	.18	.17	.14	-.17	-.05	.11	.13	-.23	.04
(3rd)	-.21	-.16	.12	-.18	.25	-.01	.05	-.19	.09	.36	.42	-.05

SST(2nd)	January			April			July			October		
Z	Jan	Feb	Mar	Apr	May	Jun	Jul	Aug	Sep	Oct	Nov	Dec
700 mb												
(1st)	-.27	-.46	-.19	.17	.02	.03	-.20	-.06	.02	-.06	-.16	.02
(2nd)	.20	-.05	-.08	.37	.17	-.11	.20	.06	-.30	.20	-.29	.18
(3rd)	.01	-.29	.08	.15	-.09	-.16	-.02	-.01	.17	.08	.05	-.23
500 mb												
(1st)	-.06	-.22	.04	-.01	.01	-.02	-.33	-.34	.19	.35	.21	.00
(2nd)	-.11	-.10	-.07	.34	-.07	.06	.04	.09	.42	-.04	-.21	-.33
(3rd)	.45	.49	.00	-.33	-.15	-.03	-.27	.17	-.10	-.18	-.10	.07
300 mb												
(1st)	.09	.23	.12	-.15	-.22	.21	.25	.39	.26	-.19	-.11	.06
(2nd)	-.01	.11	.13	-.25	.04	.12	-.13	-.14	-.03	.02	-.09	-.34
(3rd)	.05	.44	.11	-.26	.25	.14	.43	-.04	.43	-.11	-.01	.04

SST(3rd)	January			April			July			October		
Z	Jan	Feb	Mar	Apr	May	Jun	Jul	Aug	Sep	Oct	Nov	Dec
700 mb												
(1st)	-.32	.11	.03	.24	-.32	-.03	-.03	-.00	-.20	.15	-.19	.23
(2nd)	-.61	.02	-.01	-.01	-.29	.40	.43	.08	-.04	-.21	-.20	.00
(3rd)	-.01	.04	.30	-.35	.11	.18	-.18	-.34	-.26	-.13	.01	-.18
500 mb												
(1st)	-.26	.04	.11	.28	-.42	.14	-.16	-.18	.17	.08	-.02	-.19
(2nd)	.64	.04	-.04	-.05	.05	-.22	.01	-.25	.12	-.16	-.23	-.15
(3rd)	-.03	-.17	.18	-.08	.25	-.13	-.27	-.17	.09	-.03	.19	.04
300 mb												
(1st)	-.04	-.22	-.08	-.17	-.24	.04	-.09	-.22	-.29	-.05	-.01	.12
(2nd)	-.66	-.04	-.04	.12	.03	-.05	.07	-.28	-.03	.11	.17	-.23
(3rd)	-.01	-.20	.01	.01	-.18	-.07	-.04	-.01	.17	.08	.15	.17

zero and positive, and broken lines for negative.

Fig. 11 As in Fig. 10, but for the second January SST component.

Fig. 12 As in Fig. 10, but for the third January SST component.

Fig. 13 Cross-correlation patterns of coefficients of the first July SST component and 500 mb and 300 mb Z fields in July, October and January.

Fig. 14 As in Fig. 13, but for the second July SST component.

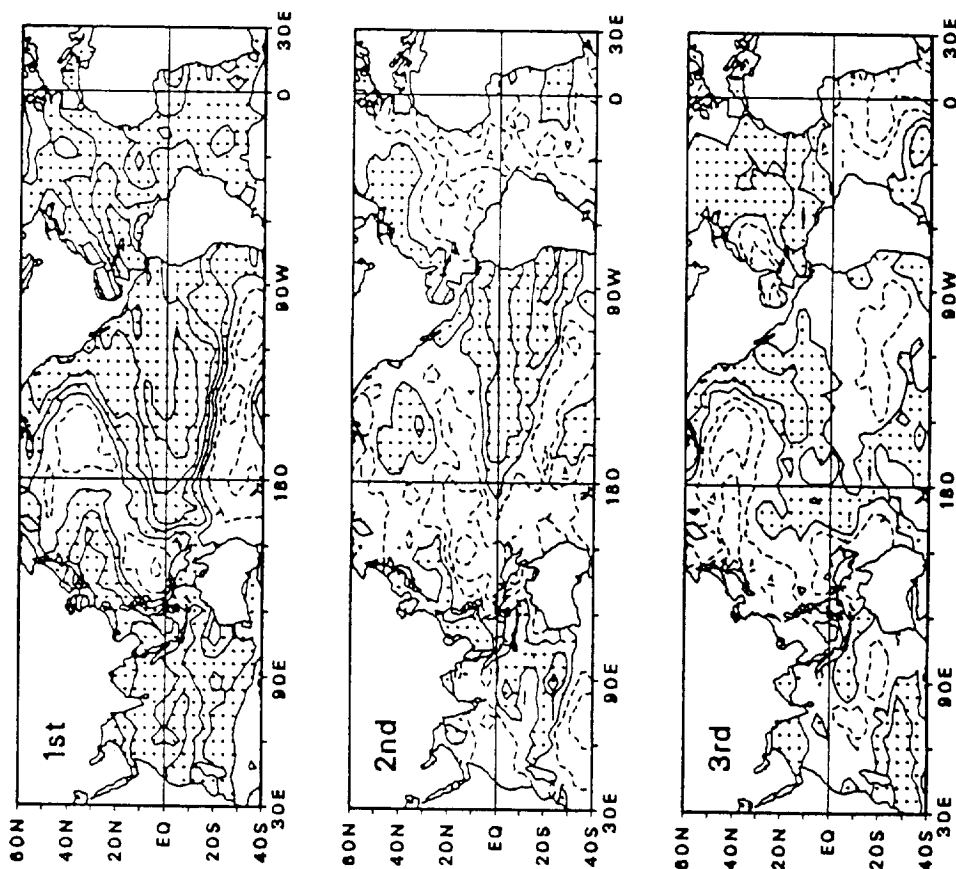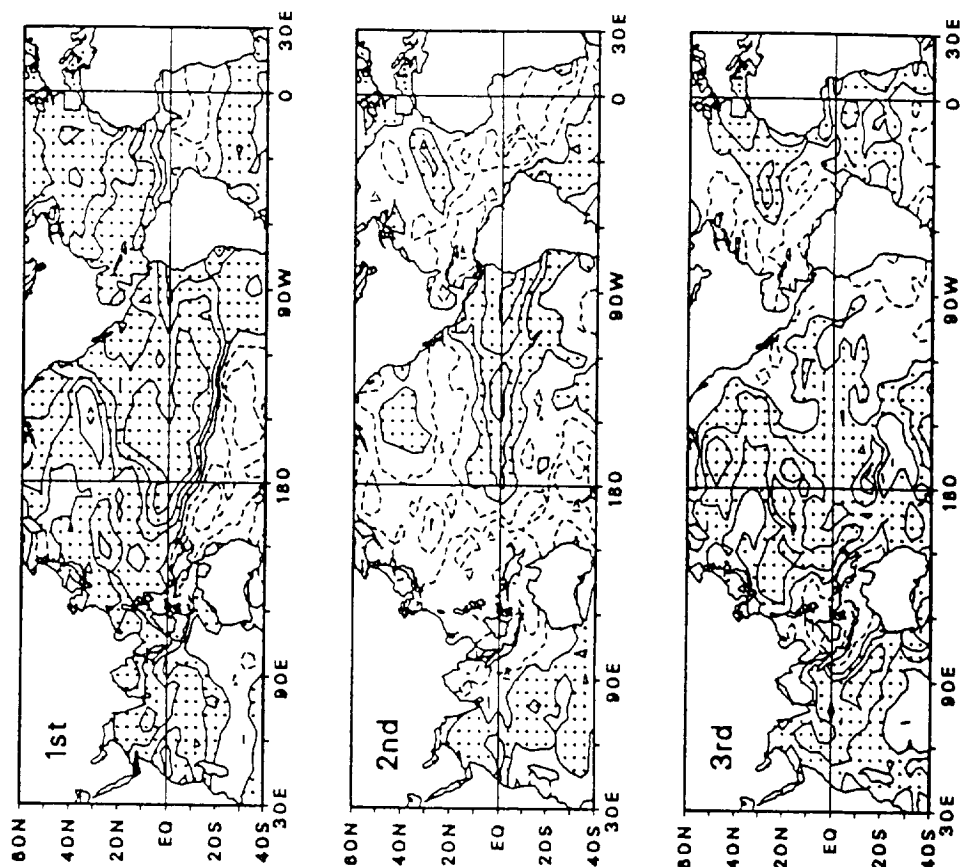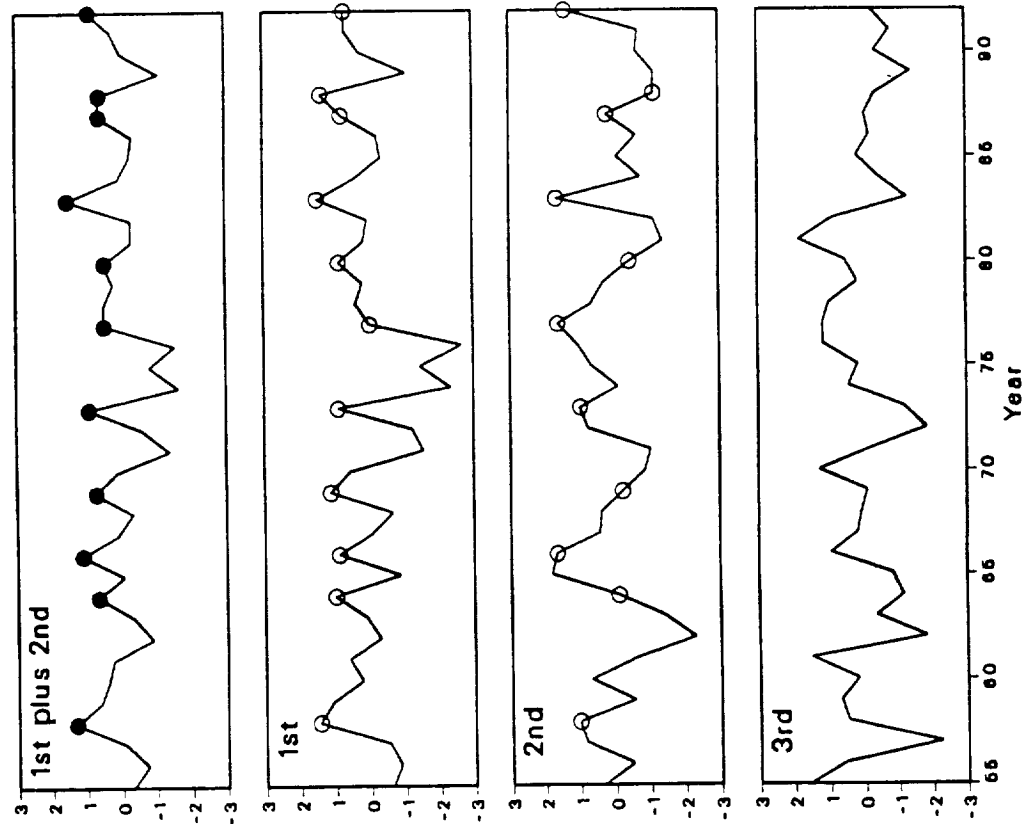Fig. 15 As in Fig. 13, but for the third July SST component.
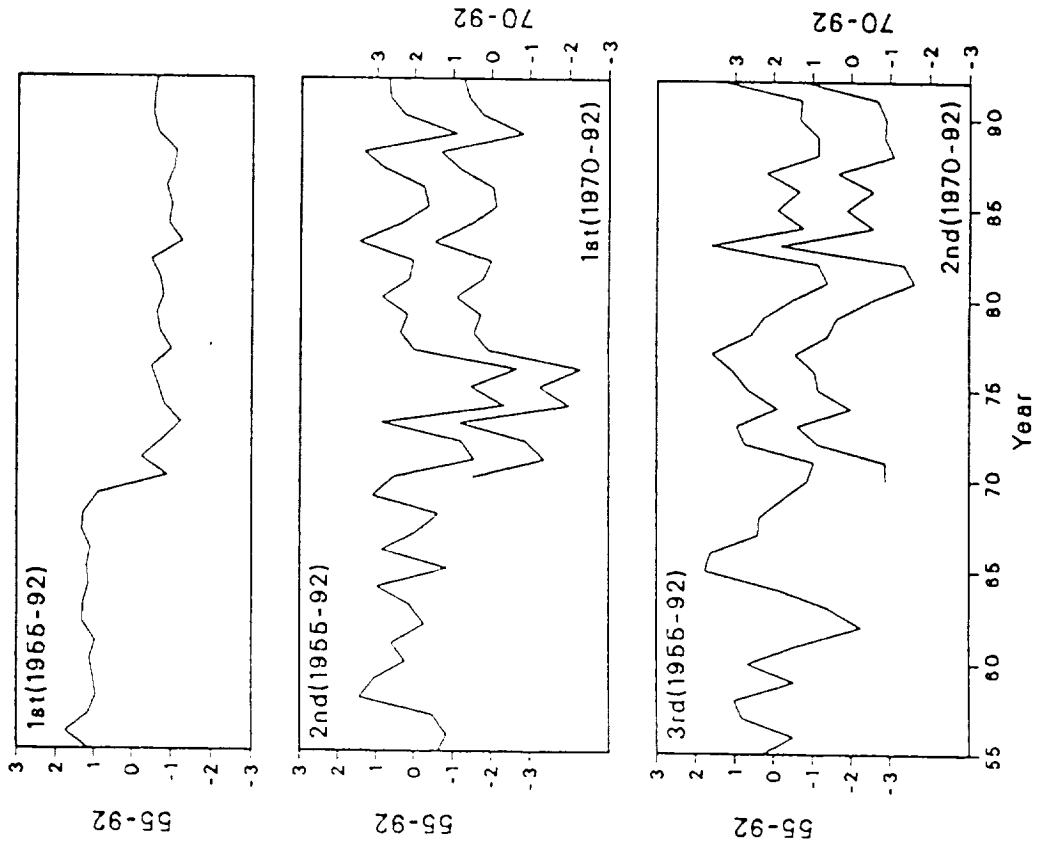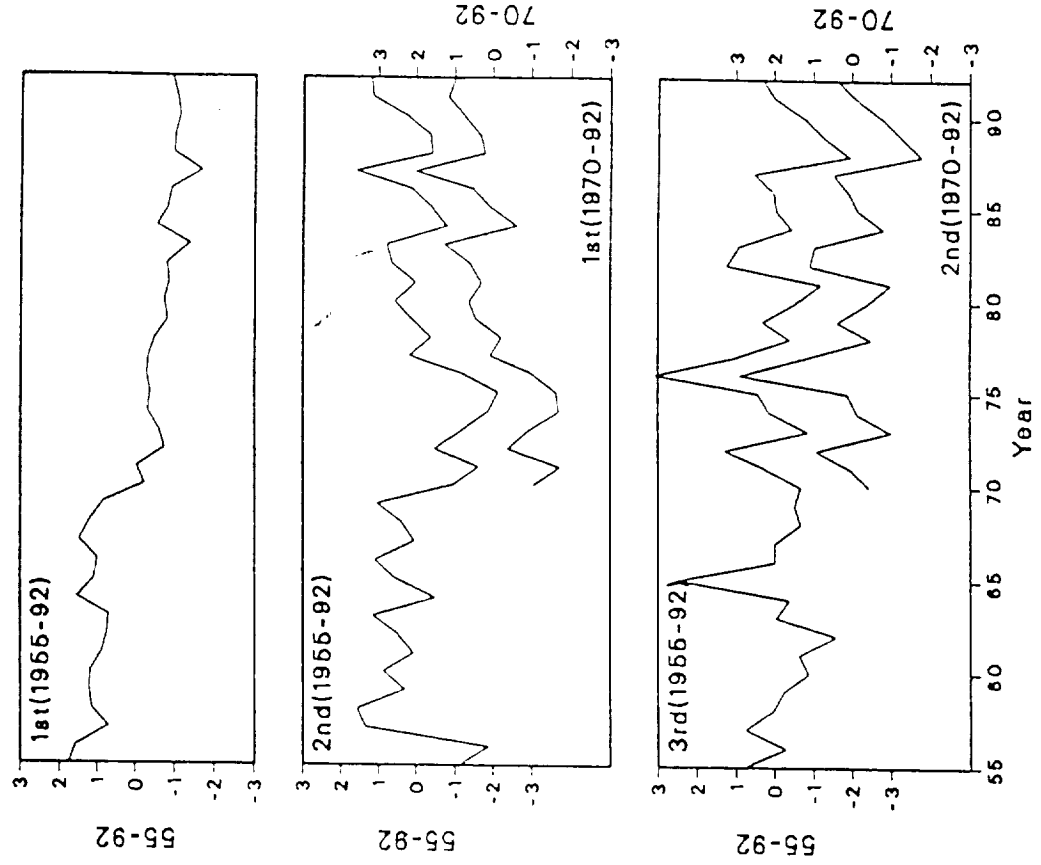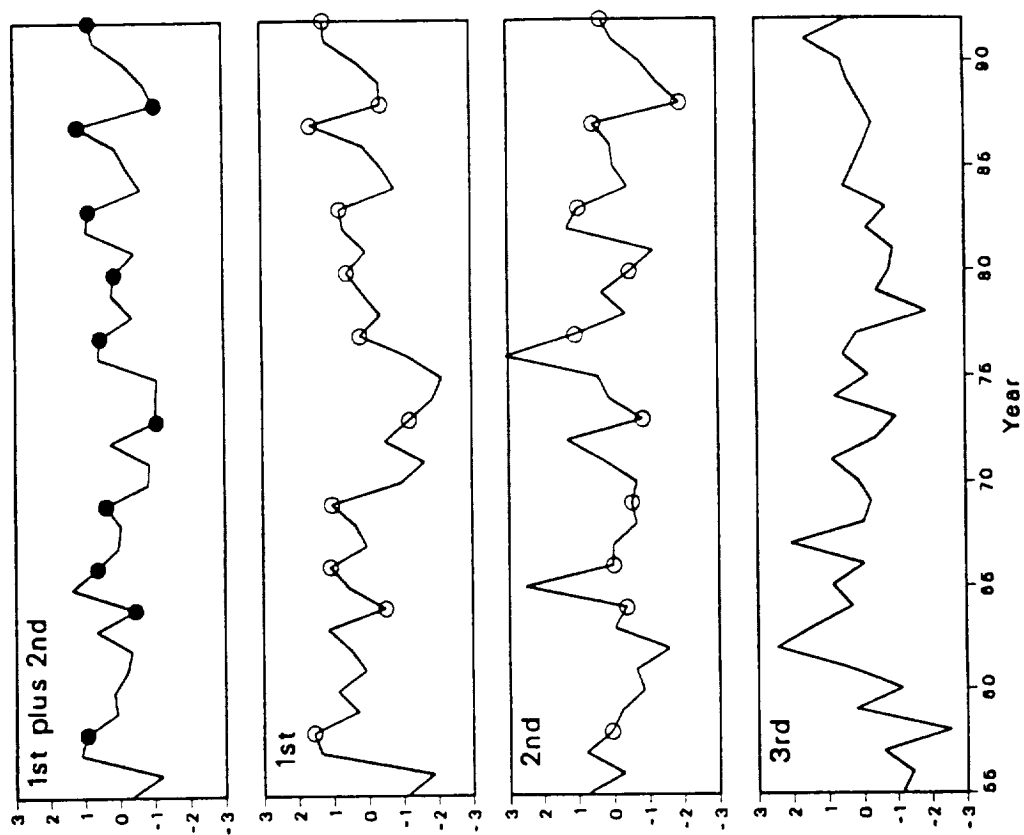
Figure 1

88

January   July

1st   1st

2nd   2nd

3rd   3rd

Figure 2

89

Figure 3

90

(a) Pattern Vector

(b) Seasonal Variation

Figure 4

91

October

April

1st

2nd

3rd

Figure 5

700mb Z

July

January

1st

2nd

3rd

Figure 6

500mb Z

January

July

1st

1st

2nd

2nd

3rd

3rd

Figure 7

94

300mb Z

January   July

Figure 8
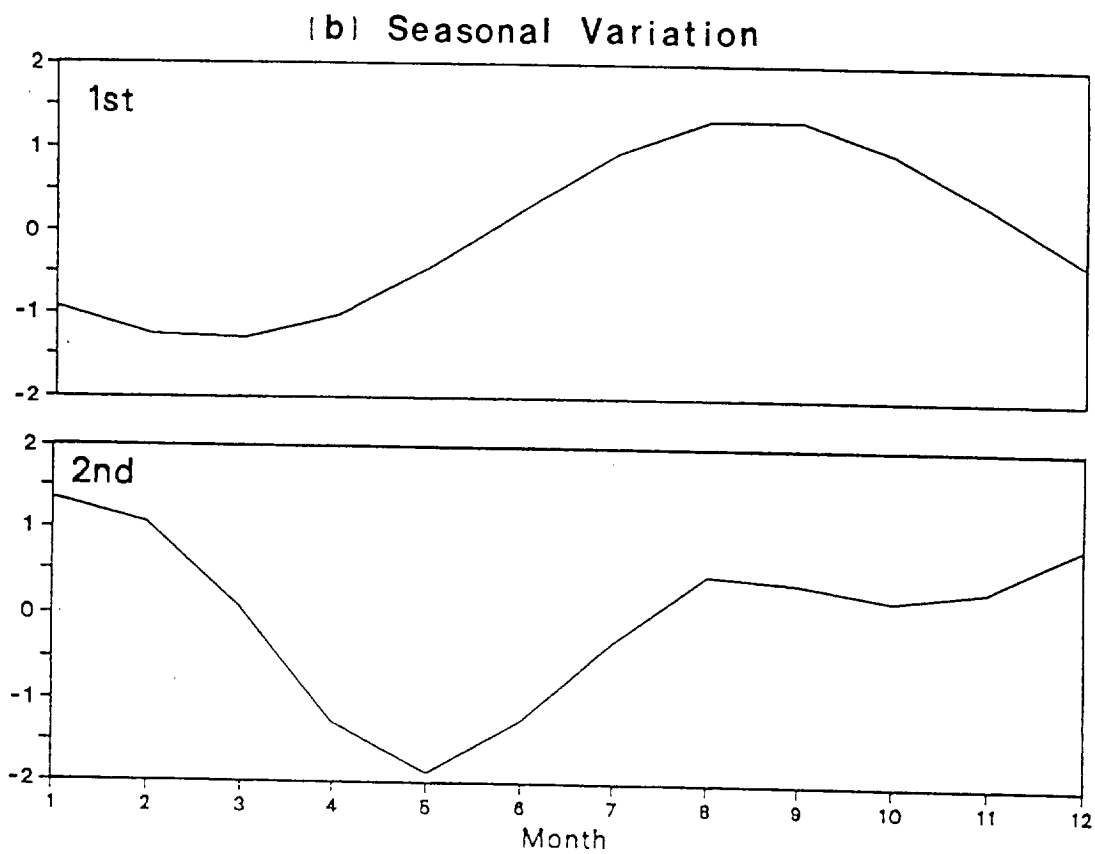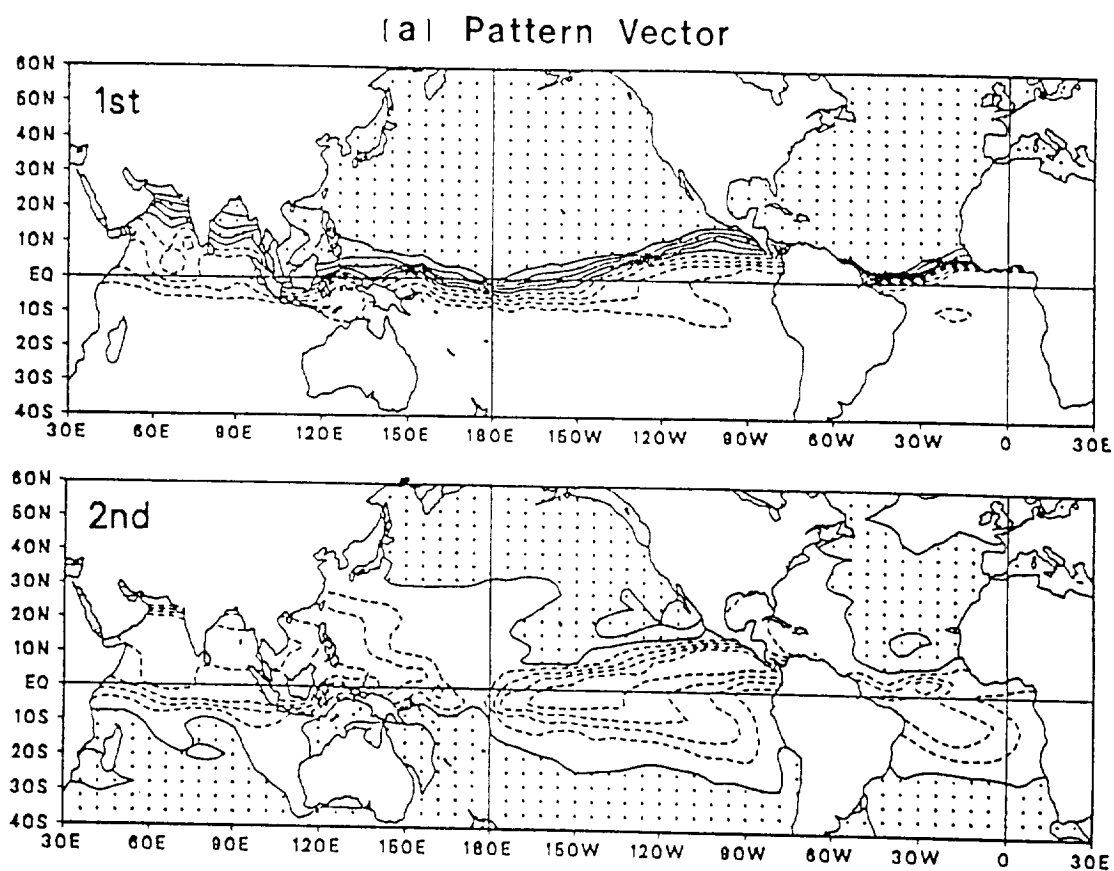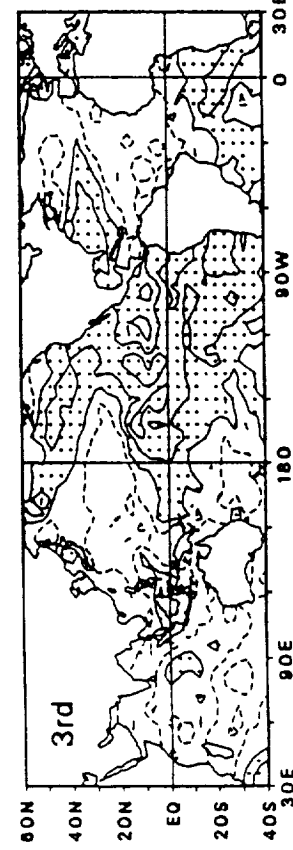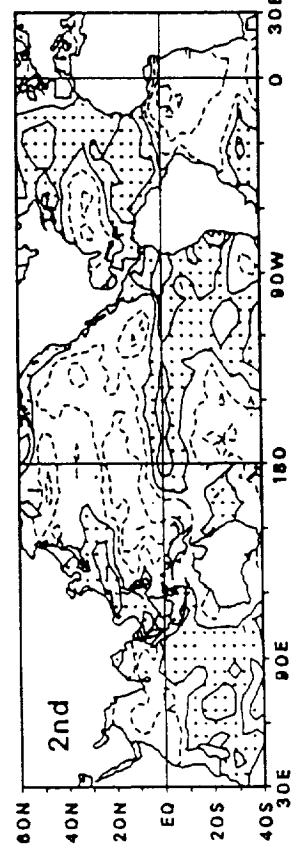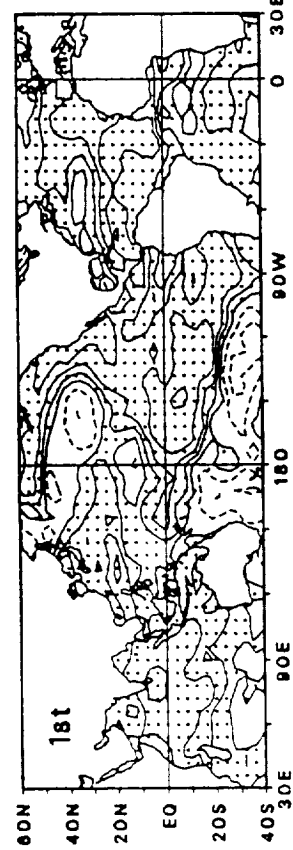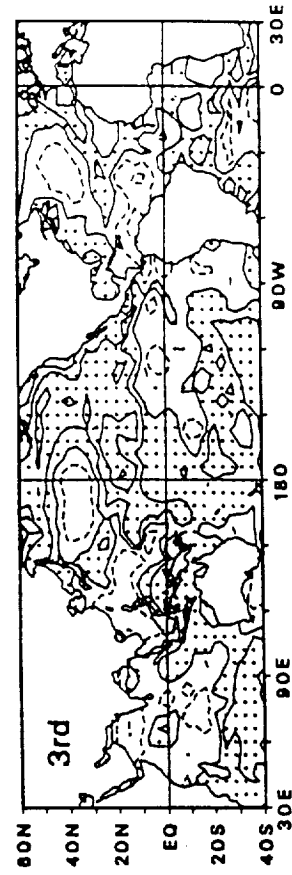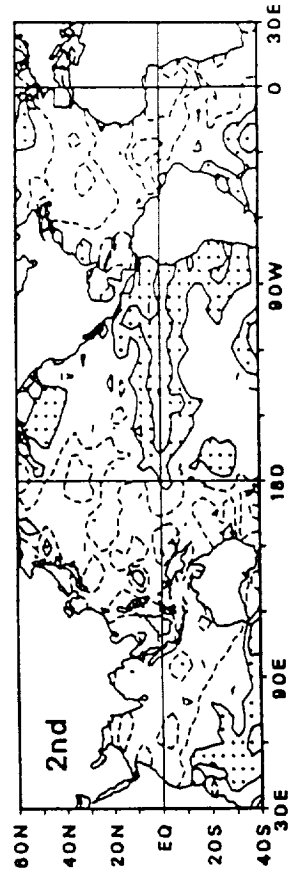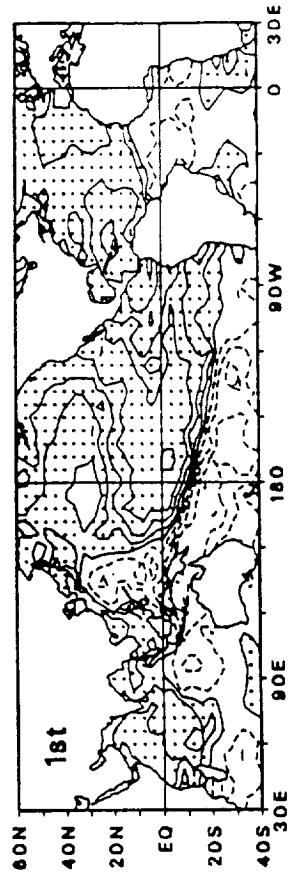
95

C-2
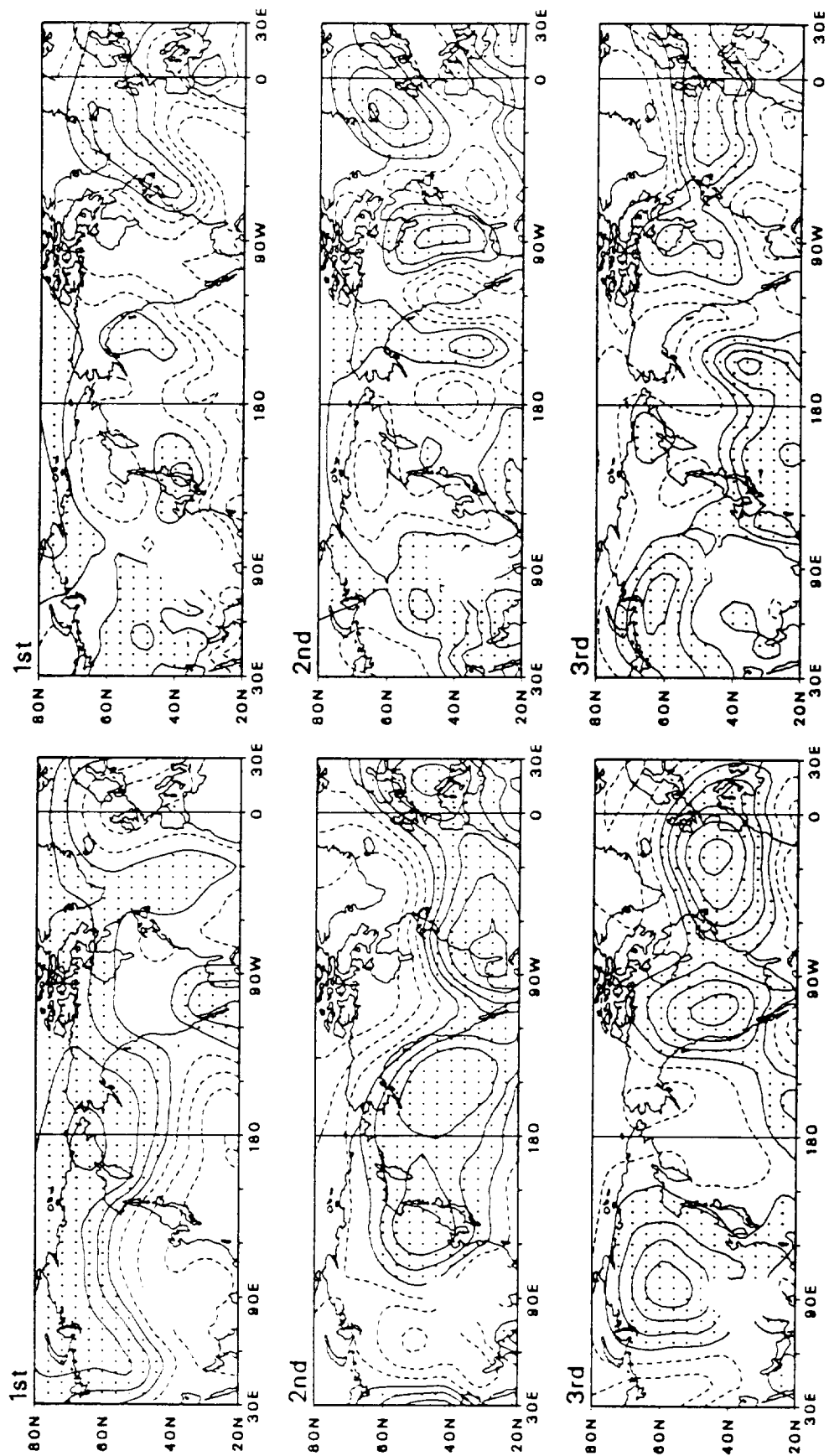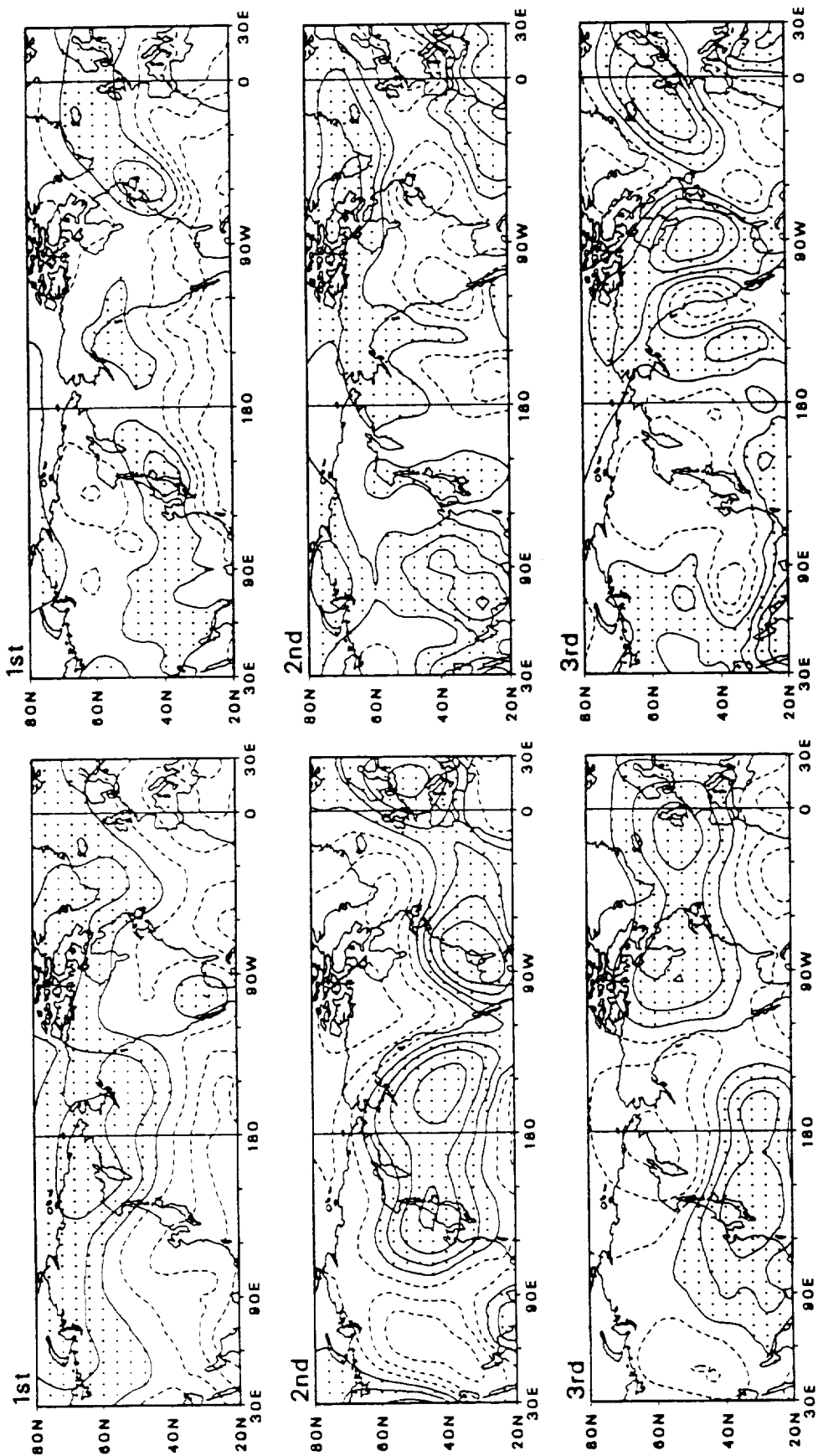
January ENSO Composite Anomalies
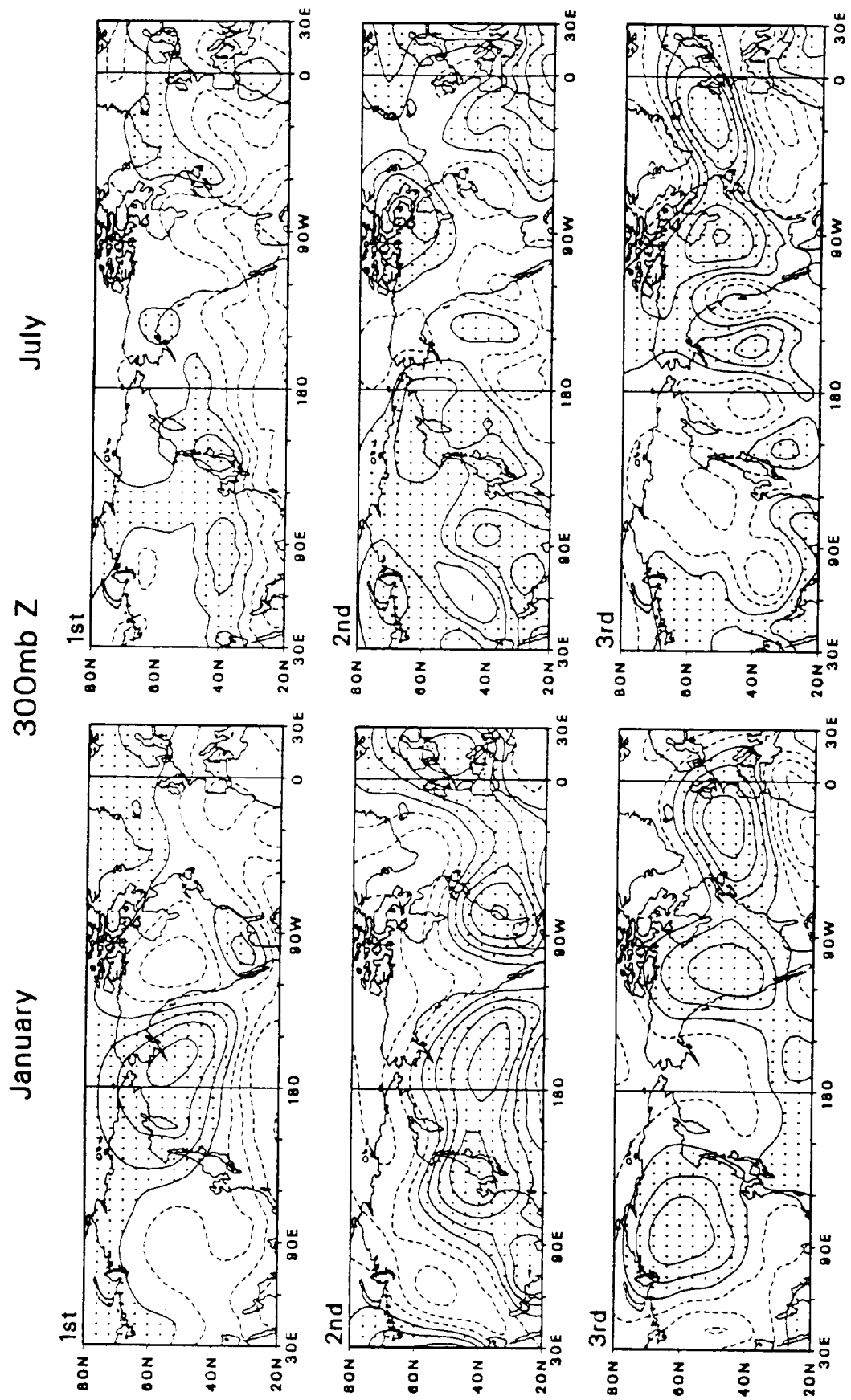
January ENSO Composite Flow Patterns

Figure 9

96
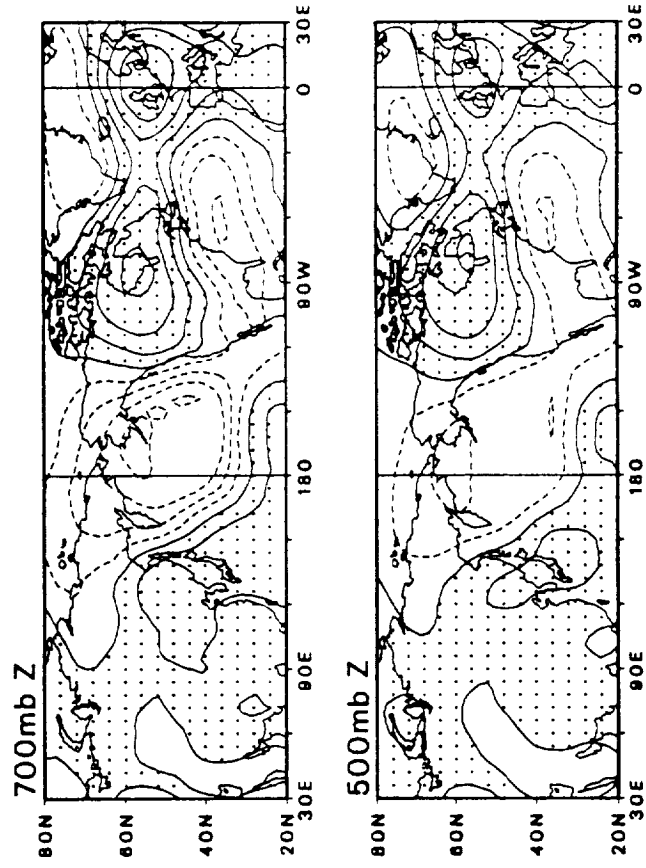
Cross-Correlations of 1st January SST Component with Upper Air Anomalies

500mb Z

300mb Z

Figure 10

97
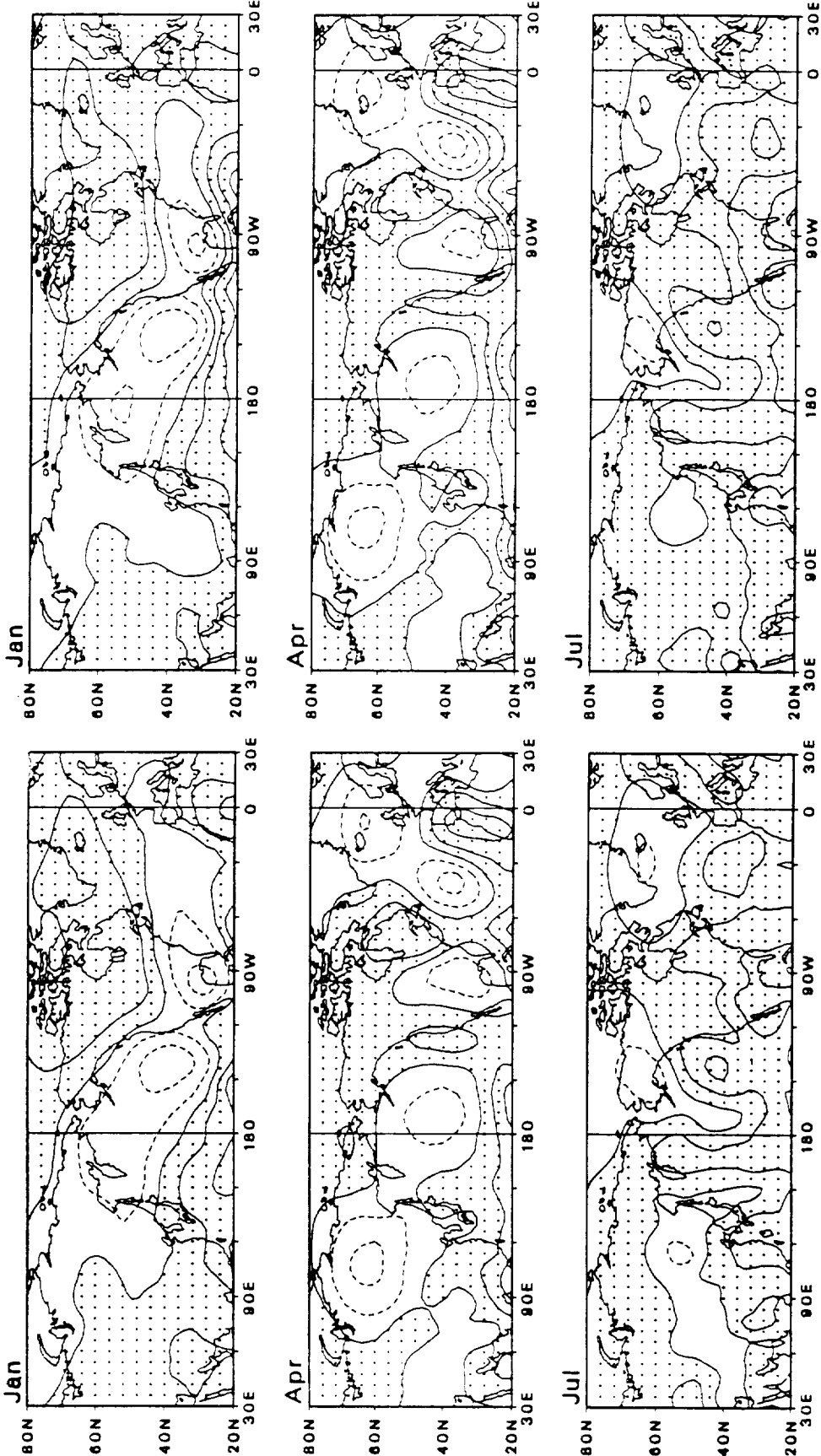
Cross-Correlations of 2nd January SST Component with Upper Air Anomalies
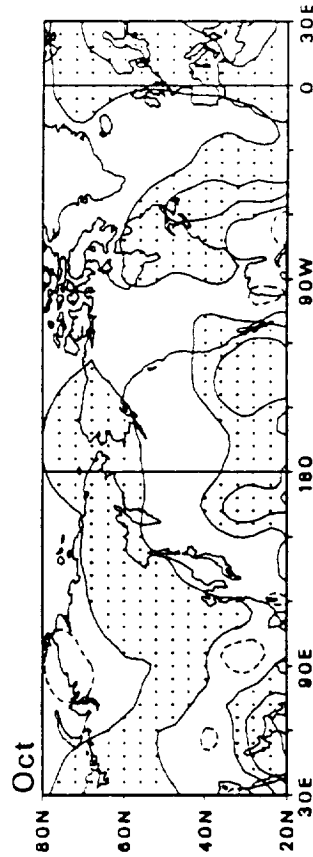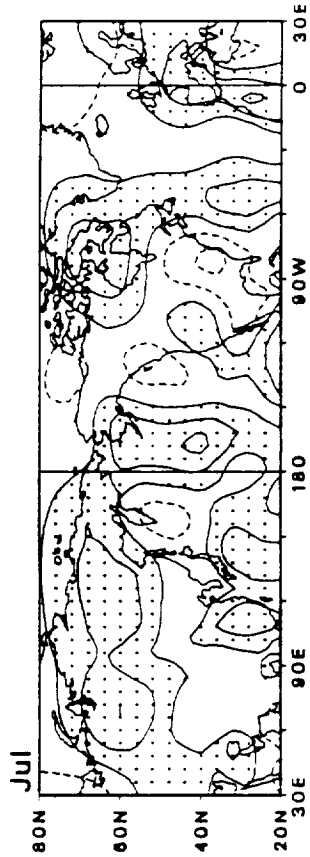
500mb Z

300mb Z

Figure 11

98
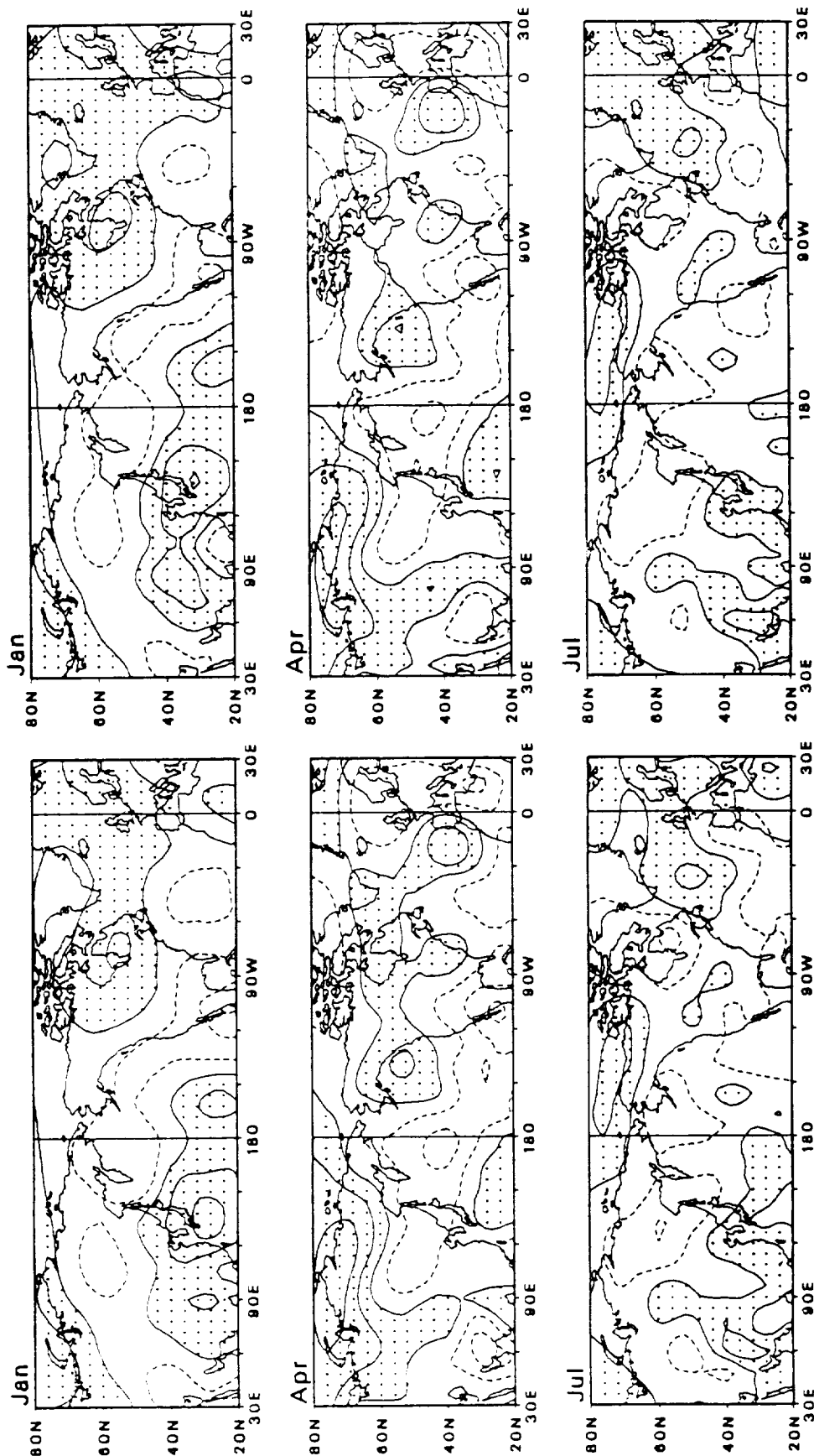
Cross-Correlations of 3rd January SST Component with Upper Air Anomalies

300mb Z

500mb Z

Figure 12

99
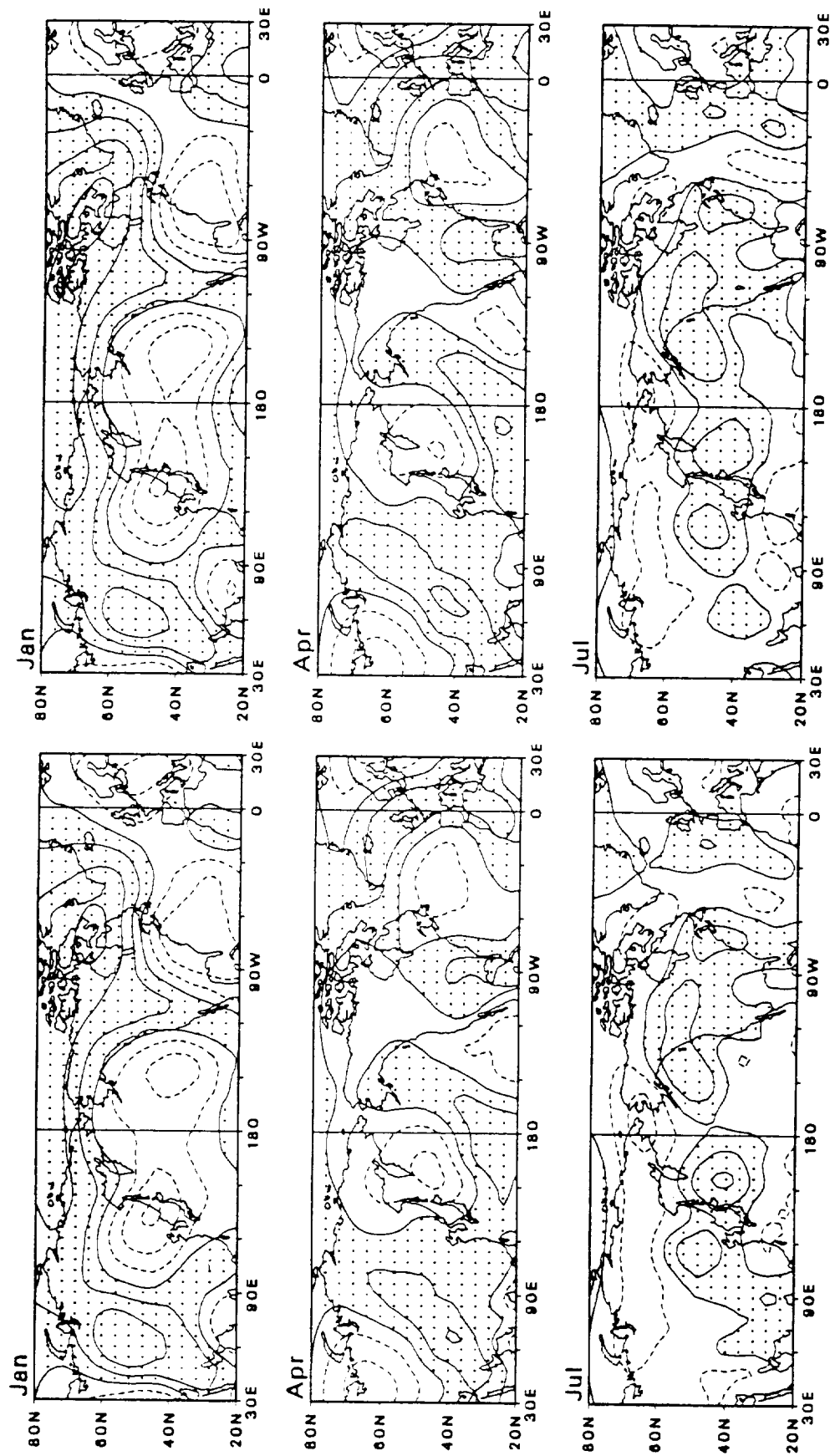
Cross-Correlations of 1st July SST Component with Upper Air Anomalies
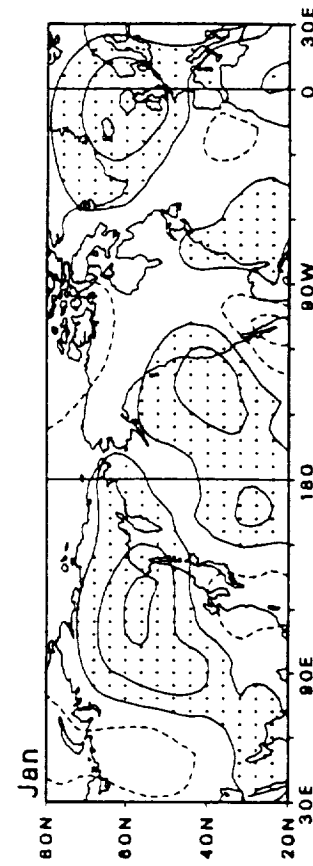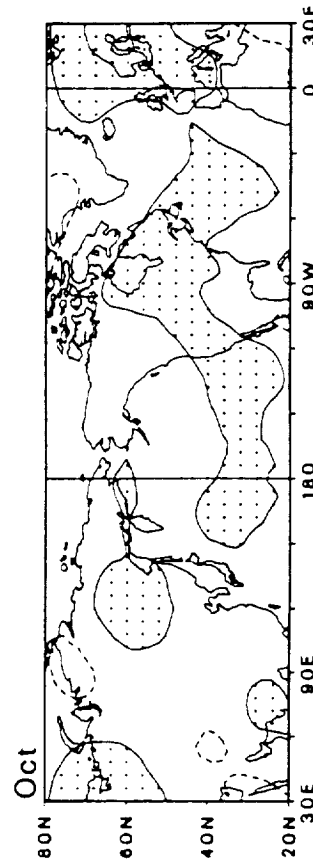
300mb Z

500mb Z

Figure 13

100
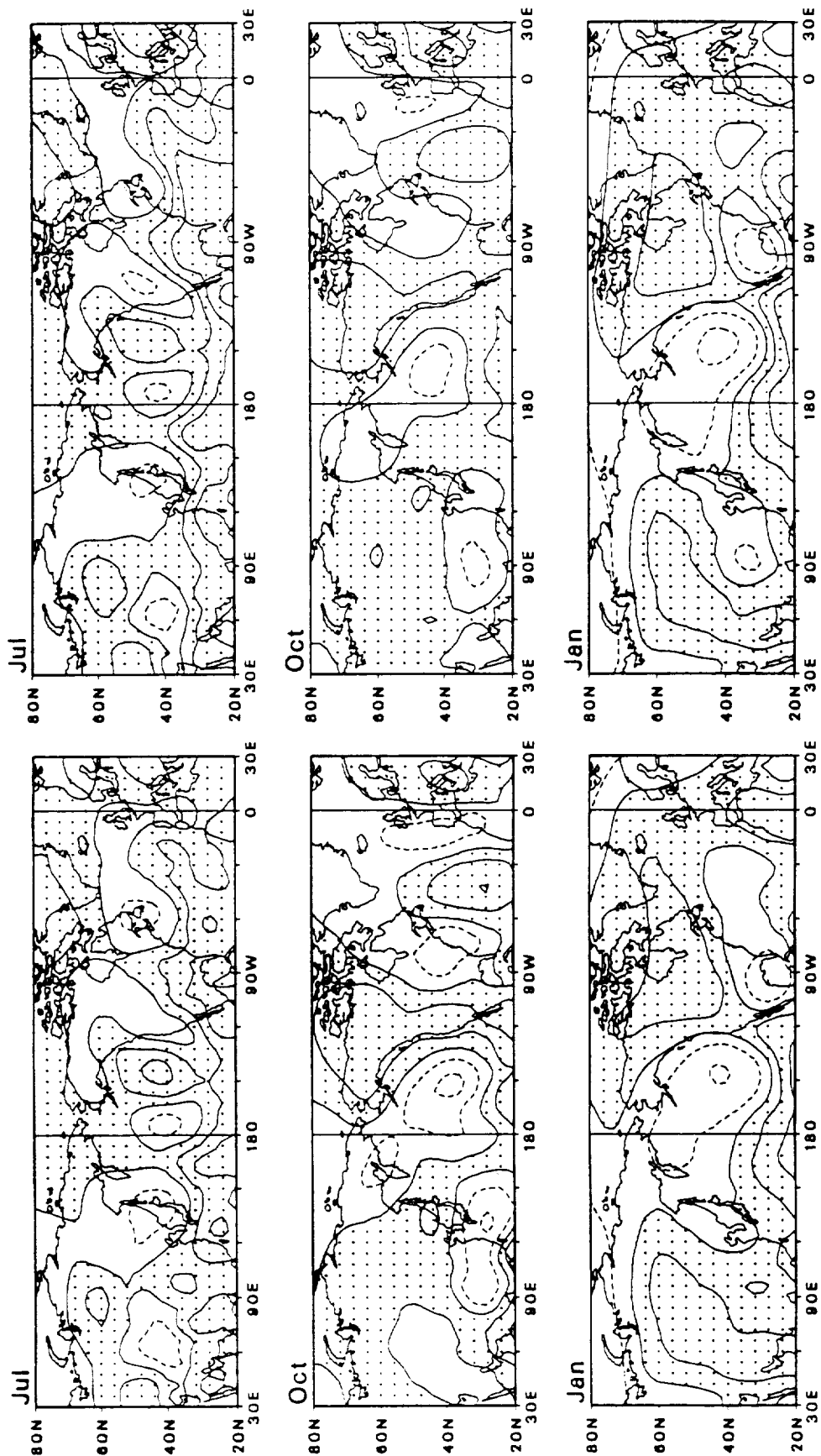
Cross-Correlations of 2nd July SST Component with Upper Air Anomalies
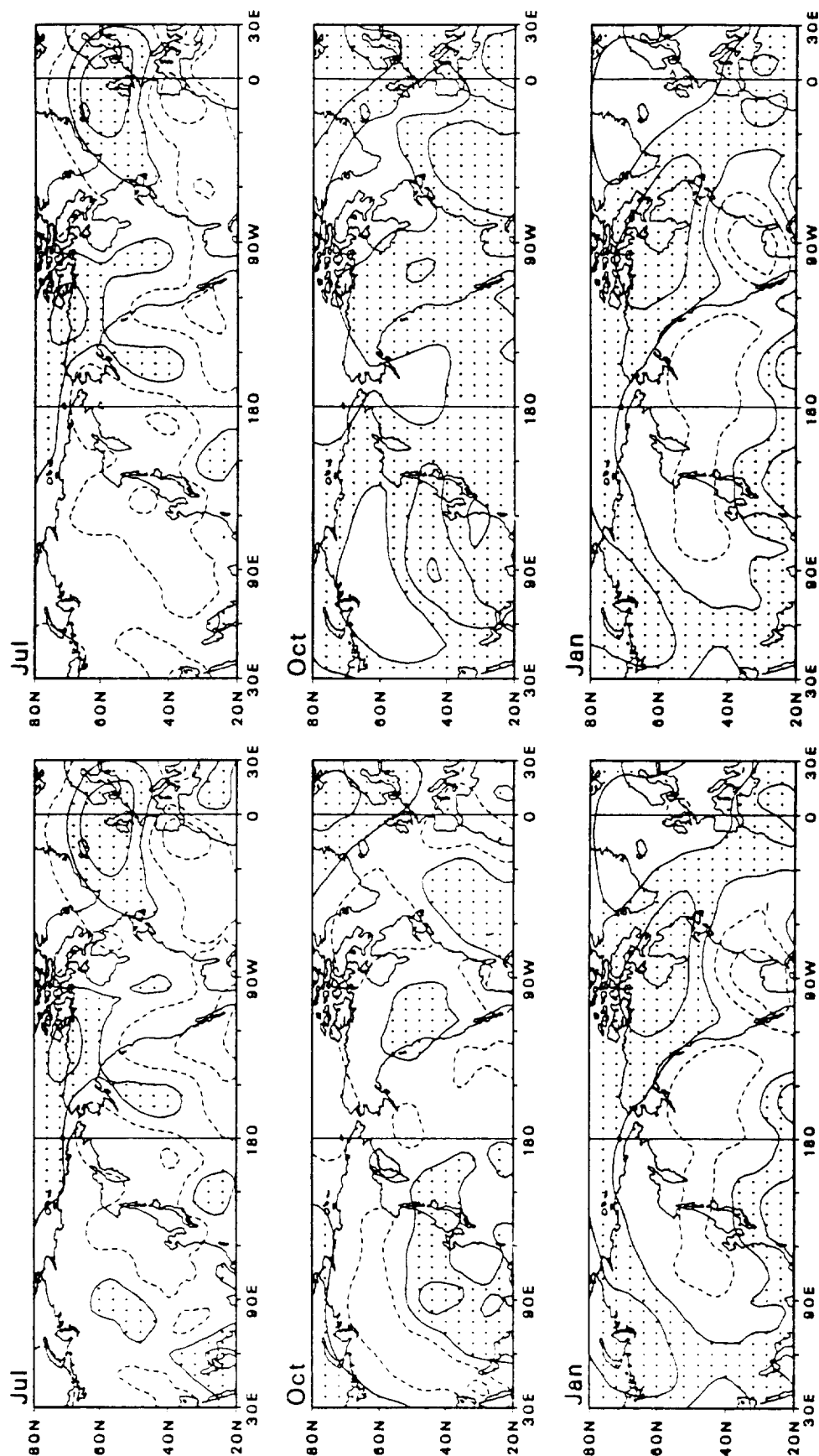
500mb Z

300mb Z

Figure 14

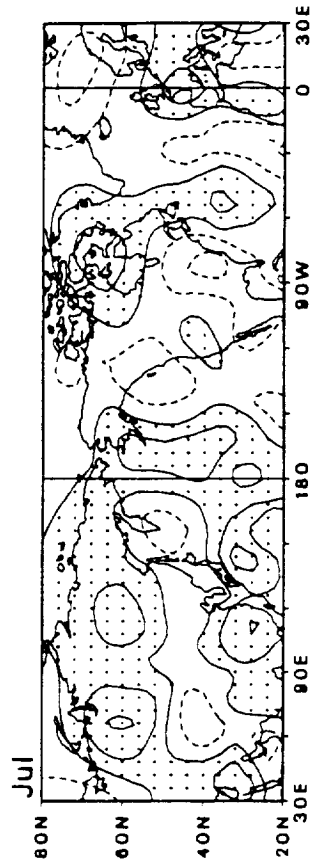## Cross-Correlations of 3rd July SST Component with Upper Air Anomalies

500mb Z

300mb Z

Figure 15

102